RETURN TO DESK
L629.051
J82

JOURNAL OF THE AERONAUTICAL SCIENCES

INSTITUTE OF THE AERONAUTICAL SCIENCES
THE NEW CRERAR LIBRARY

VOLUME 14 MAY, 1947 NUMBER 5

CONTENTS

Inelastic Column Theory ..... F. R. SHANLEY 261

Increasing the Range of Axial-Flow Compressors by Use of Adjustable Stator Blades ..... JOHN T. SINNETTE, JR. 269

Position Error of a Machmeter ..... H. W. SIBERT 283

Bending of Rotor Blade in the Plane of Rotation ..... SHAO WEN YUAN 285

Shock-Wave Oscillations in Wind Tunnels ..... HANS-WOLFGANG LIEPMANN AND HARRY ASHKENAS 295

The Rate of Descent of Parachutes from Various Altitudes ..... KENNETH E. PENROD, GEORGE L. MAISON, AND JAMES E. MCDONALD 303

Letters to the Editor 293, 310

Published by the
INSTITUTE OF THE AERONAUTICAL SCIENCES, INC.

JOURNAL OF THE AERONAUTICAL SCIENCES

Editor: HUGH L. DRYDEN, *Associate Director, National Bureau of Standards*

Associate Editor: ROBERT R. DEXTER *Associate Editor:* BERNEICE H. JARCK

The Institute of the Aeronautical Sciences publishes monthly the JOURNAL OF THE AERONAUTICAL SCIENCES and the AERONAUTICAL ENGINEERING REVIEW.

The JOURNAL OF THE AERONAUTICAL SCIENCES prints papers of scientific and technical interest to Institute members and subscribers. In general, it provides an opportunity for specialists to publish articles disclosing new knowledge and new applications in the field of the aeronautical sciences. The JOURNAL restricts itself to the aeronautical aspects of advances in science and engineering, and papers printed have either been submitted directly to the JOURNAL or have been previously presented at a meeting of the Institute.

The AERONAUTICAL ENGINEERING REVIEW keeps members and subscribers informed regarding the contents of new books and current periodicals in the field of aeronautics. It reviews new developments in the aircraft industry and reports on progress from house organs and catalogs published by aircraft and engine manufacturers and other companies engaged in aeronautical activities. It publishes papers on applied engineering and aircraft production. News of Institute activities is published in the REVIEW.

Statements and opinions expressed in the JOURNAL are to be understood as individual expressions of the authors and not those of the Institute.

SUBSCRIPTION RATES

Journal of the Aeronautical Sciences
Published Monthly

United States and Possessions		Foreign Countries Including Canada (American Currency Rates)	
1 Year	$7.00	1 Year	$9.00
Single Copies	0.70	Single Copies	1.00

Aeronautical Engineering Review
Published Monthly

United States and Possessions		Foreign Countries Including Canada (American Currency Rates)	
1 Year	$3.00	1 Year	$3.50
Single Copies	0.30	Single Copies	0.35

Notices of change of address should be sent to the Institute at least 30 days prior to actual change of address.

Manuscripts for publication, proofs, and all correspondence should be addressed to the Editorial Office of the JOURNAL.

Correspondence regarding subscriptions may be addressed to Publication Office, 20th and Northampton Sts., Easton, Pa., or to the Editorial Office of the JOURNAL OF THE AERONAUTICAL SCIENCES, 2 East 64th Street, New York 21, New York.

Copyright, 1947, by the Institute of the Aeronautical Sciences, Inc.

Entered as Second-Class Matter at the Post Office, Easton, Pa., May 1, 1937. Acceptance for mailing at a special rate of Postage provided for in the Act of August 24, 1912. Authorized April 29, 1937.

INSTITUTE of the AERONAUTICAL SCIENCES

President
P. R. BASSETT

Vice-Presidents
WELLWOOD E. BEALL
REX B. BEISEL
LUIS DE FLOREZ
JOHN K. NORTHROP

Director
S. PAUL JOHNSTON

Executive Vice-President
BENNETT H. HORCHLER

Past-Presidents
J. C. HUNSAKER
CHARLES L. LAWRANCE
DONALD W. DOUGLAS
GLENN L. MARTIN
CLARK B. MILLIKAN
T. P. WRIGHT
GEORGE W. LEWIS
JAMES H. DOOLITTLE
FRANK W. CALDWELL
HALL L. HIBBARD
HUGH L. DRYDEN
R. H. FLEET
CHARLES H. COLVIN
ARTHUR E. RAYMOND

Secretary
ROBERT R. DEXTER

Treasurer
BURDETTE S. WRIGHT

Controller
JOSEPH J. MAITAN

Counsel
ALLAN D. EMIL

COUNCIL

E. E. ALDRIN
LAWRENCE D. BELL
GEORGE W. BRADY
W. A. M. BURDEN
VICTOR E. CARBONARA
CARL DE GANAHL
JAMES H. DOOLITTLE
WILLIAM K. EBEL
SHERMAN M. FAIRCHILD
C. C. FURNAS
J. A. HERLIHY
WILLSON H. HUNTER
JEROME LEDERER
JOHN C. LESLIE
A. ELLIOTT MERRILL
EARL D. OSBORN
ELMER A. SPERRY, JR.
JOHN C. SQUIRES
M. F. STOUGHTON
ERNEST G. STOUT
C. FAYETTE TAYLOR

ADVISORY COMMITTEE

Chairman: CHARLES H. COLVIN

WALTER BEECH
FRANK W. CALDWELL
RALPH S. DAMON
KENNETH S. M. DAVIDSON
R. H. FLEET
R. PAUL HARRINGTON
R. M. HAZEN
HALL L. HIBBARD
J. C. HUNSAKER
TH. VON KÁRMÁN
THOMAS A. KNOWLES
I. M. LADDON
GROVER LOENING
GLENN L. MARTIN
CLARK B. MILLIKAN
THOMAS A. MORGAN
R. C. MUIR
ARTHUR E. RAYMOND
F. W. REICHELDERFER
L. B. RICHARDSON
RUSSELL G. ROBINSON
LAURANCE S. ROCKEFELLER
T. CLAUDE RYAN
EDWARD P. WARNER

HONORARY MEMBERS

JOHN C. ADAMS
GRIFFITH BREWER
JOHN N. BROWN
W. A. M. BURDEN
E. U. CONDON
L. C. CRAIGIE
IRA C. EAKER
HARRY F. GUGGENHEIM
HENRY G. HOUGHTON
GEORGE C. KENNEY
CURTIS E. LE MAY
GEORGE B. PEGRAM
E. M. POWERS
J. LAURENCE PRITCHARD
ARTHUR W. RADFORD
F. W. REICHELDERFER
H. B. SALLADA
CARL SPAATZ
L. C. STEVENS
NATHAN F. TWINING

HONORARY FELLOWS

H. H. ARNOLD
FRANK W. CALDWELL
SIR GEOFFREY DE HAVILLAND
DONALD W. DOUGLAS
HUGH L. DRYDEN
W. F. DURAND
SIR RICHARD FAIREY
SIR ROY FEDDEN
J. C. HUNSAKER
SIR MELVILL JONES
GEORGE W. LEWIS
GLENN L. MARTIN
GEORGE J. MEAD
SIR FREDERICK HANDLEY PAGE
D. R. PYE
IGOR I. SIKORSKY
SIR GEOFFREY I. TAYLOR
TH. VON KÁRMÁN
EDWARD P. WARNER
ORVILLE WRIGHT
T. P. WRIGHT

BENEFACTORS

E. E. ALDRIN
HART O. BERG (Deceased)
W. A. M. BURDEN
E. L. CORD
DONALD W. DOUGLAS
SHERMAN M. FAIRCHILD
SIR RICHARD FAIREY
R. H. FLEET
FLORENCE GUGGENHEIM (Deceased)
C. D. HANSCOM
JOHN P. V. HEINMULLER
ALEXANDER KLEMIN
PAUL KOLLSMAN
BELLA C. LANDAUER
WILLIAM LANDAUER
GROVER LOENING
EDMUND C. LYNCH (Deceased)
F. W. MAGIN
GLENN L. MARTIN
GEORGE J. MEAD
S. A. REED (Deceased)
LAURANCE S. ROCKEFELLER
EDWARD P. WARNER

AMERICAN FELLOWS

JOHN D. ACKERMAN
E. E. ALDRIN
HARRY G. ARMSTRONG
KARL ARNSTEIN
J. L. ATWOOD
PAUL S. BAKER
RALPH S. BARNABY
P. R. BASSETT
WELLWOOD E. BEALL
REX B. BEISEL
G. M. BELLANCA
DON R. BERLIN
HENRY A. BERLINER
WILLIAM BOLLAY
B. C. BOULTON
GEORGE W. BRADY
LYMAN J. BRIGGS
W. G. BROMBACHER
WILLIAM G. BROWN
CHARLES P. BURGESS
KENNETH CAMPBELL
CHARLES H. CHATFIELD
ALLAN CHILTON
V. E. CLARK
FRANKLIN R. COLLBOHM
CHARLES H. COLVIN
KARL T. COMPTON
EMERSON W. CONLON
JOHN W. CROWLEY, JR.
RALPH S. DAMON
LUIS DE FLOREZ
SMITH J. DE FRANCE
J. P. DEN HARTOG
WALTER S. DIEHL
JAMES H. DOOLITTLE
C. S. DRAPER
IVAN H. DRIGGS
WILLIAM K. EBEL
C. L. EGTVEDT
FREDERIC FLADER
CHARLES FROESCH
JACK FRYE
GARLAND FULTON
LESTER D. GARDNER
RICHARD C. GAZLEY
MICHAEL E. GLUHAREFF
MELVIN N. GOUGH
LEROY R. GRUMMAN
HAROLD R. HARRIS
R. M. HAZEN
ALBERT F. HEGENBERGER
EDWARD H. HEINEMANN
S. D. HERON
HALL L. HIBBARD
L. S. HOBBS
PAUL E. HOVGAARD
WILLIAM HOVGAARD
ROBERT INSLEY
EASTMAN N. JACOBS
CLARENCE L. JOHNSON
S. PAUL JOHNSTON
ALEXANDER KARTVELI
PAUL H. KEMMER
J. H. KINDELBERGER
OTTO E. KIRCHNER
ARTHUR L. KLEIN
ALEXANDER KLEMIN
W. B. KLEMPERER
PAUL KOLLSMAN
OTTO C. KOPPEN
B. V. KORVIN-KROUKOVSKY
S. M. KRAUS
I. M. LADDON
E. S. LAND
CHARLES L. LAWRANCE
JEROME LEDERER
JOHN G. LEE
JOHN C. LESLIE
CHARLES A. LINDBERGH
WILLIAM LITTLEWOOD
GROVER LOENING
ALBERT E. LOMBARD
W. RANDOLPH LOVELACE, II
EUGENE E. LUNDQUIST
R. D. MACCART
JOHN R. MARKHAM
ERLE MARTIN
WM. H. MCAVOY
C. J. MCCARTHY
CLARK B. MILLIKAN
ROBERT J. MINSHALL
JOSEPH S. NEWELL
ALFRED S. NILES
JOHN K. NORTHROP
ARTHUR NUTT
SHATSWELL OBER
ROBERT R. OSBORN
W. BAILEY OSWALD
GEORGE A. PAGE, JR.
F. W. PAWLOWSKI
F. W. PENNOYER, JR.
A. A. PRIESTER
ARTHUR E. RAYMOND
F. W. REICHELDERFER
ELLIOTT G. REID
H. J. E. REID
H. C. RICHARDSON
RUSSELL G. ROBINSON
LEONARD E. ROOT
C. E. ROSENDAHL
ADDISON M. ROTHROCK
WILLIAM T. SCHWENDLER
FRANCIS R. SHANLEY
JAMES M. SHOEMAKER
MAC SHORT
IGOR ALEXIS SIKORSKY
ABE SILVERSTEIN
SELDEN B. SPANGLER
ELMER A. SPERRY, JR.
JOHN STACK
WILLIAM B. STOUT
HARRY A. SUTTON
C. FAYETTE TAYLOR
EDWARD S. TAYLOR
PHILIP B. TAYLOR
TH. THEODORSEN
T. E. TILLINGHAST
S. TIMOSHENKO
L. B. TUCKERMAN
RALPH H. UPSON
J. PARKER VAN ZANDT
J. G. VINCENT
RICHARD VON MISES
FRANK L. WATTENDORF
P. V. H. WEEMS
FRED E. WEICK
R. D. WEYERBACHER
JOHN B. WHEATLEY
ANDREW V. WILLGOOS
DONALD H. WOOD
ROBERT J. WOODS
JOHN E. YOUNGER
ALBERT F. ZAHM
STEPHEN J. ZAND

An Appreciation
To Corporate Members of the Institute of the Aeronautical Sciences

Listed below are the leading aeronautical and industrial companies that make possible the publication of the *Journal of the Aeronautical Sciences*.

They enable the Institute to publish scientific and technical papers in the *Journal* and to devote its pages exclusively to editorial material.

Dues from individual members which would normally be used to publish this scientific and engineering monthly are thus released for additional services to the profession and industry.

The *Aeronautical Engineering Review* and the *Aeronautical Engineering Catalog*, together with the *Journal*, provide a comprehensive technical information service for the benefit of the aircraft and related industries.

Academy of Aeronautics, Inc.
Casey Jones School of Aeronautics
Aero Insurance Underwriters
Aerojet Engineering Corporation
Aeronca Aircraft Corporation
Aeroproducts Division, General Motors Corporation
Aeroquip Corporation
Agawam Aircraft Products, Inc.
Airborne Instruments Laboratory, Inc.
Airchox Company Division, Joyce Aviation, Inc.
Aircraft Radio Corporation
AiResearch Manufacturing Company
AiResearch Manufacturing Company of Arizona, Inc.
Allis-Chalmers Manufacturing Company
Allison Division, General Motors Corporation
Aluminum Company of America
American Airlines System
American Overseas Airlines, Inc.
American Bosch Corporation
American Phenolic Corporation
Associated Aviation Underwriters
Associated Foundries & Manufacturers, Inc.
Atlas Supply Company
Baker Steel & Tube Company
Beech Aircraft Corporation
Bell Aircraft Corporation
Bendix Aviation Corporation
Bendix Products Division
Bendix Radio Corporation
Eclipse-Pioneer Division
Export Division
Friez Instrument Division
Pacific Division
Scintilla Magneto Company
The BG Corporation
Boeing Aircraft Company
Breeze Corporations, Inc.
Essex Tool & Die Company
Federal Laboratories, Inc.
Cal-Aero Technical Institute, A Division of Grand Central Airport Company
Carrier Corporation
Cessna Aircraft Company
Chandler-Evans Division, Niles-Bement-Pond Company
Chase National Bank of the City of New York
The Cleveland Graphite Bronze Company
The Cleveland Pneumatic Tool Company
Automotive-Aircraft Division
Clifford Manufacturing Company
Consolidated Vultee Aircraft Corporation
Nashville Division
Stinson Aircraft Division
Continental Motors Corporation
Cox and Stevens Aircraft Corporation
Culver Aircraft Corporation
Curtiss-Wright Corporation
Airplane Division
Development Division
Propeller Division
Wright Aeronautical Corporation
Doak Aircraft Company, Inc.
Douglas Aircraft Company, Inc.
El Segundo Plant
Long Beach Plant
The Dow Chemical Company
Dzus Fastener Company, Inc.
Eastern Air Lines, Inc.
Eaton Manufacturing Company
Thomas A. Edison, Incorporated, Instrument Division
Edo Aircraft Corporation

The Electric Auto-Lite Company
Electrol Incorporated
Engineering and Research Corporation
Ethyl Corporation
Fairchild Camera & Instrument Corporation
  Fairchild Aerial Surveys, Inc.
Fairchild Engine and Airplane Corporation
  Duramold Division
  Fairchild Aircraft Division
  Ranger Aircraft Engines Division
Federal Telephone and Radio Corporation
Firestone Aircraft Company
General Aviation Equipment Company, Inc.
General Electric Company
The B. F. Goodrich Company
The Goodyear Tire & Rubber Company
Grumman Aircraft Engineering Corporation
W. & L. E. Gurley
The Hilliard Corporation
The International Nickel Company
Irving Air Chute Company, Inc.
Jack & Heintz, Inc.
Johns-Manville Sales Corporation
Kaiser Fleetwings, Inc.
Walter Kidde & Company, Inc.
Kollsman Instrument Division, Square D Company
Lavelle Aircraft Corporation
Lear Incorporated
Link Aviation Devices, Inc.
The Liquidometer Corporation
Lockheed Aircraft Corporation
Longines-Wittnauer Watch Company, Inc.
The Glenn L. Martin Company
The W. L. Maxson Corporation
Warren McArthur Corporation
McDonnell Aircraft Corporation
Menasco Manufacturing Company
Micromatic Hone Corporation
Minneapolis-Honeywell Regulator Company
Mooré Drop Forging Company
National City Bank of New York
National Credit Office, Inc.
North American Aviation, Inc.
  North American Aviation, Inc., of Texas
Northrop Aircraft, Inc.
Northwest Airlines, Inc.
Owens-Corning Fiberglas Corporation
Pan American World Airways System
The Parker Appliance Company
Pesco Products Company Division, Borg-Warner Corporation
Phillips Petroleum Company
Pioneer Parachute Company, Inc.
Piper Aircraft Corporation
Pure Oil Co.
Radioplane Company
Republic Aviation Corporation
A. V. Roe Canada Limited
John A. Roebling's Sons Company
Rohr Aircraft Corporation
The Ryan Aeronautical Company
Scott Aviation Corporation
Shell Oil Company, Inc.
Simmonds Aerocessories, Inc.
Skydyne, Inc.
Socony-Vacuum Oil Company
Solar Aircraft Company
Sperry Gyroscope Company, Inc.
Square D Company
Standard Oil Company of California
Standard Oil Company (Indiana)
Standard Oil Company of New Jersey
The Texas Company
Thompson Products, Inc.
Tinnerman Products, Inc.
Trans World Airline
Union Carbide and Carbon Corporation
  Bakelite Corporation
  Haynes Stellite Company
  Linde Air Products Company
  National Carbon Company
United Aircraft Corporation
  Chance Vought Aircraft Division
  Hamilton Standard Propellers Division
  Pratt & Whitney Aircraft Division
  Pratt & Whitney Aircraft Corporation of Missouri
  Sikorsky Aircraft Division
United Air Lines, Inc.
United States Aviation Underwriters, Inc.
United States Rubber Company
  Dominion Rubber Company, Ltd.
Vickers, Inc.
The Waco Aircraft Company
Warner Aircraft Corporation
The Weatherhead Company
Western Air Lines, Inc.
Westinghouse Electric Corporation
Weston Electrical Instrument Corporation
Willys-Overland Motors, Inc., Aircraft Research and Development Division
Wyman-Gordon Company
Young Radiator Company

EDITORIAL COMMITTEE

HUGH L. DRYDEN, *Chairman*

Aerodynamics

Francis Clauser
Howard Emmons
R. Paul Harrington
R. T. Jones
W. B. Klemperer
Otto C. Koppen
John G. Lee
H. P. Liepmann
John R. Markham
Clark B. Millikan
Shatswell Ober
W. Bailey Oswald
Allen E. Puckett
Elliott G. Reid
H. J. E. Reid
Russell Robinson
L. E. Root
G. B. Schubauer
W. R. Sears
John Stack
Th. von Kármán
Richard von Mises

Air Transport

A. W. Dallas
Charles Froesch
J. A. Herlihy
Otto E. Kirchner
John C. Leslie

Aircraft Design

W. E. Beall
Rex B. Beisel
W. K. Ebel
Hall L. Hibbard
C. L. Johnson
I. M. Laddon
C. J. McCarthy
Fred E. Weick
Robert J. Woods

Physiologic Problems

H. G. Armstrong
Louis H. Bauer
Eugene Du Bois
W. Randolph Lovelace II
Ross A. McFarland
A. D. Tuttle

Aircraft Propulsion

George W. Brady
Frank W. Caldwell
L. S. Hobbs
E. E. Johnson
Joseph Keenan
R. P. Kroon
Arthur Nutt
Hans Reissner
Abe Silverstein
C. Fayette Taylor
E. S. Taylor
P. Taylor

Structures and Materials

W. B. Bleakney
E. W. Conlon
J. P. Den Hartog
L. H. Dönnell
E. C. Hartmann
N. J. Hoff
H. L. Langhaar
E. E. Lundquist
C. F. Nagel, Jr.
J. S. Newell
Alfred S. Niles
W. Ramberg
E. Reissner
F. R. Shanley
H. W. Sibert
C. R. Strang
S. Timoshenko
H. S. Tsien

Meteorology

C. F. Brooks
D. M. Little
E. J. Minser
F. W. Reichelderfer
H. C. Willett

Fuels and Oils

A. L. Beall
J. H. Doolittle
Graham Edgar
R. T. Goodwin
S. D. Heron
A. M. Rothrock

Instruments

Allan G. Binnie
W. G. Brombacher
J. Callahan
Charles H. Colvin
C. S. Draper
O. E. Esval
David W. Moore
W. A. Reichel
C. F. Savage
O. Hugo Schuck
R. Sylvander

Rotating Wing Aircraft

Robert Coleman
M. L. Deutsch
G. Horvay
Alexander Klemin
Ralph McClarren
R. H. Prewitt
Igor I. Sikorsky
Robert A. Wolf

Vibration and Flutter

Lee Arnold
M. A. Biot
William Bollay
J. P. Den Hartog
Manfred Rauscher

Flight Testing

William K. Ebel
R. R. Gilruth
Melvin N. Gough
Robert Stanley
E. A. Stout

I.A.S. REPRESENTATIVES TO OTHER ORGANIZATIONS

Aircraft Industries Association of America, Inc.—CHARLES MARCUS

American Association for the Advancement of Science—J. C. HUNSAKER

American Society of Mechanical Engineers—CHARLES H. COLVIN

American Standards Association—P. R. BASSETT

Engineering Society of Detroit—DONALD C. HUNT, GEORGE TWENEY

Greater New York Safety Council—WILLIAM LITTLEWOOD

Daniel Guggenheim Medal Board of Award—CHARLES H. COLVIN, GROVER LOENING, LESTER D. GARDNER

Institute of Radio Engineers—L. M. HULL

Manufacturers Aircraft Association—ARTHUR E. RAYMOND

National Aeronautic Association—WILLIAM R. ENYART

National Fire Protection Association—E. E. ALDRIN

National Research Council Engineering Division—HUGH L. DRYDEN

National Safety Council—JEROME LEDERER

New York Museum of Science and Industry—LESTER D. GARDNER

Society of Automotive Engineers—STEPHEN J. ZAND

JOURNAL OF THE AERONAUTICAL SCIENCES

VOLUME 14 MAY, 1947 NUMBER 5

Inelastic Column Theory

F. R. SHANLEY*

Lockheed Aircraft Corporation

SUMMARY

The action of a column in the plastic range is analyzed on the basis that bending may proceed simultaneously with increasing axial load. This leads to a new column formula that includes both the tangent-modulus (Engesser) and the reduced-modulus (von Kármán) formulas. It is shown that bending begins at the tangent-modulus load and that the column load increases with increasing lateral deflection, approaching the reduced-modulus load as a limit if the tangent modulus is assumed to remain constant.

INTRODUCTION

IN A RECENTLY PUBLISHED PAPER,[1] the author stated that the reduced-modulus (or double-modulus) theory is not correct for predicting the maximum load up to which a perfect column will remain straight. This is because it is possible for the column to bend simultaneously with increasing axial load. Under such conditions it is possible to have bending without introducing any strain reversal, upon which the reduced-modulus theory depends. In reference 1 it was stated that the column will begin to bend as soon as the axial load exceeds the value predicted by the tangent-modulus (Engesser) theory. It appeared likely that the Engesser load could be exceeded but that the reduced-modulus load could not be reached. In this paper it will be shown that for an idealized simplified column, this is actually true.

The three basic column formulas may be written as follows (assuming pin ends and zero eccentricity):

$$\text{(Euler)} \quad P_e = \pi^2 EI/L^2 \tag{1}$$

$$\text{(Engesser)} \quad P_t = \pi^2 E_t I/L^2 \tag{2}$$

$$\text{(reduced modulus)} \quad P_r = \pi^2 E_r I/L^2 \tag{3}$$

where

P = critical load
I = moment of inertia of column cross section
L = column length
E = Young's modulus (slope of stress-strain diagram in elastic range)
E_t = tangent modulus (local slope of stress-strain diagram in inelastic range)
E_r = reduced modulus (an effective value lower than E and higher than E_t)

Eqs. (1), (2), and (3) differ only in the value used for the effective modulus of elasticity. Since the Euler equation applies only in the elastic range, the problem of column action in the inelastic (plastic) range centers around Eqs. (2) and (3). An excellent summary of the history of these two theories is given in reference 2, from which the following is quoted:

"What is here called the double-modulus theory has frequently been called also the Considère-Engesser theory and Kármán's theory. Many competent engineers are mistaken as to the origin of the theory, and a brief account of its development will not be out of place. In 1891 there was published a memoir included as an appendix (annexe) to the proceedings of the Congrès International des Procédés de Constructions, held in Paris from the 9th to the 14th of September, 1889, in which A. Considère pointed out that, as an ideal column stressed beyond the proportional limit begins to bend, the stress on the concave side increases according to the law of the compressive stress-strain diagram, and the stress on the convex side decreases according to Hooke's law, and that therefore the strength would be given by

$$P = \pi^2 \bar{E} I/L^2$$

in which $\bar{E}$ is a modulus, the value of which lies between the modulus of elasticity and the tangent modulus. Considère realized that $\bar{E}$ was a function of P/A, the average stress in the column, but did not go further than to point out this fact.

Presented at the Structures Session, Fifteenth Annual Meeting, I.A.S., New York, January 28–30, 1947.

* Division Engineer, Engineering Research.

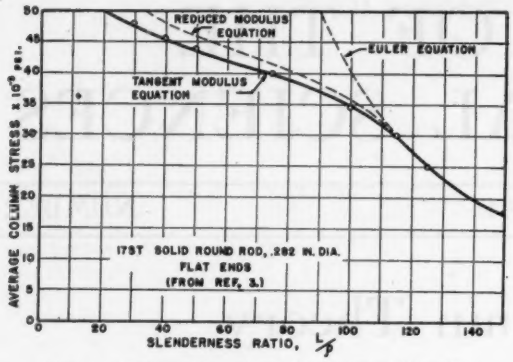

FIG. 1. Column theories and test data (Alcoa).

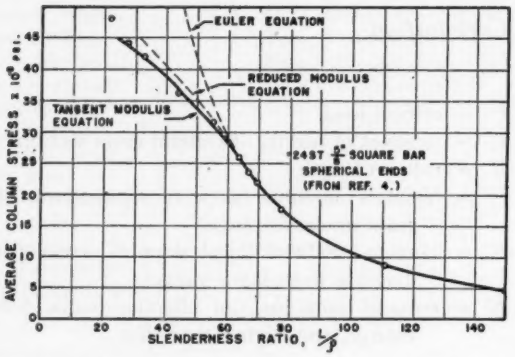

FIG. 2. Column theories and test data (Van den Broek).

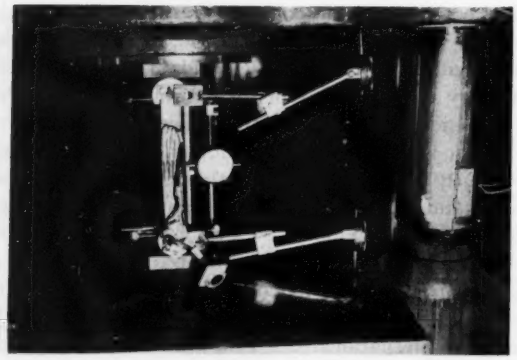

FIG. 3. Pin-end column test arrangement.

"Earlier in 1889 Fr. Engesser presented his tangent-modulus theory, and in 1895 Félix Jasinski ('Noch ein Wort zu den Knickfragen,' *Schweizerische Bauzeitung*, Vol. XXV, No. 25, p. 172, June 22, 1895) pointed out that this theory was not correct and called attention to Considère's work. He stated that at that time it was impossible, however, to determine theoretically the form of the function $\bar{E}$. Thereupon Engesser ('Ueber Knickfragen,' *Schweizerische Bauzeitung*, Vol. XXVI, No. 4, p. 24, July 27, 1895) acknowledged the error in his original theory and replied that the possibility of determining $\bar{E}$ theoretically was in no wise out of the question, and he determined it in the general form. . . . . Nothing further was done apparently until Kármán ('Untersuchungen über Knickfestigkeit,' *Forschungsarbeiten*, Nr. 81, 1910) presented the theory again, added the actual evaluation of $\bar{E}$ for the rectangular cross section and the idealized H-section (consisting of infinitely thin flanges and negligible web), and gave the theory new life by making a series of careful tests designed to afford a check on the theory. Since then $\bar{E}$ has been evaluated for other cross sections by a number of writers."

Although the reduced-modulus (or double-modulus) theory has long been accepted as the exact theory of column action, the simpler tangent-modulus theory has been found to be much easier to use, since it is not affected by the shape of the cross section. Since it gives lower critical loads than the reduced-modulus theory, it is also preferred by engineers on the basis of safety. Finally, test data indicate that the actual buckling loads are usually closer to the tangent-modulus values than to the reduced-modulus values. A typical example is shown in Fig. 1, which is reproduced from reference 3 (tests by the Aluminum Research Laboratories). Reference 4 also shows test data that agree with the Engesser theory. Fig. 2 is based on Fig. 4 of this reference, which includes a number of tests made by Professor Van den Broek.

TEST DATA

In an effort to obtain a clue, the author had a simple test performed by the Lockheed Research Laboratory. A pin-ended 24ST aluminum-alloy column of rectangular cross section (2 by $1^1/_4$ in.) was designed to fail in the plastic range and was equipped with electric strain gages on opposite sides, at the mid-section (Fig. 3). (Details of the test are omitted here but are reported in reference 5.)

The results obtained are plotted in two different ways in Figs. 4 and 5.

Fig. 4 shows that the strain distribution remained substantially constant up to a load of about 40,000 lbs. and then gradually shifted, indicating bending. Up to a load of about 87,000 lbs. there was no strain reversal. Further loading caused strain reversal to take place. At the maximum load of 92,500 lbs., considerable strain reversal had taken place and the axis of rotation of the cross section appeared to be at about one-third of the width of the column.

Fig. 5 shows the strain on opposite sides of the column plotted against load. The slight divergence corresponds to an initial eccentricity of about 0.001 in. If the column were perfect and remained straight up to the reduced-modulus load, the two curves would coincide and would be represented by the dashed line OA. (The upward curvature reflects the shape of the compression stress-strain diagram.) Point B

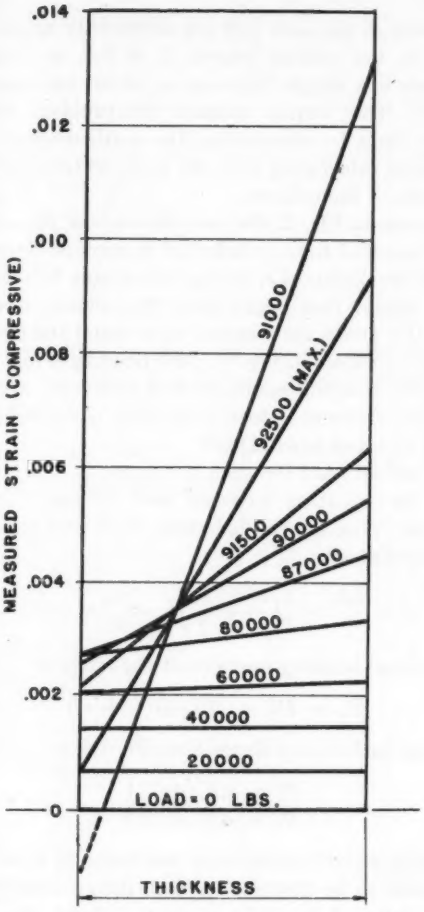

FIG. 4. Strain distribution as determined in a column test.

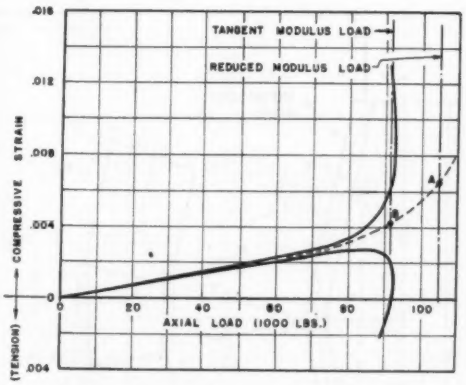

FIG. 5. Strain on opposite faces of column from test data.

represents the upper limit as predicted by the tangent-modulus theory.

Fig. 5 shows that if the column were to remain straight up to the reduced-modulus load there could be no strain reversal below that load. What, then, can supply the extra effective value of E needed to prevent buckling beyond the tangent-modulus load? The obvious answer is that the column cannot remain straight beyond the tangent-modulus load; there must be a definite amount of strain reversal as soon as the load is further increased. This should cause the two curves to separate at point B, one starting downward and the other upward.

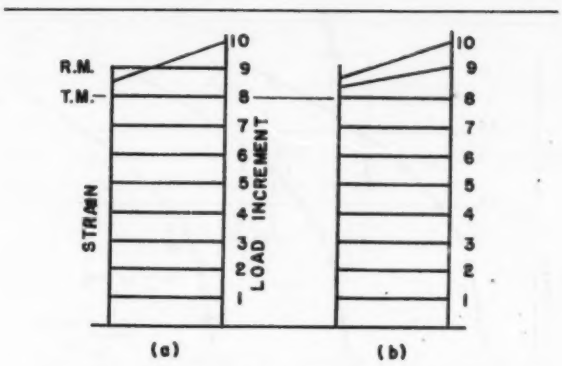

FIG. 6. Alternative types of strain distribution across column cross section.

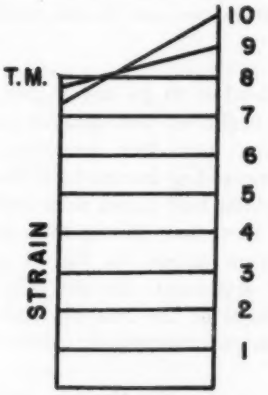

FIG. 7. Type of strain distribution needed to permit loading beyond tangent-modulus load.

It can now be seen that in the derivation of the reduced-modulus theory a questionable assumption was made. It was assumed, by implication at least, that the column remains straight while the axial load is increased to the predicted critical value, *after which* the column bends, or tries to bend. Actually, the column is free to "try to bend" at any time. There is nothing to prevent it from bending *simultaneously* with increasing axial load. Under such a condition it is possible to obtain a nonuniform strain distribution without any strain reversal taking place. The difference between the two assumptions is shown diagrammatically in Fig. 6.

Fig. 6b, however, still represents a paradox. There is no strain reversal indicated; hence, the value of E_t must apply over the entire cross section; therefore, the column load cannot exceed the tangent-modulus

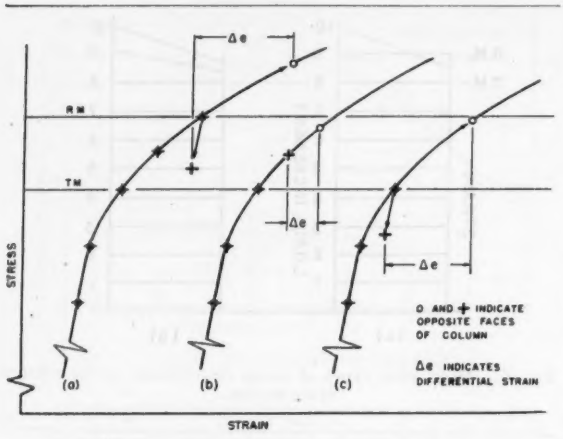

FIG. 8. Alternative types of strain progression.

value. If the load is to go any higher, some strain reversal must begin at the tangent-modulus load. The picture might then look something like Fig. 7, in which each succeeding increment of loading beyond the tangent-modulus load causes some additional strain reversal. The fact that this picture resembles the actual distribution shown in Fig. 4 is significant. (NOTE: These statements do not necessarily apply to the entire *length* of the column, since the ratio of bending moment to axial load varies from end to end.)

Another way to visualize the two different theories is shown in Fig. 8, in which the points represent conditions on opposite edges of the column. In the reduced-modulus theory it is assumed that the points stay together until the critical load is reached (Fig. 8a). Fig. 8b shows that they may separate without involving any strain reversal. Since the average stress in Fig. 8b is greater than that corresponding to the tangent-modulus theory, it represents an impossible condition. Fig. 8c shows what would have to happen if the average stress were to exceed the tangent-modulus value.

On the basis of the foregoing reasoning the author predicted, in reference 1, that (a) bending will begin as soon as the tangent-modulus load is exceeded; (b) the maximum column load will be reached somewhere between the loads predicted by the two theories.

MATHEMATICAL ANALYSIS

In order to prove the last statement, for at least one case, the problem has been greatly simplified by adopting a suggestion made by E. I. Ryder, of the Civil Aeronautics Authority. This consists in working with a two-legged hinged column in which the hinge consists of a unit "cell" formed from two small axial elements. As shown in Fig. 9, the two legs of the column are assumed to be infinitely rigid. If the dimensions of the unit cell are sufficiently small with respect to the column length, L, it can be assumed that there is a simple hinge action about the center of the cell. This device reduces the problem to elementary form by eliminating the mathematical work involved in integrating over the cross section and over the length of the column.

As shown in Fig. 9, the two elements of the column cell are assumed to have deflected in opposite directions through the distances e_1 and e_2, which may be regarded as the strains that occur after the column starts to bend. If e_1 and e_2 are assumed to be equal and opposite in sense (as shown in Fig. 9), pure bending is indicated. This restriction will *not* be applied, however; e_1 and e_2 may have different values, indicating combined bending and variation in axial load.

The critical load for such a column is easily determined by equating external and internal bending moments. The lateral deflection, d, is first expressed in terms of strain:

$$d = \frac{\alpha L}{2} = \frac{1}{2}\left(\frac{e_1}{2} + \frac{e_2}{2}\right)L = \frac{L}{4}(e_1 + e_2) \qquad (4)$$

The external bending moment at the hinge is

$$M_e = Pd = (PL/4)(e_1 + e_2) \qquad (5)$$

The axial load in each flange element, due to bending, is

$$\left.\begin{aligned} P_1 &= e_1 E_1 (A/2) \\ P_2 &= e_2 E_2 (A/2) \end{aligned}\right\} \qquad (6)$$

Note that E_1 and E_2 indicate the value of E which is considered to be effective for each flange element.

The internal bending moment (about the hinge point) may be expressed as

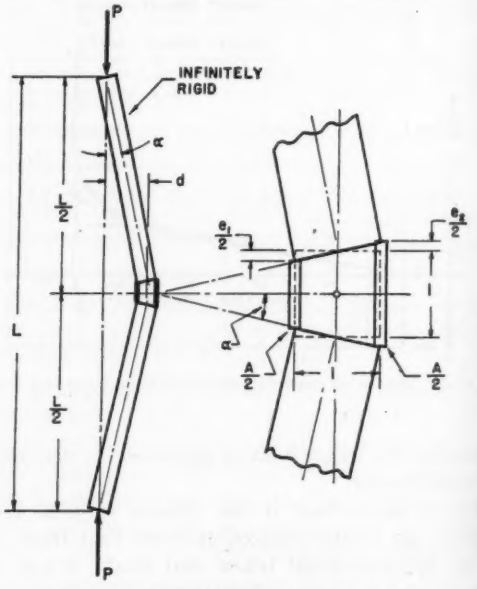

FIG. 9. Simplified two-flange column.

$$M_t = \frac{1}{2}P_1 + \frac{1}{2}P_2 = \frac{1}{2}e_1E_1\frac{A}{2} + \frac{1}{2}e_2E_2\frac{A}{2} = \frac{A}{4}(e_1E_1 + e_2E_2) \quad (7)$$

Equating internal and external bending moments [Eqs. (5) and (7)],

$$(PL/4)(e_1 + e_2) = (A/4)(e_1E_1 + e_2E_2)$$

from which

$$P = (A/L)[(e_1E_1 + e_2E_2)/(e_1 + e_2)] \quad (8)$$

Now in either the Euler or Engesser equations $E_1 = E_2$. Eq. (8) therefore reduces to the following two equations:

$$\text{(Euler)} \qquad P_e = AE/L \quad (9)$$

$$\text{(Engesser)} \qquad P_t = AE_t/L \quad (10)$$

If it is now assumed that element (1) undergoes increasing compressive stress while element (2) has a decreasing compressive stress, E_1 and E_2 may be replaced by E_t and E, respectively.

Let $k = E/E_t$. Then

$$E_1 = E_t$$

$$E_2 = kE_t$$

Substituting in Eq. (8),

$$P = (AE_t/L)[(e_1 + ke_2)/(e_1 + e_2)] \quad (11)$$

This is the same as the Engesser formula except for the added term, which will now be further examined.

From Eq. (4)

$$e_1 + e_2 = 4d/L$$

and

$$e_1 = 4d/L - e_2 \quad (12)$$

Substituting these values in Eq. (11),

$$P = \frac{AE_t}{L}\frac{L\,[(4d/L) - e_2 + ke_2)]}{4d}$$

$$P = \frac{AE_t}{L}\left[1 + \frac{L}{4d}(k-1)e_2\right] \quad (13)$$

Another expression for P may be obtained by assuming that, after the tangent-modulus load is reached, the column load continues to increase. This increase is given by the difference between the element loads P_1 and P_2, which can be expressed, from Eq. (6), as

$$\Delta P = P_1 - P_2 = e_1E_1(A/2) - e_2E_2(A/2)$$

Substituting for E_1 and E_2,

$$\Delta P = (A/2)E_t(e_1 - ke_2)$$

Substituting for e_1,

$$\Delta P = \left(\frac{A}{2}\right)E_t\left(\frac{4d}{L} - e_2 - ke_2\right) = \frac{A}{2}E_t\left[\frac{4d}{L} - (1+k)e_2\right] \quad (14)$$

This value should be added to the tangent-modulus load to obtain the total value for P.

$$P = P_t + \Delta P = \frac{AE_t}{L} + \frac{A}{2}E_t\left[\frac{4d}{L} - (1+k)e_2\right]$$

$$P = \frac{AE_t}{L}\left\{1 + \left[2d - \frac{L}{2}(1+k)e_2\right]\right\} \quad (15)$$

From Eqs. (13) and (15) the following equation can be set up:

$$\frac{L}{4d}(k-1)e_2 = 2d - \frac{L}{2}(1+k)e_2 \quad (16)$$

From this,

$$e_2 = 8d^2/L[k - 1 + 2d(1+k)] \quad (17)$$

Substituting this value of e_2 in Eq. (13),

$$P = \frac{AE_t}{L}\left[1 + \frac{2d(k-1)}{k - 1 + 2d(1+k)}\right] \quad (18)$$

This may be reduced to

$$P = \frac{AE_t}{L}\left(1 + \left\{1\Big/\left[\frac{1}{2d} + \left(\frac{k+1}{k-1}\right)\right]\right\}\right) \quad (19)$$

If the ratio E_t/E is represented by the usual symbol τ, Eq. (19) becomes

$$P = \frac{AE_t}{L}\left(1 + \left\{1\Big/\left[\frac{1}{2d} + \left(\frac{1+\tau}{1-\tau}\right)\right]\right\}\right) \quad (19a)$$

Let

$$R = P/P_t \quad (20)$$

Then, from Eq. (10),

$$R = 1 + \left\{1\Big/\left[\frac{1}{2d} + \left(\frac{k+1}{k-1}\right)\right]\right\} \quad (21)$$

or

$$R = 1 + \left\{1\Big/\left[\frac{1}{2d} + \left(\frac{1+\tau}{1-\tau}\right)\right]\right\} \quad (21a)$$

In Fig. 10, R is plotted against lateral deflection for two different values of τ. [NOTE: Eqs. (18) to (21a) do not apply when $E_t = 0$, since the limiting column load is then determined by the stress at which this occurs.]

It should be noted that Fig. 10 corresponds to the usual plot of column load against lateral deflection. If the tangent modulus had been assumed to decrease with increasing stress (as it usually does), the curves would rise to some maximum value and then start downward again. It is interesting to note that in the very short column range, where the tangent modulus approaches a constant value, test points often lie closer to the reduced-modulus curve than to the tangent-modulus curve.

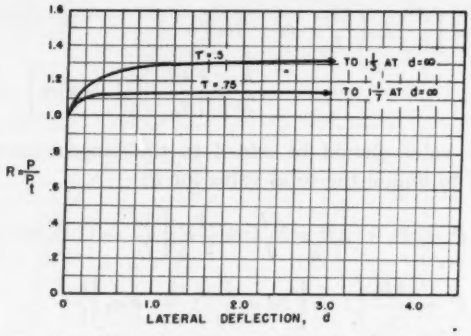

FIG. 10. Variation of column load with lateral deflection, assuming E_t constant.

COMPARISON WITH REDUCED-MODULUS THEORY

The equation for the critical column load will now be derived on the basis of the assumptions originally used in the reduced-modulus theory. It will be assumed that the column remains straight up to the critical load P_r, after which it bends. The derivation proceeds as before, up to and including Eq. (13). Now, instead of assuming that there can be an increase in load, ΔP, it will be assumed that $\Delta P = 0$. Then $P_1 = P_2$ and $E_t e_1 = E e_2$, from which

$$e_2 = e_1(E_t/E) = e_1/k \tag{22}$$

Substituting for e_1 from Eq. (12),

$$e_2 = (1/k)[(4d/L) - e_2]$$

$$e_2 = (4d/L)[1/(1 + k)] \tag{23}$$

Substitution of this value in Eq. (13) yields

$$P_r = (AE_t/L)\{1 + [(k - 1)/(k + 1)]\} \tag{24}$$

Eq. (24) obviously represents the limiting value of Eq. (19) as d approaches infinity. This proves that, for the simplified column, the reduced-modulus theory gives the limiting value for the column load as the lateral deflection approaches infinity, assuming that the value of the tangent modulus, E_t, remains constant.

The actual upper limit for the column load will depend largely on the manner in which E_t varies with increasing strain, as shown by von Kármán.[6] It is important to note, however, that, even for a perfect column, lateral deflection must take place as soon as the tangent-modulus load is exceeded and that the load predicted by the reduced-modulus theory can never be reached, even if there is no dropping off in the tangent modulus with increasing strain.

Eq. (19) represents, for the simplified column and for a constant value of E_t, the complete theory of column action. It includes the Euler equation (when $k = 1$) and the Engesser (tangent-modulus) equation (when $d = 0$) and approaches the reduced-modulus equation as a limit (as $d \to \infty$). It is suggested that an equation of this type be called the *column equilibrium equation* to avoid any question as to the definition of buckling or instability.

VARIATION OF STRAIN WITH LOAD

The equation already derived may be used to find equations for the strains in the two column elements. From Eqs. (21), (12), and (17) the following equations may be derived:

$$e_1 = \frac{2}{L}\left[\frac{k - R}{\left(\frac{k-1}{R-1}\right) - (k+1)}\right] \tag{25}$$

$$e_2 = \frac{2}{L}\left[\frac{R - 1}{\left(\frac{k-1}{R-1}\right) - (k+1)}\right] \tag{26}$$

From these equations it should be possible to obtain a graphical picture of the variation of strain against column load, to compare with the experimental curve of Fig. 5. Since Eqs. (25) and (26) apply only after the column has started to bend, at the load P_t, it is necessary to determine the average compressive strain at the load P_t. The stress, obtained from Eq. (10), is

$$P_t/A = E_t/L$$

The actual strain corresponding to this stress would be obtained from the stress-strain diagram of the material. If the stress were in the elastic range, the strain would be

$$e_t = P/AE = E_t/EL = 1/kL \tag{27}$$

This would be the value of the strain at $R = 1$. (For most materials the strain would actually be considerably higher, but this does not affect the general results.) The additional strain in each element, beyond $R = 1$, will be put in terms of the strain e_t, giving

$$\frac{\Delta e_1}{e_t} = 2\left[\frac{k(k - R)}{\left(\frac{k-1}{R-1}\right) - (k+1)}\right] \tag{28}$$

$$\frac{\Delta e_2}{e_t} = 2\left[\frac{k(R - 1)}{\left(\frac{k-1}{R-1}\right) - (k+1)}\right] \tag{29}$$

These values are plotted in Fig. 11, which represents a typical variation of strain with column load, for a value of $k = 1.333$.

Although Fig. 11 is based on extreme simplification of the problem and does not give a true picture of typical conditions, it has a general resemblance to Fig. 5, which was obtained from actual test data. It is interesting to note that on the concave side of the column the compressive strain increases rapidly after the tangent-modulus load is reached, while on the convex side the strain starts to decrease rather slowly.

The rapid increase of compressive strain which is required to obtain additional load beyond P_t will usually involve a large reduction in E_t. This indicates that in most actual cases the maximum column load will exceed the tangent-modulus load by only a slight amount.

Conclusions

Although the foregoing analysis is based on a hypothetical column that bears little resemblance to an actual column, extension of the theory to the more general case is largely a matter of mathematics. The fundamental principles of column action in the inelastic range will not be changed by such generalization. The following conclusions can therefore be drawn from the analysis of the simplified column:

(1) The tangent-modulus (Engesser) formula gives the maximum load at which an initially straight, centrally loaded column will remain straight.

(2) The column load may exceed the tangent-modulus load but cannot be greater than the reduced-modulus load. (The latter statement has not been proved for the general case.)

(3) Loading beyond the tangent-modulus load will cause bowing, which will produce permanent bending deformation (eccentricity).

(4) There will be some portion of the column cross section for which the stress will never exceed the tangent-modulus stress.

(5) After the tangent-modulus load is exceeded, the compressive strain over a portion of the cross section will increase much more rapidly than the average strain.

(6) For most engineering materials the decrease in tangent modulus with increasing strain will limit the amount by which the column load may exceed the tangent-modulus value.

(7) The idealized simplified column treated in this paper cannot sustain the reduced-modulus load unless the column is laterally supported while the axial load is being applied.

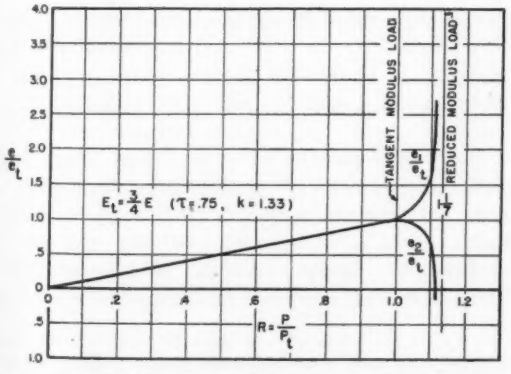

FIG. 11. Calculated strain variation with column load for a hypothetical column.

(8) When supported against bowing during axial loading, a column in the inelastic range will sustain a greater axial load (with support removed) than when loaded without such support.

(9) The tangent-modulus (Engesser) equation should be used as a basis for determining the buckling strength of members in the inelastic range.

In conclusion, it would seem fitting to repeat a statement made by von Kármán[6] to the effect that "Engesser appears to have been the first to recognize properly the nature of 'inelastic buckling.'" It is interesting that aircraft engineers, in seeking greater accuracy in the inelastic range, have gone back to the formula that was first suggested by Engesser over 50 years ago.

References

[1] Shanley, F. R., *The Column Paradox*, Journal of the Aeronautical Sciences, Vol. 13, No. 12, p. 678, December, 1948.

[2] Osgood, Wm. R., *The Double-Modulus Theory of Column Action*, Civil Engineering, Vol. 5, No. 3, pp. 173–175, March, 1935.

[3] Templin, R. L., Sturm, R. G., Hartmann, E. C., and Holt, M., *Column Strength of Various Aluminum Alloys*, Aluminum Research Laboratories Technical Paper 1, Pittsburgh, Aluminum Company of America, 1938.

[4] Van den Broek, J. A., *Column Formula for Materials of Variable Modulus (Developed by the Theory of Limit Design)*, The Engineering Journal (Canada), December, 1945.

[5] Horsfall and Sandorff, Lockheed Aircraft Corporation Report No. 5728, *Strain Distribution during Column Failure*, April, 1946.

[6] von Kármán, Th., *Untersuchungen über Knic festigkeit*, Mitt. u. Forschungsarb. d.V.D.I., Heft 81, Berlin, 1909.

Discussion

Dr. Theodore von Kármán: "The theory of buckling of a column subjected to axial load beyond the limit of elasticity has been discussed by many authors in the last three decades. Most of the objections, however, were not valid. Now Mr. Shanley comes along with an objection that is worthy of consideration.

"Both Engesser's and my own analyses of the problem were based on the assumption that the equilibrium of the straight column becomes unstable when there are equilibrium positions infinitesimally near to the straight equilibrium position under the same axial load. The correct answer to this question is given by replacing, in Euler's equation, Young's modulus by the so-called reduced modulus. Mr. Shanley's analysis represents a generalization of the question. His procedure can be formulated as follows: What is the smallest value of the axial load at which a bifurcation of the equilibrium positions can occur, regardless of whether or not the transition to the bent position requires an increase of the axial load? The answer to this question is that the first equilibrium bifurcation from the straight equilibrium configuration occurs at a load given by the Euler formula when the Young's modulus is replaced by the tangent modulus. In fact, one can construct sequences of equilbrium positions starting from any load between the two limiting values corresponding to the tangent and the reduced moduli. The inclination of the equilibrium lines representing the load as a

function of the deflection is steepest for the line starting from the lower limiting load and becomes zero for the line starting from the upper limiting load. The equilibrium lines have an envelope that starts from the lower limiting load and—at least as long as the stress-strain curve can be considered straight and the deflection small—approaches asymptotically the load computed with the reduced modulus.

"Two aspects of the question are worthy of mention:

"(a) My original analysis, and also Engesser's, is a generalization of the reasoning used in the theory of elastic buckling. Why does this not cover all possible equilibrium positions in the inelastic case? Obviously, it is not because of the nonlinearity of the stress-strain relation in the inelastic range but because of the nonreversible character of the process. There are infinite values of permanent strain which may correspond to the same stress, corresponding to different history of the loading and unloading procedure. Hence, the definition of the stability limit must be revised for nonreversible processes. This necessity was intuitively recognized by Mr. Shanley, which is, I believe, a great merit of his paper.

"(b) Although the Euler formula with the tangent modulus does not, in general, give the maximum axial load to which the column can be subjected without large deflection, it is conservative and therefore advisable to use this formula for practical computation of column loads. As I have shown in my paper of 1909, also the load deflection curve that starts from the upper limiting load in general soon assumes a negative slope. Consequently, it is difficult to determine the actual peak of the axial load. It will certainly be between the two values that correspond to the tangent and the reduced moduli. These two values can be respectively designated as the lower and upper limits of the critical load."

Changes of Address

Since the Post Office Department does not as a rule forward magazines to forwarding addresses, it is important that the Institute be notified of changes in address 30 days in advance of publishing date to ensure receipt of every issue of the JOURNAL and REVIEW.

Notices should be sent directly to:

Institute of the Aeronautical Sciences, Inc.
2 East 64th Street, New York 21, New York

Increasing the Range of Axial-Flow Compressors by Use of Adjustable Stator Blades

JOHN T. SINNETTE, JR.*

National Advisory Committee for Aeronautics

SUMMARY

A theory has been developed for resetting the blade angles of an axial-flow compressor to improve the performance at speeds and flows other than the design values and thus extend the useful operating range of the compressor. The theory is applicable to the resetting of both rotor and stator blades or to the resetting of the stator blades alone and is based on the adjustment of the blade angles to obtain lift coefficients below the stalling point of the blades.

Tests were made on the N.A.C.A. eight-stage axial-flow compressor with three different blade settings:

(1) With the design blade setting.
(2) With the stator blades reset for 75 per cent of design speed and a load coefficient of 0.48.
(3) With the stator blades reset for 75 per cent of design speed and a load coefficient of 0.65.

The test results show that a substantial increase in the useful operating range of axial-flow compressors can be obtained by adjustment of only the stator-blade angles. Considerable improvement in efficiency at compressor speeds appreciably below the design speed was obtained for both stator-blade resettings. Also, a difference of 20 to 30 per cent in the peak-efficiency flows for the two stator-blade resettings was obtained, which at high compressor speeds is about seven times the maximum flow range for any given blade setting.

INTRODUCTION

THE AXIAL-FLOW COMPRESSOR, in spite of the high efficiencies obtainable in modern designs,[1-4] has been somewhat limited in application because of its inherently narrow operating range. The useful flow range of a compressor at a given speed may be limited because of one or more of the following characteristics:

(1) A rapid change in pressure ratio with small change in flow.
(2) A marked drop in the efficiency with changes of flow.
(3) Unstable operation, referred to as "surging," which occurs when the flow is decreased beyond a certain point.

The useful speed range of a compressor may be limited by a marked drop in peak efficiency with change in speed or by a large difference between the peak-efficiency flow and the required flow at speeds appreciably different from the design speed. The explanation of those characteristics that limit the useful operating range of axial-flow compressors is the fact that the angles of attack, and hence the lift coefficients, for some of the blade rows are greatly affected by small changes in flow and speed; some of the blades are therefore operating far from their optimum lift coefficients for speeds and flows appreciably different from the design values.

An obvious remedy for these limitations on the useful range is to change the blade-angle settings with changes in operating conditions to maintain optimum lift coefficients. This method has been successfully employed in extending the high efficiency range of propeller turbines,[5, 6] and tests on axial-flow fans show that a pronounced extension of their flow range can also be obtained by the same method.[7-9] For high-speed multistage compressors, however, the adjustment of the many rows of rotor and stator blades during operation involves mechanical problems of considerable difficulty. The alternative method of adjusting only the stator blades, which is mechanically more feasible, has therefore been given particular consideration in the present investigation.

A general method for calculating blade-angle settings for a wide range of operating conditions has been developed at the Cleveland Laboratory of the N.A.C.A. The method is applicable to the resetting of both rotor and stator blades or to the resetting of stator (or rotor) blades alone and is based on the adjustment of the blade angles to obtain lift coefficients for which the blades will operate efficiently with special attention to the avoidance of blade stalling. The flow is calculated by means of one-dimensional compressible-flow equations using an estimated polytropic exponent, the cross-sectional areas at the stations between each row of blades, and the air turning angle at the mean radius for each row of blades obtained from an empirical equation based on cascade tests.

The calculation method was applied to the resetting of stator-blade angles of the N.A.C.A. eight-stage axial-flow compressor[1, 2] for 75 per cent of design speed and for a series of load coefficients ranging from 0.28 to 0.70. The load coefficient for peak efficiency at the design speed for design blade setting was 0.64. The results of tests on the N.A.C.A. eight-stage axial-flow compressor, with design blade settings and with stator blades reset for 75 per cent of design speed for load coefficients of 0.48 and 0.65, are presented herein.

Received November 26, 1946.

* Section Head, Fundamental Analysis Section, Cleveland Laboratory.

Symbols

The symbols used in this report are defined here in alphabetical order. Quantities that are a function of the radius are assumed to refer to the arithmetic mean radius unless otherwise stated. Where the subscripts are not associated with the main symbol in the definition, the significance of the subscripts is given in the list following the main symbols.

- A = cross-sectional area of passage, sq.ft.
- a = local speed of sound, ft. per sec.
- B = number of blades
- c = blade chord, ft.
- C_L = lift coefficient based on mean relative velocity
- c_p = specific heat at constant pressure, B.t.u. per lb. per °F.
- c_v = specific heat at constant volume, B.t.u. per lb. per °F.
- D/L = profile drag-lift ratio
- g = standard acceleration of gravity, 32.174 ft. per sec. per sec.
- J = mechanical equivalent of heat, 778 ft.lbs. per B.t.u.
- K = constant in empirical relation for turning angle
- m = polytropic exponent for expansion
- m' = polytropic exponent for compression
- M = local Mach Number, V/a or W/a
- n = rotor speed, revolutions per sec.
- p = absolute static pressure, lbs. per sq.ft.
- P = absolute total pressure, lbs. per sq.ft.
- Q = volume rate of flow, cu.ft. per sec.
- Q_1/n = load coefficient, cu.ft. per revolution
- $Q_1/\sqrt{\theta}$ = equivalent volume flow (volume flow corrected to N.A.C.A. standard sea-level temperature of 59°F.), cu.ft. per sec.
- r = radius to blade element, ft.
- R = gas constant, ft.lbs. per lb. per °R.
- t = static temperature, °R.
- T = total temperature, °R.
- u = ratio of rotor velocity to axial component of air velocity, U/v
- U = velocity of rotor ($2\pi rn$) at radius r, ft. per sec.
- U_t/a_1 = compressor Mach Number
- V = absolute air velocity, ft. per sec.
- v = axial component of air velocity, ft. per sec.
- W = air velocity relative to rotor, ft. per sec.
- W_a = air weight flow, lbs. per sec.
- w_i = ratio of absolute whirl component of air velocity at inlet to rotor row of blades to axial component of air velocity
- Δw = ratio of change in whirl component to axial component of air velocity
- w_m = ratio of absolute whirl component of air velocity (based on mean of inlet and outlet velocities of a row of blades) to the axial component of air velocity, $w_i + (\Delta w/2)$
- α = angle of attack measured between blade chord and entering air velocity
- α_0 = angle of attack at zero lift for isolated airfoil
- β = angle between compressor axis and absolute air velocity (referred to hereinafter as "air angle")
- ϕ = angle between compressor axis and air velocity relative to rotor (referred to hereinafter as "relative air angle")
- γ = adiabatic exponent, c_p/c_v
- δ = ratio of inlet-air total pressure P_1 to standard sea-level pressure
- ζ = loss ratio, power loss/power input (for a stage)
- η = blade-profile efficiency for stage, $1 - \zeta$

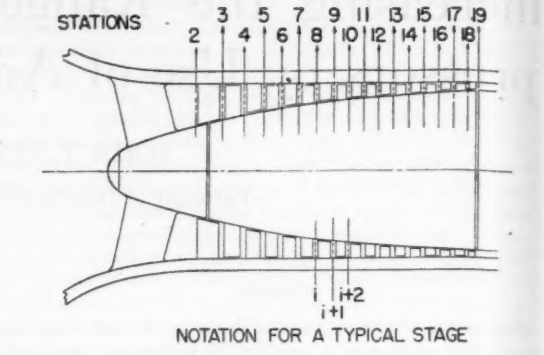

Fig. 1. Station designations used in calculations.

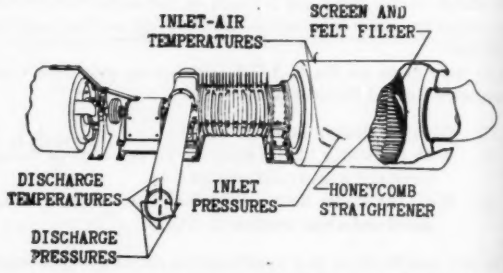

Fig. 2. Compressor setup with lagging removed showing location of pressure- and temperature-measuring stations.

- $\eta_{pol.}$ = polytropic efficiency for expansion
- $\eta_{pol.}'$ = polytropic efficiency for compression
- η_T = adiabatic temperature-rise efficiency, for constant γ,

$$\eta_T = T_1\left[(P_2/P_1)^{(\gamma-1)/\gamma} - 1\right]/(T_2 - T_1)$$

- θ = $T_1/T_{st.}$, ratio of inlet-air total temperature T_1 to N.A.C.A. standard sea-level temperature, $T_{st.}$ = 518.6°R.
- ρ = mass density of air, slugs per cu.ft.
- σ = blade-element solidity, $cB/2\pi r$ at radius r
- ψ = angle between blade chord and axis of compressor

Subscripts

- 1 = ahead of compressor where velocity is negligible (Figs. 1 and 2)
- 2 = directly ahead of entrance guide vanes (Fig. 1)
- 3 = directly ahead of first row of rotor blades (Fig. 1)
- 19 = after last row of stator blades (Fig. 1)
- 20 = measuring station in outlet pipe from compressor (Fig. 2)
- av. = flow average
- i = inlet to a row of stator blades for any stage (i = 4, 6, 8, ...) (Fig. 1)
- $i + 1$ = inlet of following row of rotor blades (Fig. 1)
- k = an integer
- m = mean of inlet and exit values for row of blades
- mr = at mean radius
- R = rotor
- S = stator
- st. = standard
- t = at rotor-blade tip (casing surface)
- w = whirl component

Blade Resetting Theory

Analysis of Problem

The losses in any stage of an axial-flow compressor may be divided into losses resulting from blade-profile drag, blade-end effects, and passage-wall friction. The profile efficiency at any given radius depends on the profile drag-lift ratio and the ratio of the various velocity components as given approximately by the following equation

$$\eta = 1 - \left(\frac{D}{L}\right)_R [1 + (u - w_m)^2] \frac{1}{u} - \left(\frac{D}{L}\right)_S \times ((1 + w^2_m)(\Delta w_S/u\,\Delta w_R) \quad (1)$$

which is essentially the same as Eq. (12) of reference 1 but is generalized to allow for cases where D/L and Δw are different in the rotor and stator blades. It is obvious from this equation that for high profile efficiency it is important to keep $(D/L)_R$ and $(D/L)_S$ small.

The value of D/L depends, among other things, upon the lift coefficient at which the blades are operating and is generally a minimum at a lift coefficient slightly below the stalling point of the blades. When the angle of attack is increased beyond the stalling point, the drag-lift ratio increases rapidly with a corresponding decrease in profile efficiency. In order to obtain good efficiency, it is therefore important to avoid stalling the blades whenever possible. Because of blade-end effects and passage-wall friction, the overall efficiency of a stage will be less than the efficiency based on the profile drag of the blade elements. Inasmuch as tip-clearance losses are proportional to the square of the lift coefficient,[10] the lift coefficient that gives best overall efficiency may be somewhat less than that indicated by profile efficiency; the difference will depend upon blade aspect ratio and blade-tip clearances.

In a well-designed axial-flow compressor, all the blades will operate in the high-efficiency range of lift coefficients at the design operating conditions; at speeds and flows differing appreciably from the design values, however, most of the blades will be operating at unfavorable angles of attack, resulting in large losses. The effects of changes of flow on the angle of attack of a typical stage are shown in Fig. 3. In order to emphasize the main effects of changes of flow, the actual flow conditions have been somewhat simplified; the axial velocity and the radius to the element have been assumed constant throughout the stage. It is evident from Fig. 3 that a decrease in flow results in an increase in the angles of attack of both rotor and stator rows of blades, whereas an increase in flow produces the opposite effect. Either change, if excessive, results in a large increase in the drag-lift ratio and a corresponding decrease in efficiency. This effect of changes of flow on angle of attack is present in all stages of a multistage

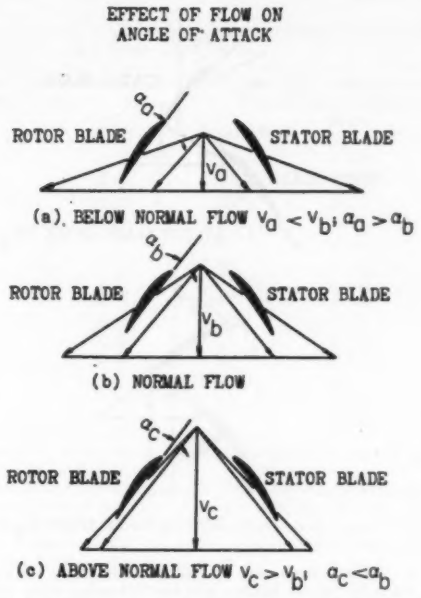

FIG. 3. Effect of flow on angle of attack for a typical stage of an axial-flow compressor.

compressor, but there is an additional effect—namely, that of density changes throughout the compressor—which makes multistage compressors much more critical to changes of flow than single-stage units.

An increase in flow, for example, reduces the angle of attack and, in general, the density rise over a stage. As this decrease in density means that the axial velocity after the stage must increase more than ahead of the stage, the change in angle of attack and density rise in the second stage will be greater than in the first stage. This amplification process continues throughout the compressor, with the result that small changes in flow at the inlet to a compressor may produce extremely large changes in axial velocity and angles of attack in the last stages.

The effect of compressor speed on performance is different in a multistage compressor than in a single-stage unit because the large density changes occurring have a marked effect on the axial-velocity distribution from stage to stage. The ratio of the mean axial velocities v_{i+k}/v_i between any two stations, represented by the subscripts i and $i + k$, is determined by the continuity equation

$$\left(\frac{v_{i+k}}{v_i}\right) = \left(\frac{\rho_i}{\rho_{i+k}}\right)\left(\frac{A_i}{A_{i+k}}\right) \quad (2)$$

In the design of the compressor the ratio of the areas at any two stations is chosen to give the desired velocity ratios at the design operating conditions. Inasmuch as the density ratio depends upon the speed at which the compressor is operating, the velocity ratios and the angles of attack will be correct only for design conditions. From the foregoing discussion it is evident

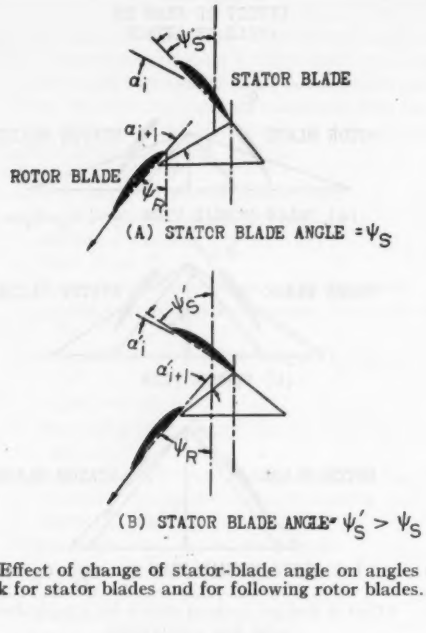

FIG. 4. Effect of change of stator-blade angle on angles of attack for stator blades and for following rotor blades.

that two important factors affecting the performance of a multistage compressor are airflow and compressor speed. Dimensional analysis shows that these factors are satisfactorily represented for a particular compressor by the load coefficient Q_1/n and the compressor Mach Number U_1/a_1.

Control of Lift Coefficients by Blade Resetting

For operation at conditions other than design, the blade angles can be reset to give arbitrary angles of attack for each row of blades at some point along the span of the blade—for example, at midspan; the angles of attack at other radii, however, cannot be arbitrarily chosen because the twist of the blades would have to be changed. The spanwise variation in lift coefficient will depend on the compressor design and on the extent of the deviations from the design blade settings. A general statement of the magnitude of the variations is therefore not possible, but the following factors should be considered in making an estimate: (1) At the compressor inlet, where the hub-tip diameter ratio is usually small and blades are twisted considerably, appreciable changes in the radial variation of the velocity may occur in re-establishing equilibrium when the blade setting is changed; whereas (2) at the compressor outlet, the development of boundary layer along the hub and casing will have an important effect on radial distribution of lift coefficients, with a tendency to load the blades more toward the ends than in the middle. If conservative lift coefficients are chosen at midspan, lift coefficients at other radii should not be excessive and satisfactory efficiencies should be obtainable for moderate deviations from the design operating conditions.

When only the stator blades are reset, it is no longer possible to choose arbitrarily the angle of attack at midspan on both the rotor and the stator blades. The stator-blade angles must be set to keep the lift coefficients on both the rotor and the stator blades within reasonable limits and, in particular, below the stalling points of the blades. The principle underlying the method of adjustment of stator blades alone is that an increase in the blade angle for a given row of stator blades not only reduces the angle of attack, hence, the lift coefficient, on that row of blades but also on the following row of rotor blades (see Fig. 4). Consequently, stalling of either stator blades or rotor blades can be prevented by the adjustment of the proper row of stator blades: in the first case by the adjustment of the row of stator blades that are stalled and, in the second case, by the adjustment of the row of stator blades ahead of the row of stalled rotor blades.

Selection of Lift Coefficients

The lift coefficient at which stalling occurs depends upon many factors, such as blade section, Reynolds Number, solidity, blade-angle setting, and degree of turbulence. Experiments on airfoil cascades with retarded flow[7, 11] indicate that stalling occurs at appreciably lower lift coefficients than for isolated airfoils, but there is some evidence that the lift coefficients at which stalling occurs on compressor blades is higher than for straight cascades.[12] Because of the spanwise variation of lift coefficients and the lack of accurate information on the stalling of compressor blades, it would appear advisable to limit the maximum lift coefficient at midspan to about 0.8.

Special Conditions at Compressor Inlet

The conditions at the compressor inlet are different from those for the typical stage (for the usual design of compressors for high speeds) because the function of the entrance guide vanes differs from that of the typical stator blades. The entrance guide vanes induce an initial whirl to the air in the direction of rotation of the rotor, whereas the typical stator row reduces this whirl component of the air velocity. When the compressor is operating at load coefficients appreciably less than the design value, the angle of attack for the first rotor row becomes excessive. This condition can be somewhat alleviated by increasing the angle of the guide vanes with respect to the axis so as to increase the whirl component of the air entering the first rotor row. Only a limited improvement can be realized by this method for two reasons: (1) Stalling of the guide vanes may result if they are turned through a sufficient angle to prevent stalling of the rotor blades; (2) turning of the guide vanes produces an appreciable shift in the radial distribution of axial velocity, which results in a small change in angle of attack at the tip of the rotor blades for a large change in guide-vane angle. An example of the effect of guide-vane settings on the angles of attack

TABLE 1

Effect of Entrance-Guide-Vane Settings on the Angles of Attack and the Theoretical Lift Coefficients on First Row of Rotor Blades at Different Load Coefficients and Radii for the N.A.C.A. Axial-Flow Compressor

Load Coefficient	Guide-Vane Setting* (Deg.)	Air Angle at Exit of Guide Vanes† (Deg.)	Angle of Attack on First Row of Rotor Blades α_2 (Deg.)			Theoretical Lift Coefficient on First Row of Rotor Blades‡		
			Hub	Mean radius	Tip	Hub	Mean radius	Tip
0.28	27	43	35.1	25.6	13.0	2.15	3.02	3.45
0.28	37	53	32.1	25.0	13.0	1.91	2.91	3.44
0.28	47	63	25.8	23.7	12.8	1.46	2.72	3.37
0.38	27	43	28.1	21.7	10.4	1.62	2.43	2.72
0.38	37	53	22.3	20.4	10.3	1.25	2.25	2.67
0.38	47	63	7.1	17.4	9.6	0.48	1.88	2.49
0.48	37	53	10.3	15.0	7.2	0.62	1.61	1.94
0.48	47	63	−18.6	8.7	5.5	− .42	1.01	1.62
0.48	57	73	−90.5	−34.6	− 3.5	−2.89	−1.33	0.24
0.65	27	43	5.5	9.0	2.3	0.41	1.03	1.05
0.65	37	53	−14.0	3.2	0.7	−0.28	0.57	0.80
0.70	17	33	11.7	9.9	1.6	0.68	1.11	0.93
0.70	27	43	.9	6.3	.6	0.23	0.80	0.78
0.70	37	53	−21.2	− 1.1	− 1.6	−0.50	0.28	0.48

* The guide-vane setting is the angle between the tangent to the concave surface of the vane and the axis of the compressor. Because there is no twist in these vanes, this angle is the same at all radii. The design setting was 27°.

† The air angle behind the guide vanes was experimentally determined for the design setting and was found to be approximately 43° for all radii. Because of the high solidity of the entrance guide vanes, it was assumed that for other settings the change of the air angle from the design value was the same as the change of the guide-vane setting—that is, K in Eq. (6) was assumed equal to 1.0.

‡ The lift coefficients (based on assumption that blades do not stall) are used to indicate the favorable or adverse conditions existing at the entrance to the rotor blades rather than actual lift coefficients that would be expected.

and the lift coefficients at different radii on the first row of rotor blades is shown in Table 1, the values of which were calculated for the N.A.C.A. eight-stage axial-flow compressor by the method given in Appendix I.

For load coefficients appreciably below the design value, it is therefore not generally possible to avoid appreciable losses in the first row of rotor blades by the adjustment of the stator blades alone. The improvement in the performance of the succeeding stages and the shift of the surge limit by the adjustment of the stator blades should, however, make it possible to operate the compressor satisfactorily at lower load coefficients than is possible with the design blade setting.

Mach Number Limitations

When the local relative Mach Number at the entrance to a row of blades appreciably exceeds a certain value, referred to as the critical Mach Number, large compression-shock losses may result. For a given compressor Mach Number U_1/a_1, any change in blade-angle settings will alter the velocity diagrams and, hence, the local Mach Numbers through the compressor. When the compressor is operating near the design speed, the local Mach Numbers on many of the blades will be near the critical values, and changes in blade-angle settings (especially changes that make the velocity diagrams asymmetrical) may cause the critical Mach Numbers on some of the blades to be exceeded. At high compressor speeds, changes in blade angles required to produce large changes in the flow may therefore lead to appreciable compression-shock losses. On the other hand, the useful flow range for a single blade setting may be extremely narrow at these high compressor speeds. Consequently, the extension of useful flow range by using different blade settings may be large compared to the range with a single blade setting. At low compressor speeds, other factors than compression shock will usually determine how much extension of useful flow range is possible by blade adjustment.

Method of Calculation

For the determination of blade resettings for particular operating conditions (given in terms of compressor Mach Number and load coefficient), flow conditions and blade resettings are calculated progressively from the inlet to the outlet of the compressor. The stations at which flow conditions are calculated are taken midway between the various rows of blades, as well as immediately ahead of the entrance guide vanes and after the last row of blades. The station designations used in the presentation are shown in Fig. 1. Unless otherwise stated, all flow conditions and blade angles refer to radii midway between the hub and casing.

Because the entrance guide vanes have a function essentially different from that of the typical row of stator blades, the calculation procedure for the entrance guide vanes is treated separately from that of the typical stage. When the stator blades alone are reset, it is necessary to reset the entrance guide vanes only when the load coefficient for which the blades are reset is appreciably different from the design value. The most desirable guide-vane setting may be determined by calculating the lift coefficient on the first row of rotor blades for several guide-vane settings within the unstalled range of these vanes (see Appendix I). For a typical stage (consisting of a row of stator blades followed by a row of rotor blades), the calculations are carried out for different stator-blade-angle settings

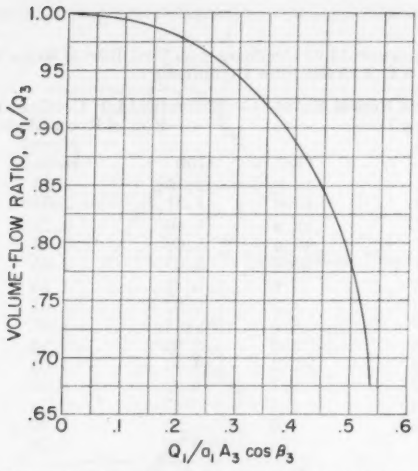

FIG. 5. Determination of volume flow ahead of first rotor row of blades. $\eta_{pol.} = 0.90$.

until satisfactory lift coefficients are obtained on both the stator and the rotor blades.

If both the stator and the rotor blades are to be reset, adjustment of the entrance guide vanes are unnecessary unless it is desired to obtain a more favorable radial distribution of lift or more symmetrical velocity diagram in the first stage. The calculations for the rest of the compressor are then carried out on one row of blades at a time, using several blade angle settings on each row until a satisfactory lift coefficient is obtained on that row.

Calculation Procedure for Entrance Guide Vanes

For any given guide-vane setting, the flow conditions between the entrance guide vanes and the first row of rotor blades (station 3, Fig. 1) are calculated by the following procedure: The value of Q_1/a_1 is determined from the compressor Mach Number U_t/a_1 and the load coefficient Q_1/n or from the flow corrected to standard sea-level temperature $Q_1/\sqrt{\theta}$ or $W_a\sqrt{\theta}/\delta$ by the relations:

$$Q_1/a_1 = (U_t/a_1)\,(Q_1/n)\,(1/2\pi r_t) \tag{3}$$

$$\frac{Q_1}{a_1} = \frac{Q_1}{\sqrt{\gamma g R T_1}} = \frac{1}{\sqrt{\gamma g R T_{st.}}}\frac{Q_1}{\sqrt{\theta}} \tag{4}$$

$$\frac{Q_1}{a_1} = \frac{W_a R T_1}{P_1\sqrt{\gamma g R T_1}} = \frac{\sqrt{R T_{st.}}}{P_{st.}\sqrt{\gamma g}}\frac{W_a\sqrt{\theta}}{\delta} \tag{5}$$

The leaving air angle β_3 from the guide vanes may be determined either from direct tests on the guide vanes or estimated from design data or from cascade tests on similar vanes. If the value of β_3 is known for one guide-vane setting ψ, its value β_3' for any other unstalled setting ψ' can be determined with sufficient accuracy by the empirical relation based on airfoil-cascade tests.

$$\beta_3 - \beta_3' = K\,(\psi - \psi') \tag{6}$$

where K is a constant (depending on the solidity) between 0.9 and 1.0.

The value of Q_3/a_1 is then determined from the following implicit equation [derived in Appendix I as Eq. (38)]:

$$\frac{Q_1}{a_1 A_3 \cos \beta_3} = \frac{Q_3}{a_1 A_3 \cos \beta_3} \times \left[1 - \left(\frac{\gamma - 1}{2}\right)\left(\frac{Q_3}{a_1 A_3 \cos \beta_3}\right)^2\right]^{1/(m-1)} \tag{7}$$

where m is the polytropic exponent which is related to the polytropic expansion efficiency by the equation

$$(m - 1)/m = [(\gamma - 1)/\gamma]\eta_{pol.} \tag{8}$$

The solution of Eq. (7) based on $\eta_{pol.} = 0.90$ is shown in Fig. 5 with Q_1/Q_3 plotted against $Q_1/a_1A_3 \cos \beta_3$. The value of V_3/a_1 is given by

$$V_3/a_1 = (Q_1/a_1 A_3 \cos \beta_3)\,(Q_3/Q_1) \tag{9}$$

and the axial component and whirl component are determined from the relations

$$v_3/a_1 = (V_3/a_1)\cos \beta_3 = Q_3/a_1 A_3 \tag{10}$$

$$V_{w3}/a_1 = (V_3/a_1)\sin \beta_3 \tag{11}$$

The density ratio across the guide vanes is obtained from the continuity relation

$$\rho_3/\rho_1 = Q_1/Q_3 \tag{12}$$

and pressure ratio, temperature ratio, and velocity-of-sound ratio are obtained from the polytropic relations

$$\frac{p_3}{p_1} = \left(\frac{\rho_3}{\rho_1}\right)^m = \left(\frac{t_3}{t_1}\right)^{m/(m-1)} = \left(\frac{a_3}{a_1}\right)^{2m/(m-1)} \tag{13}$$

For convenience of calculation, these four ratios are

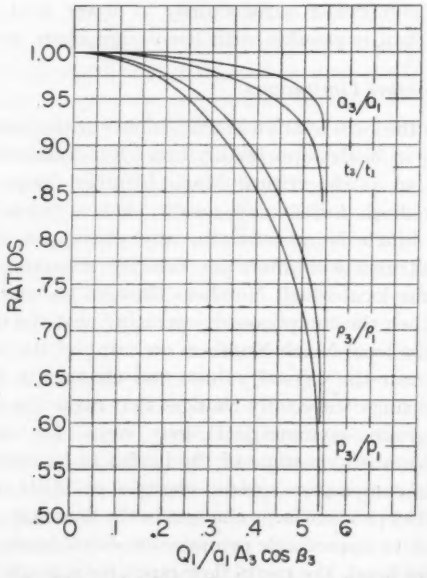

FIG. 6. Determination of pressure ratio, density ratio, temperature ratio, and velocity-of-sound ratio over entrance guide vanes. $\eta_{pol.} = 0.90$.

plotted in Fig. 6 as a function of the variable $Q_1/a_1A_3 \cos \beta_3$ for $\eta_{pol.} = 0.90$.

The whirl component of air velocity relative to the rotor can now be obtained from the relation

$$W_{w3}/a_1 = (U_3/a_1) - (V_{w3}/a_1) \tag{14}$$

The relative air angle and the resultant relative air velocity ahead of the first row of rotor blades can be readily calculated from the two velocity components if the small radial component of velocity is neglected.

Calculation for Typical Stage

The calculation procedure for the first row of rotor blades is essentially the same as that used in a typical stage and need not be presented separately. The special conditions encountered in the first row of rotor blades will be discussed after the general method for a typical stage is presented. A velocity diagram for a typical row of blades (stators) is shown in Fig. 7. The air enters the stator row of blades with a velocity V_i at an angle β_i with respect to the compressor axis. The air in passing through the stator blades is deflected through an angle $\beta_i - \beta_{i+1}$ and leaves the blades with a velocity V_{i+1} at an angle β_{i+1}. The air enters the following row of rotor blades with a velocity relative to the rotor of W_{i+1} at an angle ϕ_{i+1} with respect to the compressor axis and leaves the rotor row with a velocity W_{i+2} at an angle ϕ_{i+2}. The axial component of velocity v is shown in Fig. 7 as increasing from station to station, as is the case in the N.A.C.A. eight-stage axial-flow compressor. The value of U may also be changed slightly from station to station because of the change in mean radius.

In order to obtain the conditions at the exit of a row of blades from the conditions at the entrance to the row, it is necessary to know the angle through which the air is turned while passing through the blades. Cascade tests have indicated that, for solidities in the neighborhood of unity, a good approximation to the turning angle is given by the empirical rule

$$\beta_i - \beta_{i+1} = K(\alpha_i - \alpha_0) \tag{15}$$

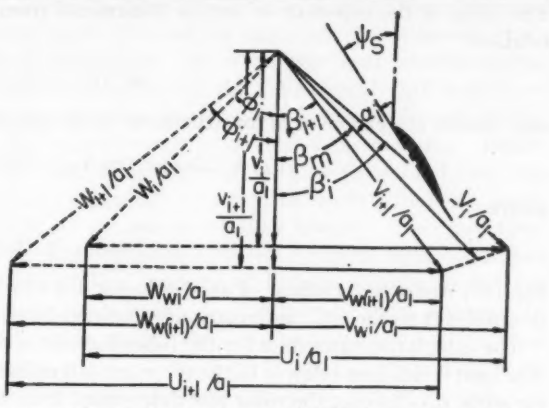

FIG. 7. Velocity diagram for a typical blade row (stator) of an axial-flow compressor.

where K is a constant slightly less than 1 and α_0 is the angle of attack for zero lift for an isolated airfoil. For a solidity of unity, a value of K equal to 0.9 was found satisfactory. Although a value of 0.9 was used with satisfactory results in the resetting of the blades of the N.A.C.A. eight-stage axial-flow compressor, somewhat greater accuracy might be obtained by taking K as a function of the solidity increasing with an increase in solidity. Other empirical relations for turning angle, of course, may be used in place of Eq. (15), or, if sufficient cascade data for the blade-sections used in the compressor are available, the turning angle may be obtained from these data.

The air angle β_{i+1} leaving the stator row can be expressed in terms of β_i, α_0, and ψ_S (Fig. 7) by the use of Eq. (15) and the relation

$$\alpha_i = \beta_i - \psi_S \tag{16}$$

thus obtaining

$$\beta_{i+1} = (1 - K)\beta_i + K\psi_S + K\alpha_0 \tag{17}$$

The corresponding relation for the following row of rotor blades is

$$\phi_{i+2} = (1 - K)\phi_{i+1} + K\psi_R + K\alpha_0 \tag{18}$$

With given stator-blade-angle setting and inlet conditions, the leaving air angle is calculated from Eq. (17) and the value of v_{i+1}/a_1 is determined by a trial-and-error solution of the following equation [derived in Appendix II as Eq. (50)]:

$$\frac{v_i}{a_1} = \frac{v_{i+1}}{a_1}\left(\frac{A_{i+1}}{A_i}\right)\left\{1 + \frac{\gamma - 1}{2}\left(\frac{a_1}{a_i}\right)^2\left[\frac{(v_i/a_1)^2}{\cos^2 \beta_i} - \frac{(v_{i+1}/a_1)^2}{\cos^2 \beta_{i+1}}\right]\right\}^{1/(m'-1)} \tag{19}$$

Inasmuch as v_{i+1}/a_1 will be nearly equal to v_i/a_1, a satisfactory approximation can usually be obtained by a few trials. The density ratio ρ_{i+1}/ρ_1 is determined in carrying out the foregoing approximations and is equal to the expression in the braces raised to the indicated power in Eq. (19). The pressure ratio, temperature ratio, and velocity of sound ratios are determined from the polytropic relations

$$p_{i+1}/p_i = (\rho_{i+1}/\rho_i)^{m'} = (t_{i+1}/t_i)^{m'/(m'-1)} = (a_{i+1}/a_i)^{2m'/(m'-1)} \tag{20}$$

The value of the exponent m' can be determined from the estimated polytropic efficiency of compression by the relation

$$m'/(m' - 1) = [\gamma/(\gamma - 1)]\, \eta_{pol.} \tag{21}$$

and (unlike the exponent m for expansion) is greater than γ. The lift coefficient is calculated from the relation[1]

$$C_L = (2\Delta w/\sigma) \cos \beta_m = (2/\sigma)\, (\tan \beta_i - \tan \beta_{i+1}) \cos \beta_m \tag{22}$$

where

$$\tan \beta_m = (\tan \beta_i + \tan \beta_{i+1})/2 \tag{23}$$

Eq. (23) neglects variations of axial velocity and effect of drag, but, because of uncertainties regarding the most desirable lift coefficient, this equation is considered adequate.

The calculation procedure for the following row of rotor blades is essentially the same as for the stator blades. The inlet conditions relative to the rotor are determined from the conditions leaving the stator row and the relative air angle ϕ_{i+2} leaving the rotor row determined from Eq. (18). The value of v_{i+2}/a_i is then determined from the equation [derived in Appendix II as Eq. (51)]:

$$\frac{v_{i+1}}{a_1} = \frac{v_{i+2}}{a_1}\left(\frac{A_{i+2}}{A_{i+1}}\right)\left\{1 + \frac{\gamma - 1}{2}\left(\frac{a_1}{a_{i+1}}\right)^2\left[\frac{(v_{i+1}/a_1)^2}{\cos^2 \phi_{i+1}} - \frac{(v_{i+2}/a_1)^2}{\cos^2 \phi_{i+2}} + \left(\frac{U_{i+2}}{a_1}\right)^2 - \left(\frac{U_{i+1}}{a_1}\right)^2\right]\right\}^{1/(m'-1)} \tag{24}$$

and the lift coefficient is calculated from the equations analogous to Eqs. (22) and (23), with the air angles relative to the rotor replacing those relative to the stator.

Special Conditions for First Row of Rotor Blades

When only the stator blades are reset, conditions are somewhat different for the first row of rotor blades than for a typical stage, because, as has already been pointed out, it is not practical to control the lift coefficients on the first row of rotor blades to an appreciable extent by the adjustment of the entrance guide vanes. Consequently, when the stator blades are reset for a load coefficient considerably below the design value, the first row of rotor blades will be stalled and the method presented here will not be accurate for that row of blades. The actual turning angle and density rise will be less and the axial velocity leaving the blades higher than calculated. At a somewhat lower inlet airflow, however, the axial velocity and the air angle leaving the following row of stator blades (station 5, Fig. 1), and, hence, the flow conditions in the subsequent stages, should be substantially correct as calculated. Somewhat higher accuracy, of course, could be obtained by basing the turning angle and density rise for the first row of rotor blades on cascade tests under similar stalled conditions.

Application and Test of Theory

Calculation of Stator-Blade Resettings for N.A.C.A. Eight-Stage Axial-Flow Compressor

The preceding theory has been used to calculate stator-blade resettings for the N.A.C.A. eight-stage axial-flow compressor[1,2] for 75 per cent of design speed for a number of different load coefficients ranging from 0.28 to 0.70. The results of these calculations are summarized in Table 2. The blade resettings were calculated for load coefficients appreciably less than the design value of 0.64, because computations indicated that for certain practical gas-turbine applications the compressor would have to operate at appreciably reduced load coefficients at speeds below the design. The design theory, the theory of operation, and the complete details of construction of the N.A.C.A. eight-stage axial-flow compressor (Fig. 8) are given in reference 1.

The changes of blade angles from the design settings are extremely large in some cases, amounting to approximately 36° for the first four stator rows at the lowest load coefficient calculated. (See Table 2 at a load coefficient of 0.28.) Changes required are fairly large for all resettings (over 20° for some of the rows) because the speed for which the blades were reset was appreciably below the design speed.

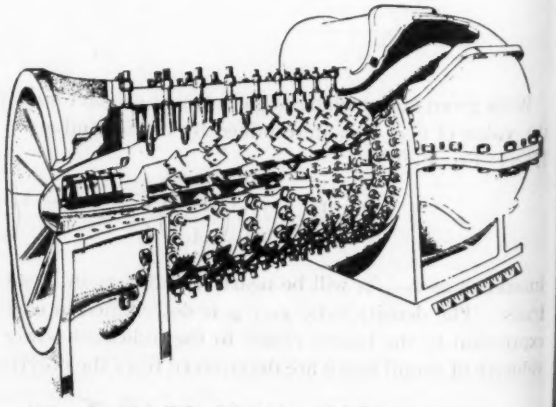

FIG. 8. N.A.C.A. eight-stage axial-flow compressor.

TABLE 2

Summary of Calculations on Resetting of Stator Blades of N.A.C.A. Eight-Stage Axial-Flow Compressor for 75 Per Cent of Design Speed

Blade Row	Blade Angle at Midspan (Deg.)	Increase of Blade Angle over Design Angle (Deg.)	Lift Coefficient at Midspan	Static-Pressure Ratio at Midspan	Diffusion Velocity Ratio at Mean Radius	M Ahead of Blade Row at Mean Radius	U/a
Load coefficient, 0.28							
Entrance vanes	37.0	10	1.08	0.985	1.88	0.07	...
First rotor*	55.4	0	2.91	1.143	0.28	0.48	7.3
First stator	84.9	35.9	0.28	1.013	0.95	0.49	7.2
Second rotor	47.9	0	0.80	1.014	0.81	0.16	6.7
Second stator	83.1	35.6	0.38	1.028	0.91	0.52	6.3
Third rotor	45.3	0	0.80	1.014	0.82	0.18	5.8
Third stator	80.6	35.3	0.42	1.035	0.89	0.53	5.4
Fourth rotor	43.1	0	0.77	1.014	0.84	0.21	5.0
Fourth stator	77.3	35.0	0.42	1.044	0.86	0.54	5.0
Fifth rotor	42.3	0	0.72	1.015	0.83	0.24	4.3
Fifth stator	73.3	30.7	0.48	1.051	0.84	0.53	4.0
Sixth rotor	41.6	0	0.71	1.018	0.83	0.28	3.7
Sixth stator	68.2	28.1	0.55	1.054	0.83	0.53	3.4
Seventh rotor	40.1	0	0.71	1.020	0.84	0.32	3.1
Seventh stator	63.2	25.5	0.53	1.057	0.81	0.53	2.9
Eighth rotor	37.7	0	0.71	1.029	0.78	0.35	2.8
Eighth stator	56.9	19.4	0.70	1.091	0.69	0.53	2.8
Load coefficient, 0.38							
Entrance vanes	37.0	10.0	1.08	0.975	1.89	0.10	...
First rotor*	55.4	0	2.25	1.114	0.41	0.45	5.3
First stator	79.2	30.2	0.32	1.015	0.94	0.46	5.2
Second rotor	47.9	0	0.83	1.019	0.80	0.22	4.9
Second stator	46.7	29.2	0.47	1.035	0.87	0.50	4.6
Third rotor	45.3	0	0.79	1.019	0.82	0.24	4.3
Third stator	73.1	27.9	0.51	1.041	0.86	0.51	4.0
Fourth rotor	43.1	0	0.74	1.019	0.85	0.27	3.7
Fourth stator	67.9	25.6	0.55	1.055	0.82	0.52	3.4
Fifth rotor	42.3	0	0.73	1.025	0.82	0.32	3.2
Fifth stator	62.0	19.4	0.62	1.059	0.79	0.51	3.0
Sixth rotor	41.6	0	0.71	1.029	0.82	0.36	2.8
Sixth stator	55.1	15.0	0.69	1.058	0.79	0.51	2.6
Seventh rotor	40.1	0	0.71	1.034	0.83	0.41	2.4
Seventh stator	48.4	10.7	0.68	1.061	0.79	0.51	2.3
Eighth rotor	37.7	0	0.72	1.051	0.77	0.45	2.2
Eighth stator	45.2	7.7	0.70	1.078	0.72	0.52	2.2
Load coefficient, 0.48							
Entrance vanes	47.0	20.0	1.37	0.926	2.60	0.12	...
First rotor*	55.4	0	1.00	1.041	0.74	0.33	3.0
First stator	69.5	20.5	0.46	1.024	0.88	0.43	3.8
Second rotor	47.9	0	0.80	1.029	0.80	0.31	3.6
Second stator	65.7	18.2	0.62	1.044	0.82	0.48	3.4
Third rotor	45.3	0	0.80	1.031	0.81	0.34	3.2
Third stator	60.0	14.7	0.70	1.054	0.80	0.49	3.0
Fourth rotor	43.1	0	0.79	1.036	0.82	0.38	2.8
Fourth stator	52.1	9.8	0.77	1.065	0.76	0.50	2.6
Fifth rotor	42.3	0	0.78	1.048	0.79	0.44	2.5
Fifth stator	46.9	4.3	0.75	1.060	0.78	0.50	2.3
Sixth rotor	41.6	0	0.68	1.045	0.83	0.47	2.2
Sixth stator	41.1	.9	0.73	1.049	0.82	0.50	2.0
Seventh rotor	40.1	0	0.61	1.042	0.86	0.51	1.9
Seventh stator	33.3	− 4.4	0.71	1.050	0.83	0.52	1.8
Eighth rotor	37.7	0	0.62	1.071	0.80	0.56	1.7
Eighth stator	31.4	− 6.1	0.70	1.068	0.77	0.53	1.7
Load coefficient, 0.65							
Entrance vanes	27.0	0	0.82	0.948	1.57	0.17	...
First rotor*	55.4	0	1.04	1.069	0.72	0.45	3.0
First stator	55.6	6.7	0.60	1.025	0.86	0.40	2.9
Second rotor	47.9	0	0.84	1.047	0.78	0.40	2.8
Second stator	53.7	6.2	0.70	1.041	0.82	0.45	2.6
Third rotor	45.3	0	0.72	1.039	0.84	0.42	2.5
Third stator	48.5	3.2	0.70	1.042	0.83	0.48	2.3
Fourth rotor	43.1	0	0.63	1.036	0.87	0.45	2.2
Fourth stator	40.4	− 1.9	0.70	1.047	0.83	0.49	2.0
Fifth rotor	42.3	0	0.57	1.043	0.87	0.51	1.9
Fifth stator	33.1	− 9.6	0.70	1.041	0.86	0.50	1.8
Sixth rotor	41.6	0	0.51	1.043	0.89	0.57	1.7
Sixth stator	24.9	−15.2	0.70	1.028	0.91	0.52	1.5
Seventh rotor	40.1	0	0.47	1.045	0.91	0.64	1.4
Seventh stator	15.5	−22.2	0.70	1.025	0.93	0.56	1.3
Eighth rotor	37.7	0	0.52	1.115	0.81	0.73	1.3
Eighth stator	14.5	−23.1	0.70	1.053	0.86	0.57	1.3
Load coefficient, 0.70							
Entrance vanes	27.0	0	0.82	0.939	1.58	0.18	...
First rotor	55.4	0	0.81	1.055	0.79	0.44	2.8
First stator	52.7	3.7	0.50	1.017	0.90	0.39	2.7
Second rotor	47.9	0	0.70	1.042	0.83	0.42	2.5
Second stator	48.5	1.0	0.70	1.037	0.83	0.45	2.4
Third rotor	45.3	0	0.65	1.040	0.86	0.45	2.3
Third stator	42.8	− 2.5	0.70	1.038	0.85	0.48	2.1
Fourth rotor	43.1	0	0.58	1.037	0.89	0.50	2.0
Fourth stator	34.2	− 8.2	0.70	1.041	0.85	0.50	1.8
Fifth rotor	42.3	0	0.52	1.046	0.88	0.56	1.7
Fifth stator	26.4	−16.3	0.70	1.034	0.89	0.52	1.6
Sixth rotor	41.6	0	0.47	1.046	0.91	0.63	1.5
Sixth stator	18.0	−22.1	0.70	1.017	0.95	0.54	1.4
Seventh rotor	40.1	0	0.45	1.052	0.82	0.72	1.3
Seventh stator	8.6	−29.1	0.70	1.009	0.98	0.59	1.2
Eighth rotor	37.7	0	0.50	1.115	0.80	0.83	1.2
Eighth stator	8.6	−28.9	0.70	1.045	0.89	0.60	1.2

* The calculations are based on the assumption that the blades do not stall. For the first row of rotor blades, where a high lift coefficient is sometimes obtained by the calculation method presented herein, the blades would probably stall, making the actual lift coefficient and pressure ratio considerably less than the values indicated for this row of blades.

The most favorable flow conditions at the compressor inlet were obtained for the blade resettings for high-load coefficients. At the lower load coefficients the angles of attack and the "theoretical" lift coefficients were excessively high on the first row of rotor blades, which should result in stalling of these blades. Different entrance-guide-vane settings were tried, but the improvement was found to be small (Table 1), especially at the tips of the rotor blades. The most desirable entrance-guide-vane setting under these conditions is uncertain. Because of increased losses in the entrance guide vanes resulting from large increases in guide-vane angles, the increase over design setting was limited to 20°. This large increase in guide-vane angle was used only for a load coefficient of 0.48, because the improvement in rotor-blade conditions at lower-load coefficients appeared to be so slight that increasing the guide-vane losses by large changes in the guide-vane settings was hardly warranted.

Not only is the angle of attack on the first row of rotor blades excessively high for blade resettings for low load coefficients but the relative Mach Number at the entrance to these blades increases as the load coefficient decreases because of the small whirl component of velocity produced by the entrance guide vanes. Inasmuch as the critical Mach Number is low for high angles of attack, large compression shock losses may also occur at the low load coefficients even when the compressor is operating at only 75 per cent of design speed. Because of the uncertainty regarding the losses through the first row of rotor blades, it is difficult to estimate the overall performance that might be expected from the compressor with the stator blades reset for low load coefficients.

The maximum practicable load coefficients for resetting stator blades appear to be determined principally by the relative Mach Number on the last row of rotor blades. At a load coefficient of 0.70 (Table 2) the relative Mach Number at the entrance to the last rotor is 0.83, which should be appreciably above the critical Mach Number for these blades even for the low lift coefficient of 0.50.

Tests with Design Blade Settings and with Two Stator-Blade Resettings

The effect on the performance of an axial-flow compressor of resetting the stator blades according to the theory presented was determined by comparing the performance of the N.A.C.A. eight-stage axial-flow compressor with the design blade setting and with the stator blades reset for 75 per cent of design speed for load coefficients of 0.48 and 0.65 (Table 2). The original blading for this compressor[1] was modified to improve the strength. The principal changes were that the rotor blades were tapered in thickness, larger fillets were used, and a semicircular cut was made at the root of the overhanging portion of the blade (Fig. 9). Modification of the original blading as used in the present

FIG. 9. Construction of modified rotor blades used in present tests.

FIGS. 10

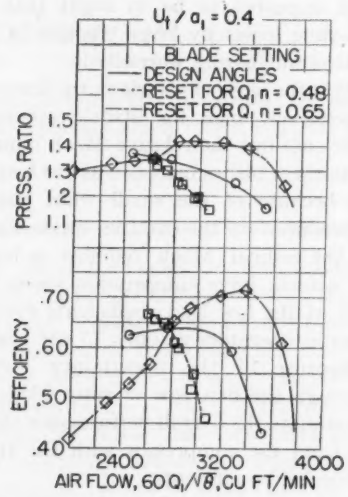

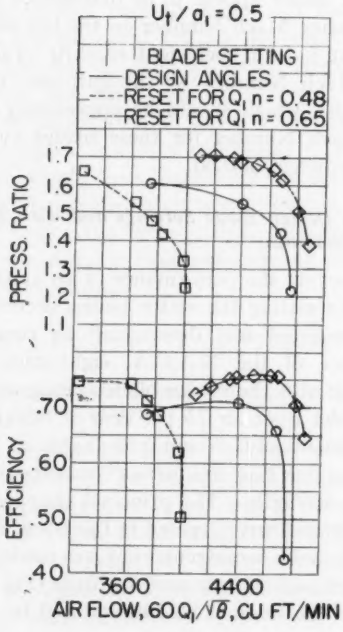

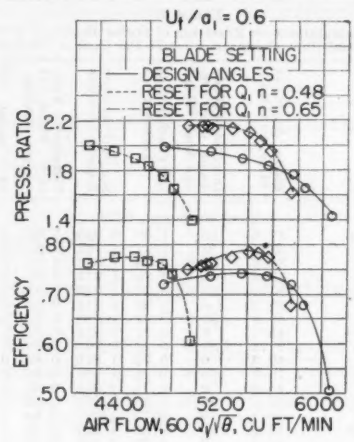

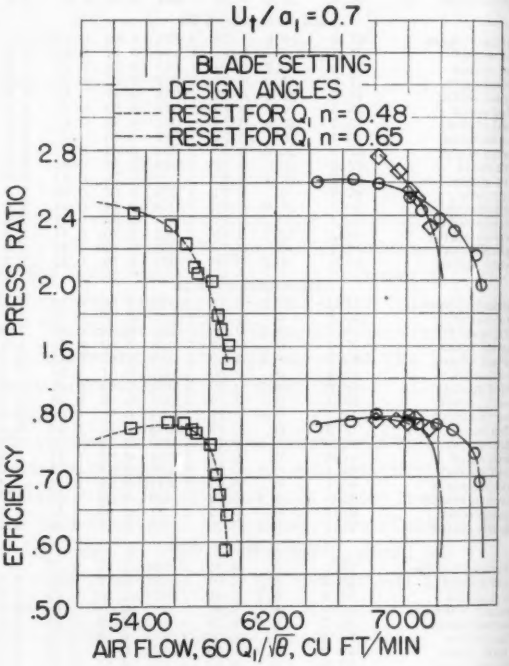

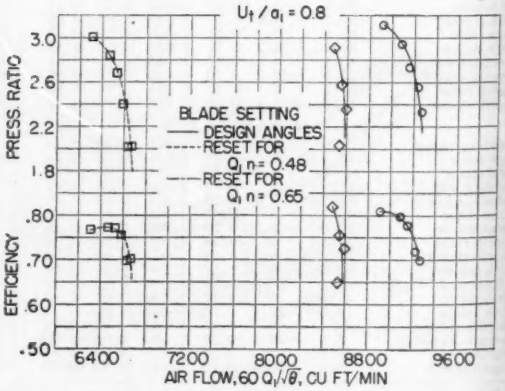

FIGS. 10. Comparison of performance characteristics of N.A.C.A. axial-flow compressor with design blade setting and with two stator-blade resettings for 75 per cent of design speed.

tests are described in reference 2. The test setup and principal instrumentation are shown in Fig. 2. Tests were conducted over a range of compressor Mach Numbers from 0.2 to 0.8; the design Mach Number of 0.968 was therefore not reached in the present tests. Because of limitations of power and outlet-air temperature at high speeds, the tests were run with an inlet-air pressure of 10.16 in. of mercury absolute (corresponding to a pressure altitude of 27,000 ft.) and an inlet-air temperature of 0°F. At Mach Numbers of 0.2 and 0.3 with design blade settings, it was impossible to throttle the inlet air to the desired pressure and still cover the normal flow range of the compressor because of imperfect fitting of the inlet throttle. These data are not presented here because other tests have indicated that inlet conditions have a large effect on compressor performance at these speeds. The inlet throttle was modified when the stator blades were reset so that the subsequent tests could be run at the selected inlet pressure.

At the high speeds, the flow ranges for each compressor Mach Number were selected by starting with a low pressure ratio and progressively decreasing the flow until a definite surge occurred. At a compressor Mach Number of 0.8, however, the compressor was not surged except for the first blade resetting (load coefficient 0.48) because of power limitation. At the lower compressor speeds, where no definite surging occurred, the flow was decreased as far as possible by closing the inlet throttle.

A comparison of the performance characteristics for the different blade settings is shown in Fig. 10. Fig. 11 presents a comparison of the peak adiabatic temperature-rise efficiencies, the peak pressure ratios, and the load coefficients at the peak-efficiency points for the three blade settings as a function of the compressor Mach Number.

The effect on the useful flow range is striking at the higher compressor speeds, as is shown in Fig. 10 for $U_t/a_1 = 0.8$. At this compressor speed the useful flow range is small for a single blade setting. By using different stator blade settings it is possible to increase the useful flow range some seven-fold and still maintain high efficiency. At lower compressor speeds, the flow range for a given blade setting is much greater, so that the extension produced by different blade settings is less striking although still significant.

For both stator-blade resettings, appreciable increases in peak efficiencies were obtained over those with design angles at compressor Mach Numbers below that for which the blades were reset (Figs. 10 and 11), and the peak-efficiency curves are much flatter over the range of Mach Numbers from 0.4 to 0.8. This shift of the high-efficiency range to lower compressor Mach Numbers was expected because the blades were reset for 75 per cent of the design compressor Mach Number. At the Mach Number for which the blades were reset, however, the three different blade settings gave about

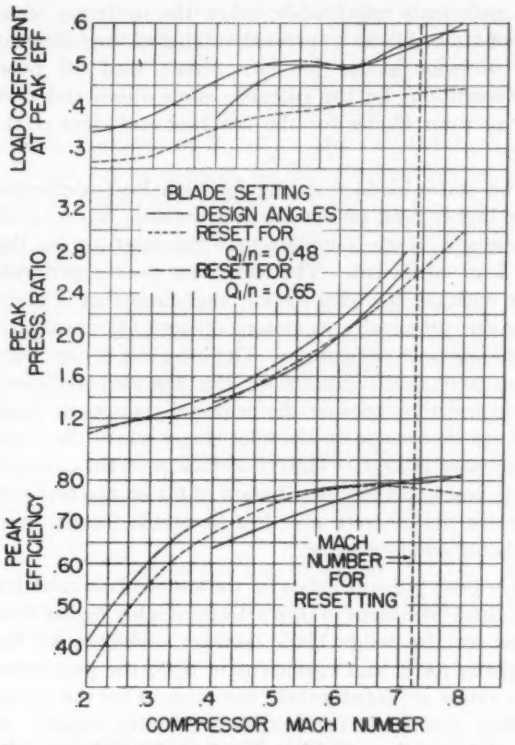

FIG. 11. Comparison of peak-performance characteristics of N.A.C.A. axial-flow compressor with design blade setting and with two stator-blade resettings for 75 per cent of design speed.

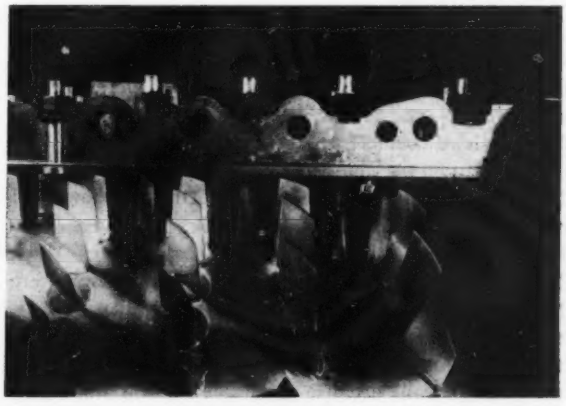

FIG. 12. Close-up of N.A.C.A. axial-flow compressor showing effect of blade-angle resetting on clearances at tips of stator blades. Clearances increased at trailing edge, decreased at leading edge.

the same efficiency. At this compressor speed the slight gain that might have been expected from somewhat more favorable lift coefficients was counteracted by other unfavorable factors, such as: (1) rather large deviations from a symmetrical velocity diagram (Table 2), (2) increase in blade-tip clearances (Fig. 12) and poor fairing of the blade bases with the casing resulting from changes of blade setting, (3) necessity for using

lift coefficients appreciably below the optimum on a row of stator blades to prevent stalling of the following row of rotor blades (or vice versa), and (4) poor flow conditions for the entrance guide vanes and first row of rotor blades for the low load-coefficient resetting.

The stator-blade resetting for high load coefficient gave higher peak efficiencies and pressure ratios at all compressor Mach Numbers than the resetting for the low load coefficient. The somewhat poorer performance with the resetting for low load coefficient is probably due principally to factors (2) and (4) mentioned in the previous paragraph. The increases in tip clearances were much greater for the low-load-coefficient blade resetting, because the principal changes in blade settings were made on the inlet stages where the taper of the rotor is large. The lift coefficient on the entrance guide vanes and the distribution of lift on the first row of rotor blades were also less favorable for the low-load-coefficient resetting.

The peak pressure ratios for the stator-blade resetting for a load coefficient of 0.65 are appreciably higher than those for the design blade settings; whereas for the resetting for a load coefficient of 0.48, the peak pressure ratios are substantially the same as for the design setting over most of the Mach Number range. At compressor Mach Number of 0.8, peak pressure ratios were not reached with the design blade setting and with the resetting for a load coefficient of 0.65 because of power limitations.

The tests with the two stator-blade resettings also show that a substantial change in the peak-efficiency flow at a given speed can be obtained by changing the stator-blade settings. With the stator-blade resetting for high load coefficient, the peak-efficiency flows were about 20 to 30 per cent greater over the range of Mach Numbers tested than with the resetting for low load coefficient. For both stator-blade resettings, the load coefficient obtained at the compressor Mach Number for which the blades had been reset were lower than calculated. The differences may be attributed to several assumptions made in the calculation, especially the neglect of retardation of flow along the passage walls because of surface friction and blade-end losses. The test results indicate that the calculated flow should be multiplied by a flow coefficient between 0.85 and 0.90 to obtain the actual flow.

Conclusions

By the adjustment of only the stator-blade angles, substantial improvement of the peak efficiencies can be obtained at speeds below the design speed; by the use of different blade settings, the flows for peak efficiency can be varied so as to extend greatly the useful flow range of the compressor.

Appendix I
Entrance-Guide-Vane Calculations

An exact calculation of the flow at all radii throughout a multistage compressor, which involves problems of considerable difficulty, has not been attempted in the calculation procedure. For the entrance guide vanes, however, more detailed calculations of the flow conditions at different radii have been made because the small value of the hub-tip diameter ratio at the compressor inlet makes the radial distribution especially important here.

Velocity Distribution After Entrance Guide Vanes

An approximation of the radial distribution of air velocity and velocity components behind the guide vanes can be obtained if it is assumed that radial equilibrium has been established at this point (station 3, Fig. 1). Although this assumption is not strictly true because, in general some radial flow will exist at this station, the assumption should give a better approximation than the assumption of constant axial velocity at all radii. The condition for radial equilibrium is

$$\partial p/\partial r = \rho V_w^2/r \tag{25}$$

For the present calculation, losses through the entrance guide vanes will be neglected in order that Bernoulli's equation

$$^1/_2\, V^2 + \int dp/\rho = K \tag{26}$$

with the same constant at all radii can be used. This equation can then be differentiated with respect to r, which gives

$$V(\partial V/\partial r) + (1/\rho)(\partial p/\partial r) = 0 \tag{27}$$

The whirl velocity component in Eq. (25) can be eliminated by the relation

$$V_w = V \sin \beta \tag{28}$$

and the pressure can be eliminated by use of Eq. (27) to obtain

$$-(1/V)\,(\partial V/\partial r) = \sin^2 \beta/r \tag{29}$$

which, when integrated with respect to the radius, gives

$$\log_e (V_t/V) = -\int_r^{r_t} (\sin^2\beta/r)dr \tag{30}$$

The indicated integration can then be carried out if β is known as a function of r. For compressors in which β is constant with respect to the radius, as is approximately the case with the N.A.C.A. eight-stage axial-flow compressor, Eq. (30) can be directly integrated to obtain

$$V/V_t = (r/r_t)^{-\sin^2\beta} \tag{31}$$

Eq. (30) gives the distribution of the resultant velocity as a function of the radius. The distribution of the whirl component and the axial component of velocity

can also be readily obtained when β is known as a function of the radius.

Mean Velocity Behind Guide Vanes

The continuity equation applied to the flow between stations 1 and 3 (Fig. 1) can be written

$$\int \rho_1 v_1 2\pi r dr = \int \rho_3 v_3 2\pi r dr \tag{32}$$

where the integrations are made over the flow passages at these two stations. Because station 1 is chosen where the cross-sectional area is large and the velocity negligible, and the fluid is assumed to be homogeneous, the density at station 1 is constant, and the first integral can be replaced by $\rho_1 Q_1$. The right side of Eq. (32) can be expressed

$$\int \rho_3 v_3 2\pi r dr = \rho_{3\,av.} \int v_3 2\pi r dr = \rho_{3\,av.} Q_3 \tag{33}$$

where $\rho_{3_{av.}}$ is the flow-average density. Eq. (32) then becomes

$$Q_3 = Q_1 (\rho_1/\rho_{2\,av.}) \tag{34}$$

The condition for constant total enthalpy between stations 1 and 3 can be written (assuming V_1 to be negligible)

$$1 - (t_3/t_1) = V_3^2/2gJc_p t_1 \tag{35}$$

By use of the polytropic relation between temperature and density, the perfect-gas laws, and the relation for the velocity of sound, the following density ratio is obtained

$$\rho_3/\rho_1 = \left\{1 - [(\gamma - 1)/2]\,(V_3/a_1)^2\right\}^{1/(m-1)} \tag{36}$$

If this equation is applied at the mean radius and if the density at the mean radius is assumed to be equal to flow-average density, Eq. (36) can be substituted in Eq. (34), giving

$$Q_1 = Q_3\left[1 - \left(\frac{\gamma - 1}{2}\right)\left(\frac{V_3}{a_1}\right)^2_{mr}\right]^{1/(m-1)} \tag{37}$$

Hereinafter, the mean radius subscript *mr* will be omitted and all quantities will refer to the mean radius unless otherwise indicated.

If the axial velocity at the mean radius $V_3 \cos \beta_3$ is assumed to be equal to the average axial velocity Q_3/A_3, then V_3/a_1 may be replaced by $Q_3/a_1A_3 \cos \beta_3$. If this substitution is made and Eq. (37) is divided by $a_1A_3 \cos \beta_3$, the following relation is obtained

$$\frac{Q_1}{a_1A_3 \cos \beta_3} = \frac{Q_3}{a_1A_3 \cos \beta_3}\left[1 - \left(\frac{\gamma - 1}{2}\right) \times \left(\frac{Q_3}{a_1A_3 \cos \beta_3}\right)^2\right]^{1/(m-1)} \tag{38}$$

which is the same as Eq. (7). The value of V_3/a_1 at the mean radius is given by Eq. (9) and can be obtained at other radii by use of Eq. (30).

Angles of Attack and Lift Coefficients on First Row of Rotor Blades

The angle of attack and the lift coefficient on the first row of rotor blades can now be calculated as follows: The relative whirl component of velocity at any radius is obtained from the absolute whirl component by the relation

$$W_{u3}/a_1 = (U_3/a_1)\,(V_{u3}/a_1) \tag{39}$$

and the relative air angle ϕ_3 is obtained from the relation

$$\tan \phi_3 = (W_{u3}/a_1)/(v_3/a_1) \tag{40}$$

The angle of attack α_3 (relative to the entrance velocity W_3) is given by

$$\alpha_3 = \phi_3 - \psi_R \tag{41}$$

The angle of the air leaving the first row of rotor blades ϕ_4 is obtained from the relation

$$\phi_4 = (1 - K)\phi_3 + K\psi_R + K\alpha_0 \tag{42}$$

and the lift coefficient is obtained from Eqs. (22) and (23).

Appendix II—Derivation of Eqs. (19) and (24)

For the row of stator blades the energy equation is

$$\frac{(V_i)^2}{2} - \frac{(V_{i+1})^2}{2} = gJc_p t_i\left(\frac{t_{i+1}}{t_i} - 1\right) \tag{43}$$

For compression with a polytropic exponent m', this relation can be written

$$\frac{(V_i)^2}{2} - \frac{(V_{i+1})^2}{2} = \frac{\gamma}{\gamma - 1}\left(\frac{p_i}{\rho_i}\right)\left[\left(\frac{\rho_{i+1}}{\rho_i}\right)^{m'-1} - 1\right] = \frac{(a_i)^2}{\gamma - 1}\left[\left(\frac{\rho_{i+1}}{\rho_i}\right)^{m'-1} - 1\right] \tag{44}$$

which, when solved for ρ_{i+1}/ρ_i, gives

$$\frac{\rho_{i+1}}{\rho_i} = \left\{1 + \frac{\gamma - 1}{2}\left(\frac{a_1}{a_i}\right)^2\left[\left(\frac{V_i}{a_1}\right)^2 - \left(\frac{V_{i+1}}{a_1}\right)^2\right]\right\}^{1/(m'-1)} \tag{45}$$

For the following row of rotor blades the energy equation is

$$\frac{(W_{i+1})^2}{2} - \frac{(W_{i+2})^2}{2} + \frac{(U_{i+2})^2}{2} - \frac{(U_{i+1})^2}{2} = gJc_p t_{i+1}\left(\frac{t_{i+2}}{t_{i+1}} - 1\right) \tag{46}$$

where U is the rotor velocity at the radius midway between the hub and casing at the station indicated by the subscript. The terms containing the U's are required because of the centrifugal-force field existing in the rotating frame of reference; the effect of these terms is generally small in axial-flow compressors where the change in radius from station to station is small. The density ratio for the row of rotor blades may be obtained in a manner similar to that for the stator blades, the result being

$$\frac{\rho_{i+2}}{\rho_{i+1}} = \left\{1 + \frac{\gamma - 1}{2}\left(\frac{a_1}{a_{i+1}}\right)^2\left[\left(\frac{W_{i+1}}{a_1}\right)^2 - \left(\frac{W_{i+2}}{a_1}\right)^2 + \left(\frac{U_{i+2}}{a_1}\right)^2 - \left(\frac{U_{i+1}}{a_1}\right)^2\right]\right\}^{1/(m'-1)} \tag{47}$$

In order to use Eqs. (45) and (47) together with the relations for turning angle [Eqs. (17) and (18)] and the continuity relation, it is convenient to express the air velocities in terms of the axial components and the relative air angles. Eq. (45) for the stator blades becomes

$$\frac{\rho_{i+1}}{\rho_i} = \left\{1 + \frac{\gamma - 1}{2}\left(\frac{a_1}{a_i}\right)^2\left[\frac{(v_i/a_1)^2}{\cos^2\beta_i} - \frac{(v_{i+1}/a_1)^2}{\cos^2\beta_{i+1}}\right]\right\}^{1/(m'-1)} \tag{48}$$

and Eq. (47) for the rotor blades becomes

$$\frac{\rho_{i+2}}{\rho_{i+1}} = \left\{1 + \frac{\gamma - 1}{2}\left(\frac{a_1}{a_{i+1}}\right)^2\left[\frac{(v_{i+1}/a_1)^2}{\cos^2\phi_{i+1}} - \frac{(v_{i+2}/a_1)^2}{\cos^2\phi_{i+2}} + \left(\frac{U_{i+2}}{a_1}\right)^2 - \left(\frac{U_{i+1}}{a_1}\right)^2\right]\right\}^{1/(m'-1)} \tag{49}$$

The density ratio can be eliminated from these equations by use of the continuity equation, which for the stator blades is

$$\rho_{i+1}/\rho_i = (v_i/v_{i+1})\ (A_i/A_{i+1})$$

to obtain

$$\frac{v_i}{a_1} = \frac{v_{i+1}}{a_1}\frac{A_{i+1}}{A_i}\left\{1 + \frac{\gamma - 1}{2}\left(\frac{a_1}{a_i}\right)^2\left[\frac{(v_i/a_1)^2}{\cos^2\beta_i} - \frac{(v_{i+1}/a_1)^2}{\cos^2\beta_{i+1}}\right]\right\}^{1/(m'-1)} \tag{50}$$

and

$$\frac{v_{i+1}}{a_1} = \frac{v_{i+2}}{a_1}\left(\frac{A_{i+2}}{A_{i+1}}\right)\left\{1 + \frac{\gamma - 1}{2}\left(\frac{a_1}{a_{i+1}}\right)^2\left[\frac{(v_{i+1}/a_1)^2}{\cos^2\phi_{i+1}} - \frac{(v_{i+2}/a_1)^2}{\cos^2\phi_{i+2}} + \left(\frac{U_{i+2}}{a_1}\right)^2 - \left(\frac{U_{i+1}}{a_1}\right)^2\right]\right\}^{1/(m'-1)} \tag{51}$$

which are Eqs. (19) and (24) of the text.

REFERENCES

[1] Sinnette, John T., Jr., Schey, Oscar W., and King, J. Austin, *Performance of NACA Eight-Stage Axial-Flow Compressor Designed on the Basis of Airfoil Theory*, N.A.C.A. A.C.R. No. E3H18, 1944.

[2] King, J. Austin, and Regan, Owen W., *Performance of NACA Eight-Stage Axial-Flow Compressor at Simulated Altitudes*, N.A.C.A. A.C.R. No. E4L21, 1944.

[3] Betz, A., *Axial Blowers*, N.A.C.A. T.M. No. 1073, August, 1944.

[4] Seippel, C., *The Development of the Brown-Boveri Axial Compressor*, Brown-Boveri Rev., Brown, Boveri & Co., Ltd. (Switzerland), Vol. XXVII, No. 5, pp. 108–113, May, 1940.

[5] White, William Monroe, *American Hydraulic Turbines*, Mechanical Engineering, Vol. 52, No. 4, pp. 390–395, April, 1930.

[6] Daugherty, R. L., *Hydraulics*, 4th Ed., p. 407; McGraw-Hill Book Company, Inc., New York, 1937.

[7] Keller, Curt, and Marks, L. S., *The Theory and Performance of Axial-Flow Fans*; McGraw-Hill Book Company, Inc., New York, 1937.

[8] Keller, C., *Multi-Stage Axial-Flow Fans of Today and Yesterday Design*, Escher Wyss News, Vol. XI, No. 2, pp. 39–44, April-June, 1938.

[9] Bell, E. Barton, *Test of a Single-Stage Axial-Flow Fan*, N.A.C.A. Report No. 729, 1942.

[10] Meldahl, A., *End Losses of Turbine Blades*, Jour. Am. Soc. Naval Eng., Vol. 54, No. 3, pp. 454–466, August, 1942.

[11] Harris, R. G., and Fairthorne, R. A., *Wind Tunnel Experiments with Infinite Cascades of Aerofoils*, R. & M. No. 1206, British A.R.C., 1928.

[12] Weske, John R., and Marble, Frank E., *Characteristics of Airfoils in a Cylindric Axial-Flow Grid*, Journal of the Aeronautical Sciences, Vol. 10, No. 8, pp. 289–294, October, 1943.

Position Error of a Machmeter

H. W. SIBERT*
University of Colorado

SUMMARY

A simple formula is given for the position error of a Machmeter in terms of the Machmeter reading corrected for instrument error, the altimeter position error, and the standard-atmosphere density and pressure ratios corresponding to the altimeter reading corrected for instrument error.

INTRODUCTION

DURING THE WAR the U.S. Army Air Forces initiated the development of a Machmeter for use in fighter aircraft. In the future, Machmeters will probably be used not only in fighter aircraft but also in heavier jet-propelled aircraft, both military and civilian. Since no formula for the position error of this instrument has yet been given, it appears desirable to derive such a formula.

From the well-known relation

$$p_t = p\{1 + [(\gamma - 1)/2]M^2\}^{\gamma/\gamma - 1}$$

connecting the total pressure p_t, the static pressure p, the Mach number M, and the ratio of specific heats γ, it is evident that the airplane Mach Number relative to the free stream can be found from the relation

$$p_{ts} = p_s(1 + 0.2M^2_{\text{plane}})^{3.5} \qquad (1)$$

(when $\gamma = 1.4$), where p_{ts} is the free-stream total pressure and p_s is the free-stream static pressure. It appears from Eq. (1) that a Machmeter can be actuated by the two pressures from an ordinary air-speed head.

The Army Air Forces Machmeter is an instrument with an airtight case containing two diaphragm capsules, of which one is evacuated and the other has led into it the pressure p_{th} from the opening at the end of the air-speed head. The pressure p_h from the openings in the side of the air-speed head is led into the space between the capsules and the outside case. Thus the movement of the diaphragms of the two capsules is proportional to p_h and $(p_{th} - p_h)$, respectively. By a suitable mechanism an A.A.F. Machmeter with a correctly graduated dial gives values of M_i according to the relation

$$(p_{th} - p_h)/p_h = (1 + 0.2\,M_i^2)^{3.5} - 1 \qquad (2)$$

when it is connected to an air-speed head.

Stating that the dial of a Machmeter is correctly graduated is equivalent to saying that it has no instrument error, which is the error due to the failure of the dial readings to follow Eq. (2) exactly. Thus M_i in Eq. (2) is either the reading of a Machmeter free of instrument error or the reading of a Machmeter corrected for instrument error.

An air-speed head when properly located with respect to the airplane will transmit the free-stream total pressure p_{ts} and the free-stream static pressure p_s to the altimeter, air-speed indicator, and Machmeter. Any change in the dial readings of these instruments because of the failure of p_{th} to equal p_{ts} and p_h to equal p_s is called a position error. Instrument readings that have been corrected for both instrument and position error are called "calibrated" values and are designated by the subscript c. Thus when there is no instrument or position error, $p_{th} = p_{ts}$, $p_h = p_s$, $M_i = M_c$ and Eq. (2) becomes

$$(p_{ts} - p_s)/p_s = (1 + 0.2\,M_c^2)^{3.5} - 1 \qquad (3)$$

It is evident from a comparison of Eqs. (1) and (3) that M_c as given in Eq. (3) is actually the airplane Mach Number.

The determination of the position error of a given Machmeter attached to a given air speed-head installation consists in finding the difference between M_c and M_i from Eqs. (2) and (3). In deriving a formula for the difference between M_c and M_i the following symbols will be used.

SYMBOLS

p_{th} = pressure at the opening in the end of the air-speed head
p_h = pressure at the openings in the side of the air-speed head
ρ = density
a = speed of sound
h = altitude
g = acceleration of gravity
$\sigma = \rho/\rho_0$ = density ratio
γ = ratio of specific heats = 1.4 in this paper
M_i = Mach Number from Machmeter, corrected for instrument error only
M_c = Mach Number from Machmeter, corrected for both instrument and position error
h_i = altitude from altimeter, corrected for instrument error only
h_c = altitude from altimeter, corrected for both instrument and position error
$\Delta M = M_c - M_i$ = Machmeter position error
$\Delta h = h_c - h_i$ = altimeter position error
$F(M) = 3.5 \log (1 + 0.2M^2)$
$f(h) = \log p$
p_i = standard-atmosphere value of p corresponding to h_i
ρ_i = standard-atmosphere value of ρ corresponding to h_i
σ_i = standard-atmosphere value of σ corresponding to h_i

Received December 9, 1946.

* Professor of Aeronautical Engineering.

Subscript 0 refers to standard-atmosphere sea-level conditions.
Subscript s refers to free-streams conditions at altitude at which airplane is flying.

NOTE: All logarithms are to the base e.

DERIVATION OF FORMULAS

High-speed wind-tunnel data have demonstrated that a well-designed air-speed head will transmit free-stream total pressure with negligible error provided the head is not yawed more than 15° or 20°. Thus, $p_{th} = p_{ts}$ except for unusual airplane attitudes.

A pressure altimeter is graduated to give pressure altitude h according to the standard-atmosphere relation between altitude and pressure. Since h_i is the altitude from the altimeter corrected for instrument error, and p_i is the standard-atmosphere value of p corresponding to h_i, p_i is the actual pressure transmitted from the air-speed head to the altimeter. In other words, $p_i = p_h$.*

From Eqs. (2) and (3) and the relations $p_{th} = p_{ts}$ and $p_h = p_i$,

$$p_s(1 + 0.2M_c^2)^{3.5} = p_i(1 + 0.2M_i^2)^{3.5} \qquad (4)$$

Taking logarithms of Eq. (4),

$$3.5 \log (1 + 0.2M_c^2) - 3.5 \log (1 + 0.2M_i^2) = \log p_i - \log p_s$$

By virtue of the definitions of $F(M)$, $f(h)$, ΔM and Δh, this equation can be written in the following forms:

$$F(M_c) - F(M_i) = f(h_i) - f(h_c)$$

$$F(M_i + \Delta M) - F(M_i) = -[f(h_i + \Delta h) - f(h_i)] \qquad (5)$$

In differential calculus it is shown that the derivative dH/dx at a point x of any function H of x is given fairly accurately by the formula

$$(dH/dx)_{x=x} = [H(x + \Delta x) - H(x)]/\Delta x$$

provided Δx is sufficiently small. By means of this relation, Eq. (5) can be written as

$$(dF/dM)_{M=M_i} \Delta M = -(df/dh)_{h=h_i} \Delta h \qquad (6)$$

provided ΔM and Δh are sufficiently small. From the definition of $F(M)$,

$$(dF/dM)_{M=M_i} = 1.4M_i/(1 + 0.2M_i^2) \qquad (7)$$

The difference in pressure dp in the atmosphere at two points whose elevation differs by dh is equal to the weight of a column of air of height dh and unit cross section. Hence, $dp = -g\rho dh$. Since $f(h) = \log p$ by definition, it follows from the above formula for dp that

$$\frac{df}{dh} = \left(\frac{df}{dp}\right)\left(\frac{dp}{dh}\right) = \frac{1}{p}(-g\rho) = -\left(\frac{\gamma g}{a_0^2}\right)\left(\frac{\rho/\rho_0}{p/p_0}\right)$$

since $a^2 = \gamma p/\rho$. Hence, for $\gamma = 1.4$,

$$(df/dh)_{h=h_i} = -1.4g\sigma_i/(a_0^2 p_i/p_0) \qquad (8)$$

It follows from Eqs. (6), (7), and (8) that

$$\Delta M = [(1 + 0.2M_i^2)/M_i][g\sigma_i \Delta h/(a_0^2 p_i/p_0)] \qquad (9)$$

the units of length and time in g, a_0, and h being the same. Thus the Machmeter position error ΔM has been found in terms of the altimeter position error Δh, which can be obtained by the usual fly-by method. Note that σ_i and p_i/p_0 are, respectively, the standard-atmosphere density and pressure ratios corresponding to h_i.

* Provided, of course, that lag in the system is neglected. The effect of lag must be determined separately from the position error. However, in installations similar to those made by the N.A.C.A., the effect of lag is usually negligibly small.

Changes of Address

Since the Post Office Department does not as a rule forward magazines to forwarding addresses, it is important that the Institute be notified of changes in address 30 days in advance of publishing date to ensure receipt of every issue of the JOURNAL and REVIEW.

Notices should be sent directly to:

Institute of the Aeronautical Sciences, Inc.
2 East 64th Street, New York 21, New York

Bending of Rotor Blade in the Plane of Rotation*

SHAO WEN YUAN†

Polytechnic Institute of Brooklyn

SUMMARY

A theoretical analysis of the bending of the rotor blade in the plane of rotation is given with consideration of the elasticity of the blade. The analysis also includes the bending of a blade with variable mass distribution along the span. The results lead to matrix equations that are convenient for arithmetic calculation.

The application of this theoretical analysis is illustrated by numerical calculations. The results found in the case of a typical rotor blade show that the maximum deflection in the plane of rotation is about one-tenth of that in the flapping plane and that the maximum bending moment in the plane of rotation is about one-fourth of that in the flapping plane. When a blade with variable section is compared with one with an equivalent constant blade section, the bending moment for the variable section is found to be appreciably greater than that for the equivalent constant section in the region of the inner half span.

INTRODUCTION

THE BENDING OF THE ROTOR BLADE in the plane of rotation is of particular importance in the design of the present steel spar and fabric-covered blade since the bending rigidity in the plane of rotation is about equal to that in the flapping plane. The deflection of the rotor blade in the plane of rotation gives, as observed in flight tests, a certain amount of pitching moment that has an adverse effect upon control. It is expected that this pitching moment can be reduced to a minimum by initially bending the blade forward if the amount of deflection in the plane of rotation is known.

In the solution of the problem of the bending of the rotor blade in the plane of rotation, the differential equation of motion of the blade is derived from a consideration of the forces that act on a blade element of length dr. They are the so-called aerodynamic torque, the component of the centrifugal force perpendicular to dr, the inertia force, and the Coriolis force.

Since the weight of the blade is seldom distributed uniformly over the span, a method of calculating the bending of the blade with variable mass distribution is developed. If the mass distribution and the bending rigidity distribution are known for a given rotor blade of variable mass distribution, the bending moments and the deflections can be calculated in a manner similar to that used in the case of the uniformly distributed mass. The differential equations are then solved by the method of collocation. The same degree of accuracy is obtained as in the case of constant mass distribution along the blade span.

In this paper the analysis is carried out for the nontwisted blade with constant chord. However, for a twisted blade with tapered chord, only the blade loading expression need be modified. The expressions presented were developed on the basis of the first three terms of the Fourier series expansions because the consideration of more terms would lead to entirely unwieldy equations. On the other hand, the numerical example was worked out using five terms of the Fourier series. The maximum bending moment found when five terms were considered was about 20 per cent higher than that obtained when three terms were used.

The results found in the case of a typical rotor blade show that the maximum deflection in the plane of rotation is about one-tenth of that in the flapping plane and that the maximum bending moment in the plane of rotation is about one-fourth of that in the flapping plane.

When a blade with variable section is compared with one with an equivalent constant blade section, in the region of the inner half span the bending moment for the variable section is found to be appreciably greater than that for the equivalent constant section.

The reason for this phenomenon is that the variable blade section has a greater bending rigidity in the inner portion of the blade span. It is somewhat unconservative to assume an equivalent constant section, as done in present practice, since the maximum bending moment of the rotor blade in the plane of rotation generally occurs at about 20 per cent of the span.

SYMBOLS

a	=	slope of life curve of blade element
C	=	chord of blade element
EI	=	bending rigidity
m	=	mass of blade per unit length
M_{BG}	=	bending moment of rigid blade
M_{EL}	=	bending moment of blade with consideration of blade elasticity
r	=	radius to the blade element
R	=	tip radius
R_r	=	distance between center of rotation and lag hinge
θ_0	=	blade pitch angle

Presented at the Rotating Wing Aircraft Session, Fourteenth Annual Meeting, I.A.S., New York, January 29–31, 1946. Received December 20, 1946.

* A considerable portion of the work presented here was carried out while the author was associated with the Helicopter Research Division of the McDonnell Aircraft Corporation.

† Research Advisor. Also, Consulting Engineer.

λ = axial flow coefficient
μ = coefficient of advance
ρ = mass density of air
ψ = angle of rotation of blade measured from neutral position back
ω = angular velocity of rotor

Fundamental Assumptions

In the derivation of the differential equation of the bending of the blade with consideration of the blade elasticity, the following simplifying assumptions are made and the following definitions are used:

(1) The chord is constant along the span of the blade.

(2) The twisting of the blade is neglected.

(3) The distance r from the center of rotation to an element of the blade does not change when the blade is bent.

(4) The flapping motion is represented by the first three terms of a Fourier expansion:

$$\beta = a_0 - a_1 \cos \psi - b_1 \sin \psi$$

(5) The lag motion is also represented by the first three terms of a Fourier expansion:

$$\zeta = A_0 + A_1 \cos \psi + B_1 \sin \psi$$

(6) The instantaneous lag angle of an element of length dr is defined as the angle $\zeta' = \zeta + (z/r)$ formed by the ray from the lag hinge to the element in question with the reference line that connects the center of the rotor with the lag hinge. In the defining equation z is the elastic backward deflection of the element at r (see Fig. 4).

(7) The direction of the tangent to the blade element at r is measured by the angle $\Gamma = \zeta + (dz/dr)$. This is shown in Fig. 4.

(8) Squares and products of the small angles ζ, ζ', and Γ are neglected.

(9) In the expressions obtained for the aerodynamic forces only those corresponding to the first three terms of a Fourier expansion are considered.

(10) The tip loss of the blade is disregarded.

(11) The flow through the rotor disc is considered uniform.

(12) The deflection of the blade is assumed to be of the form $Z = Z_1 + Z_2 \cos \psi + Z_3 \sin \psi$.

(13) The profile drag coefficient of a blade element is approximated by the following function of the operating angle of attack of an element:

$$C_{d_0} = \delta_0 + \delta_2 \alpha_r^2$$

where $\delta_0 = 0.0075$, $\delta_2 = 0.8$.

Bending of an Infinitely Rigid Blade

When investigating the bending of a blade with consideration of blade elasticity, it is convenient to discuss first the bending of an infinitely rigid blade.

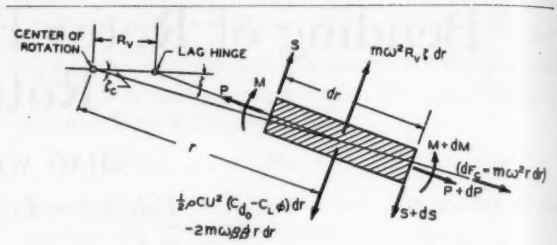

FIG. 1. Forces acting on an element of a rigid blade.

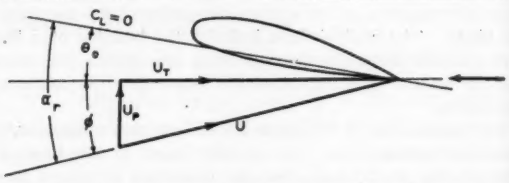

FIG. 2. Velocities and angles at a section of a blade.

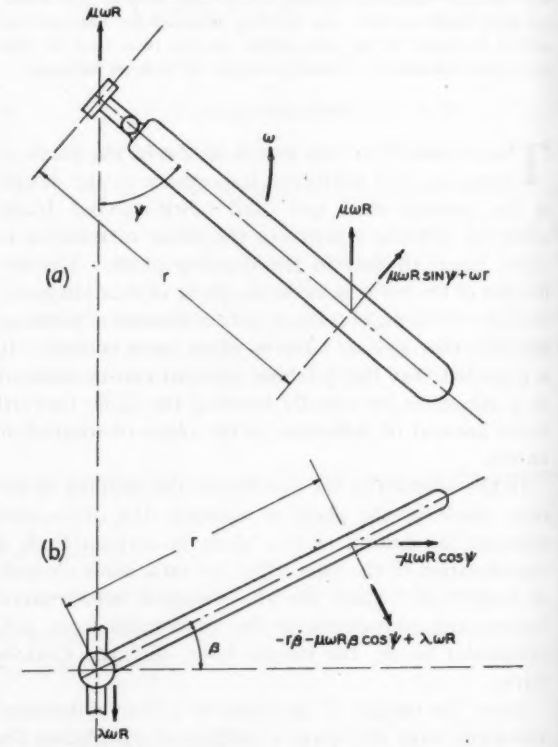

FIG. 3. Velocities at the blade: (a) in plane of disc; (b) in plane containing rotor axis and blade.

The forces acting on an infinitesimal element of length dr are shown in Fig. 1. The aerodynamic forces may be reduced to a resultant acting through the centerline of the span and perpendicular to the blade element. The centrifugal force introduces a term whose component perpendicular to the element

dr is $mdr\omega^2 R_V\zeta$, and the Coriolis force is a term equal to $2m\omega\beta\dot{\beta}rdr$. The shearing force, the bending moment, and the longitudinal tension along the blade element are represented by S, M, and P, respectively.

The acceleration of the element of length dr normal to the blade and in the plane of rotation is given by the equation of motion:

$$mdr\ddot{\zeta} = dS + {}^1/_2\rho CU^2(C_d - C_L\varphi)dr - mdr\omega^2 R_V\zeta - 2mdr\omega\beta\dot{\beta} \quad (1)$$

The bending moment at any point r is given by

$$M_{RG} = -\int_R^r\int_R^r dsdr = -\int_R^r\int_R^r mr\ddot{\zeta}drdr - \int_R^r\int_R^r mR_V\omega^2\zeta drdr - \int_R^r\int_R^r 2m\omega\dot{\beta}\beta rdrdr + {}^1/_2\rho C\int_R^r\int_R^r U^2(C_{d_0} - C_L)drdr \quad (2)$$

In the evaluation of the last integral of Eq. (2), which represents the aerodynamic torque, the following assumptions are employed:

(14) The influence of the radial velocity on the blade forces is negligible.

(15) The acute angle φ between the resultant U of the velocities UT and UP and the rotor disc is small. Consequently, the following expressions can be used:

$$U_T = U,\ U_P = \varphi U$$

(16) The lift coefficient C_L of the blade is proportional to the angle of attack:

$$C_L = a\alpha_r = a(\theta_0 + \varphi)$$

Hence, the expressions for the components of the resultant flow velocities for a blade section at distance r are (see Fig. 3):

$$U_T = \omega r + \mu\omega R\sin\psi$$
$$U_P = \lambda\omega R - r\dot{\beta} - \mu\omega R\beta\cos\psi$$

Substitution of the expressions for ζ, $\ddot{\zeta}$, β, $\dot{\beta}$, U, C_L and C_{d_0} in Eq. (2) and integration yield the following expression for the bending moment of the infinitely rigid blade in the plane of rotation:

$$\left.\begin{aligned} M_{RG} = {} & -m\omega^2 R_V R_A A_0 + \frac{\rho}{2}C\omega^2[(\delta_0 + \delta_2\theta_0^2)(R_C + \frac{\mu^2}{2}R^2R_A) + (2\delta_2 - a)(RR_B\lambda) + (\delta_2 - a)(R^2R_A\lambda^2 + \\ & \mu R^2R_A\lambda a_1) + R_C\left(\frac{a_1^2}{2} + \frac{b_1^2}{2}\right) + \frac{\mu^2}{2}R^2R_A\left(a_0^2 + \frac{3}{4}a_1^2 + \frac{b_1^2}{4}\right) - \mu RR_Ba_0b_1] + \{m\omega^2[A_1(R_B - \\ & R_VR_A) + 2R_Ba_0b_1] + \frac{\rho}{2}C\omega^2[(2\delta_2 - a)\theta_0\{-\mu RR_Ba_0 + (R_C + \frac{\mu^2}{4}R^2R_A)b_1\} + \{2RR_B\lambda b_1 + \\ & \mu^2R^2R_A\left(-\frac{3}{2}a_0a_1\right) - 2\mu R^2R_A\lambda a_0 + \mu RR_Ba_1b_1\}(\delta_2 - a)]\}\cos\psi + \{m\omega^2[B_1(R_B - R_VR_A) - \\ & 2R_Ba_0a_1] + \frac{\rho}{2}C\omega^2[(\delta_0 + \delta_2\theta_0^2)(2\mu RR_B) + (2\delta_2 - a)\theta_0\{R^2R_A\mu\lambda - (R_C - \frac{\mu^2}{4}R^2R_A)a_1\} + (\delta_2 - a) \\ & \{-2RR_B\lambda a_1 - \frac{\mu^2}{2}R^2R_Aa_0b_1 + {}^1/_2\mu RR_B(b_1^2 - a_1^2)\}]\}\sin\psi \end{aligned}\right\} \quad (3)$$

where

$$R_A = R^2\left[\frac{1}{2}\left(\frac{r}{R}\right)^2 - \frac{r}{R} + \frac{1}{2}\right],\ R_B = R^3\left[\frac{1}{6}\left(\frac{r}{R}\right)^3 - \frac{1}{2}\left(\frac{r}{R}\right) + \frac{1}{3}\right],\ R_C = R^4\left[\frac{1}{12}\left(\frac{r}{R}\right)^4 - \frac{1}{3}\left(\frac{r}{R}\right) + \frac{1}{4}\right]$$

The coefficients A_0, A_1, and B_1 are determined from the condition $M_{RG} = 0$ at $r = R_V$. They are:

$$\left.\begin{aligned} A_0 = {} & \frac{\rho C}{2mR_VR_{AV}}\left\{(\delta_0 + \delta_2\theta_0^2)\left(R_{CV} + \frac{\mu^2}{2}R^2R_{AV}\right) + (2\delta_2 - a)\theta_0(RR_{BV}\lambda) + (\delta_2 - a)\left[R^2R_{AV}\lambda^2 + \right.\right. \\ & \left.\left.\mu R^2R_{AV}\lambda a_1 + \frac{R_{CV}}{2}(a_1^2 + b_1^2) + \frac{\mu^2}{2}R^2R_{AV}\left(a_0^2 + \frac{3}{4}a_1^2 + \frac{b_1^2}{4}\right) - \mu RR_{BV}a_0b_1\right]\right\} \\ A_1 = {} & \frac{\rho C}{2m(R_VR_{AV} - R_{BV})}\left\{(2\delta_2 - a)\theta_0\left[-\mu RR_{BV}a_0 + \left(R_{CV} + \frac{\mu^2R^2R_{AV}}{4}\right)b_1\right] + (\delta_2 - a)\times\right. \\ & \left.\left[2RR_{BV}\lambda b_1 + \mu^2R^2R_{AV}\left(-\frac{3}{2}a_0a_1\right) - 2\mu R^2R_{AV}\lambda a_0 + \mu RR_{BV}a_1b_1\right]\right\} + \left(\frac{2R_{BV}}{R_VR_{AV} - R_{BV}}\right)a_0b_1 \\ B_1 = {} & \frac{\rho C}{2m(R_VR_{AV} - R_{BV})}\left\{(\delta_0 + \delta_2\theta_0^2)[2\mu RR_{BV}] + (2\delta_2 - a)\theta_0\left[R^2R_{AV}\mu\lambda - \left(R_{CV} - \frac{\mu_2}{4}R^2R_{AV}\right)a_1\right] + \right. \\ & \left.(\delta_2 - a)\left[-2RR_{BV}\lambda a_1 - \frac{\mu^2}{2}R^2R_{AV}a_0b_1 + \frac{1}{2}\mu RR_{BV}(b_1^2 - a_1^2)\right]\right\} - \left(\frac{2R_{BV}}{R_{AV}R_V - R_{BV}}\right)a_0a_1 \end{aligned}\right\} \quad (4)$$

where

$$R_{AV} = R^2\left[\frac{1}{2}\left(\frac{R_V}{R}\right)^2 - \frac{R_V}{R} + \frac{1}{2}\right],\ R_{BV} = R^3\left[\frac{1}{6}\left(\frac{R_V}{R}\right)^3 - \frac{1}{2}\frac{R_V}{R} + \frac{1}{3}\right],\ R_{CV} = R^4\left[\frac{1}{12}\left(\frac{R_V}{R}\right)^4 - \frac{1}{3}\frac{R_V}{R} + \frac{1}{4}\right]$$

Bending of a Blade with Consideration of Its Elasticity

The forces acting on an element dr of an elastic blade are shown in Fig. 4. The equations of motion of the blade element are as follows:

(*a*) *Normal to the element in the plane of rotation:*

$$mdrr\ddot{\zeta}' = {}^1/_2\rho CU^2(C_{d_0} - C_L\varphi)dr\cos(\Gamma - \zeta') - 2m\omega\beta\dot{\beta}rdr\cos(\Gamma - \zeta') - mdrr\omega^2\sin(\Gamma - \zeta_C) + P'd\Gamma + dS' \quad (5)$$

The component $P'd\Gamma$ perpendicular to the element appears on account of the curvature of the element. It may be noted that the equation of motion of an infinitely rigid blade can be obtained from Eq. (5) by putting $\zeta' = \Gamma = \zeta$.

(*b*) *Parallel to the element in the plane of rotation:*

$$0 = mdrr\omega^2\cos(\Gamma - \zeta_C) - {}^1/_2\rho CU^2(C_{I0} - C_L\varphi)dr\sin(\Gamma - \zeta') + 2m\omega\beta\dot{\beta}rdr\sin(\Gamma - \zeta_C') + dP' \quad (6)$$

Neglecting second order terms in ζ, ζ', and Γ and integrating, one obtains

$$P' = {}^1/_2m\omega^2(R^2 - r^2) \quad (7)$$

When Eq. (1) is subtracted from Eq. (5) and use is made of the connection $\ddot{\zeta}' = \ddot{\zeta} + (\ddot{z}/r)$:

$$mdrr(\ddot{z}/r) = [{}^1/_2\rho CU^2(C_{d_0} - C_L\varphi)dr - 2m\omega\beta\dot{\beta}rdr] \times [\cos(\Gamma - \zeta') - 1] + P'd\Gamma + dS' - dS - mr\omega^2dr[\sin(\Gamma - \zeta_C) - \sin(\zeta - \zeta_C)] \quad (8)$$

With second order terms in ζ, ζ', and Γ omitted from Eq. (8) and upon substitution of the expression given for P' in Eq. (7),

$$m\ddot{z} = -mr\omega^2\frac{dz}{dr} + \frac{dS'}{dr} + {}^1/_2m\omega^2(R^2 - r^2)\frac{d^2z}{dr^2} - \frac{dS}{dr} \quad (9)$$

From the theory of strength of materials the following relation between shear force and deflection is known:

$$S' = dM'/dr = -EI(d^3z/dr^3)$$

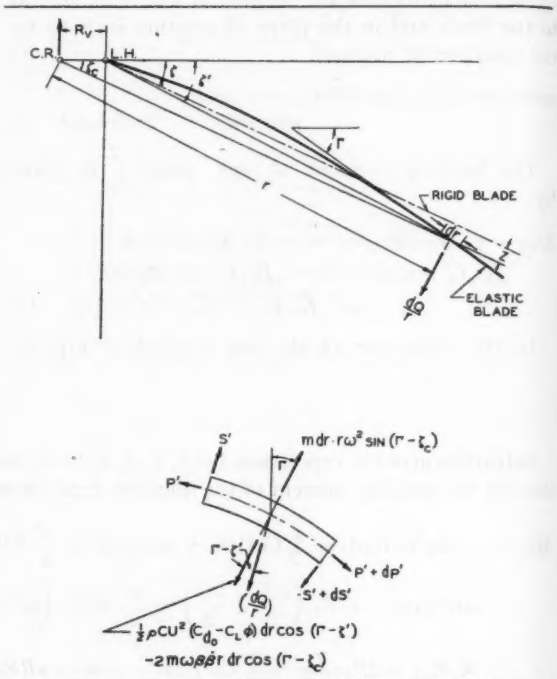

FIG. 4. Forces acting on an element of elastic blade in plane of rotation.

With substitution of the above well-known relation in Eq. (9) and the new symbols $X = (r - R_V)/(R - R_V)$, $Z = (z/R)$, and $k = (mR^4\omega^2)/(2EI)$, the differential equation of bending becomes

$$\frac{d^4Z}{dX^4} - k\left(1 - \frac{R_V}{R}\right)^2\left[\frac{R_V}{R}\left(2 - \frac{R_V}{R}\right)X^2 - 2\frac{R_V}{R}\left(1 - \frac{R_V}{R}\right)X - \left(\frac{R_V}{R}\right)^2 + 1 - X^2\right]\frac{d^2Z}{dX^2} + 2k\left(1 - \frac{R_V}{R}\right)^3\left[\left(1 - \frac{R_V}{R}\right)X + \frac{R_V}{R}\right]\frac{dZ}{dX} + \frac{2k}{\omega^2}\left(1 - \frac{R_V}{R}\right)^4\frac{d^2Z}{dt^2} = -\frac{R^3(1 - R_V/R)^4}{EI}\left(\frac{dS}{dr}\right) \quad (10)$$

The term on the right-hand side of Eq. (10) represents a rigid blade loading that is given in Eq. (1) and can be expressed as follows:

$$-\frac{R^3}{EI}\left(1 - \frac{R_V}{R}\right)^4\frac{dS}{dr} = [J_{1,1}X^2 + J_{1,2}X + J_{1,3}] + [J_{2,1}X^2 + J_{2,2}X + J_{2,3}]\cos\psi + [J_{3,1}X^2 + J_{3,2}X + J_{3,3}]\sin\psi \quad (11)$$

where

$$J_{n,1} = \left(1 - \frac{R_V}{R}\right)^2 j_{n,1},\ J_{n,2} = \left(1 - \frac{R_V}{R}\right) j_{n,2} + 2\frac{R_V}{R}\left(1 - \frac{R_V}{R}\right) j_{n,1},\ J_{n,3} = j_{n,3} + \frac{R_V}{R} j_{n,2} + \left(\frac{R_V}{R}\right)^2 j_{n,1}$$

$n = 1, 2, 3$; and

$$\left.\begin{aligned}
j_{1,1} &= \frac{R^3}{EI}\left(1 - \frac{R_V}{R}\right)^4\left(\frac{\rho}{2} CR^2\omega^2 \{(\delta_0 + \delta_2\theta_0^2) + [(\delta_2 - a)/2](a_1^2 + b_1^2)\}\right)\\
j_{1,2} &= \frac{R^3}{EI}\left(1 - \frac{R_V}{R}\right)^4\left(\frac{\rho}{2} CR^2\omega^2\right)[(2\delta_2 - a)\theta_0\lambda - (\delta_2 - a)\mu a_0 b_1]\\
j_{1,3} &= \frac{R^3}{EI}\left(1 - \frac{R_V}{R}\right)^4\left(\frac{\rho}{2} CR^2\omega^2\right)\left\{(\delta_0 + \delta_2\theta_0^2)\frac{\mu^2}{2} + (\delta_2 - a) \times \right.\\
&\qquad \left.\left[\lambda^2 + \mu\lambda a_1 + \frac{\mu^2}{2}\left(a_0^2 + \frac{3}{4}a_1^2 + \frac{b_1^2}{4}\right)\right] - mR_V\omega^2 A_0\right\}\\
j_{2,1} &= \frac{R^3}{EI}\left(1 - \frac{R_V}{R}\right)^4\left(\frac{\rho}{2} CR^2\omega^2\right)[(2\delta_2 - a)\theta_0 b_1]\\
j_{2,2} &= \frac{R^3}{EI}\left(1 - \frac{R_V}{R}\right)^4\left(\frac{\rho}{2} CR^2\omega^2\right)[-(2\delta_2 - a)\theta_0\mu a_0 + (\delta_2 - a)(2\lambda b_1 + \mu a_1 b_1) + mR_V\omega^2(A_1 + 2a_0 b_1)]\\
j_{2,3} &= \frac{R^3}{EI}\left(1 - \frac{R_V}{R}\right)^4\left(\frac{\rho}{2} CR^2\omega^2\right)\left[(2\delta_2 - a)\frac{\theta_0\mu^2 b_1}{4} - (\delta_2 - a)\left(\frac{3}{2}\mu^2 a_0 a_1 + 2\mu a_0\lambda\right) - mR_V\omega^2 A_1\right]\\
j_{3,1} &= (R^3/EI)[1 - (R_V/R)]^4[(\rho/2)CR^2\omega^2][-(2\delta_2 - a)\theta_0 a_1]\\
j_{3,2} &= \frac{R^3}{EI}\left(1 - \frac{R_V}{R}\right)^4\left(\frac{\rho}{2} CR^2\omega^2\right)\left\{2\mu(\delta_0 + \delta_2\theta_0^2) + (\delta_2 - a) \times \right.\\
&\qquad \left.\left[-2\lambda a_1 + \frac{1}{2}\mu(b_1^2 - a_1^2)\right] + mR_V\omega^2(B_1 - 2a_0 a_1)\right\}\\
j_{3,3} &= \frac{R^3}{EI}\left(1 - \frac{R_V}{R}\right)^4\left(\frac{\rho}{2} CR^2\omega^2\right)\left[(2\delta_2 - a)\theta_0\left(\mu\lambda + \frac{\mu^2}{4} a_1\right) - (\delta_2 - a)(\mu^2 a_0 b_1/2) - mR_V\omega^2 B_1\right]
\end{aligned}\right\} \quad (12)$$

The coefficients A_0, A_1, and B_1 are given in Eq. (4).

It must be borne in mind that the moment of this loading about the hinge should be zero for all values of ψ. This requires:

$$\int_0^1\int_x^1 (J_{1,1}X^2 + J_{1,2}X + J_{1,3})dXdX = 0,\ \int_0^1\int_x^1 (J_{2,1}X^2 + J_{2,2}X + J_{2,3})dXdX = 0,$$
$$\int_0^1\int_x^1 (J_{3,1}X^2 + J_{3,1}X + J_{3,2})dXdX = 0 \quad (13)$$

The above conditions can easily be verified by substituting the corresponding values of $J_{1,1}$, $J_{1,2}$, $J_{1,3}$.... This serves as a valuable check of the arithmetical calculations.

Solution of the Differential Equation

In solving Eq. (10) the form $Z = Z_1 + Z_2\cos\psi + Z_3\sin\psi$ is assumed, where Z_1, Z_2, Z_3 are functions of X only. This is the same harmonic form as that of the loading function dS/dr. By substituting Z and the right-hand side member of Eq. (11) in Eq. (10), the following differential equations are obtained.

$$\left.\begin{aligned}
&\frac{d^4Z_1}{dX^4} - k\left(1 - \frac{R_V}{R}\right)^2 R_1(X)\frac{d^2Z_1}{dX^2} + 2k\left(1 - \frac{R_V}{R}\right)^3 R_2(X)\frac{dZ_1}{dX} = J_{1,1}X^2 + J_{1,2}X + J_{1,3}\\
&\frac{d^4Z_2}{dX^4} - k\left(1 - \frac{R_V}{R}\right)^2 R_1(X)\frac{d^2Z_2}{dX^2} + 2k\left(1 - \frac{R_V}{R}\right)^3 R_2(X)\frac{dZ_2}{dX} - 2k\left(1 - \frac{R_V}{R}\right)^4 Z_2 = J_{2,1}X^2 + J_{2,2}X + J\\
&\frac{d^4Z_3}{dX^4} - k\left(1 - \frac{R_V}{R}\right)^2 R_1(X)\frac{d^2Z_3}{dX^2} + 2k\left(1 - \frac{R_V}{R}\right)^3 R_2(X)\frac{dZ_3}{dX} - 2k\left(1 - \frac{R_V}{R}\right)^4 Z_3 = J_{3,1}X^2 + J_{3,2}X + J_{3,3}
\end{aligned}\right\} \quad (14)$$

where

$$R_1(X) = \frac{R_V}{R}\left(2 - \frac{R_V}{R}\right)X^2 - 2\frac{R_V}{R}\left(1 - \frac{R_V}{R}\right)X - \left(\frac{R_V}{R}\right)^2 + 1 - X^2$$

$$R_2(X) = [1 - (R_V/R)]X + (R_V/R)$$

The hinged root end of the blade and the free tip end give the following boundary conditions:

$$Z = 0,\ d^2Z/dX^2 = 0 \text{ (for } X = 0)$$
$$dZ/dX = 0,\ d^2Z/dX^2 = 0 \text{ (for } X = 1)$$

The second and third differential coefficients are, of course, proportional to the bending moment and shearing force, respectively.

Eqs. (14) can be solved by the method of Frobenius. This, however, is extremely laborious because of the rather slow convergence of the series. A more convenient method is provided by the "collocation" approximations of Frazer and Jones. The assumed form of approximation is:

$$Z_s = C_1^i X + \sum_{j=3}^{s+1} C_i^j \times \left[X^j - \frac{2(j-1)}{j+1} X^{j+1} + \frac{j(j-1)}{(j+1)(j+2)} X^{j+2}\right] \quad (15)$$

Hence, all the independent polynominals satisfy the boundary conditions. J. A. Beavan found that the approximation was sufficiently close to the solution calculated by the method of Frobenius when s was taken as 5 so that the differential equation was satisfied at $x = 0,\ ^1/_4,\ ^1/_2,\ ^3/_4$, and 1.

Substitution of the right-hand side member of Eq. (15) in Eqs. (14) yields the following matrix equations:

$$Z_1 = C_1^1 X + c_3^1(X^3 - X^4 + 0.3X^5) + C_4^1(X^4 - 1.2X^5 + 0.4X^6) + C_5^1\left(X^5 - \frac{4}{3}X^6 + \frac{10}{21}X^7\right) + C_6^1\left(X^6 - \frac{10}{7}X^7 + \frac{15}{28}X^8\right)$$

$$\begin{bmatrix} A_{1,1} & A_{1,2} & A_{1,3} & A_{1,4} & A_{1,5} \\ A_{2,1} & A_{2,2} & A_{2,3} & A_{2,4} & A_{2,5} \\ A_{3,1} & A_{3,2} & A_{3,3} & A_{3,4} & A_{3,5} \\ A_{4,1} & A_{4,2} & A_{4,3} & A_{4,4} & A_{4,5} \\ A_{5,1} & A_{5,2} & A_{5,3} & A_{5,4} & A_{5,5} \end{bmatrix} \begin{bmatrix} C_1^1 \\ C_3^1 \\ C_4^1 \\ C_5^1 \\ C_6^1 \end{bmatrix} = \begin{bmatrix} J_{1,3} \\ 0.0625J_{1,1} + 0.25J_{1,2} + J_{1,3} \\ 0.25\ J_{1,1} + 0.5\ J_{1,2} + J_{1,3} \\ 0.5625J_{1,1} + 0.75J_{1,2} + J_{1,3} \\ J_{1,1} + J_{1,2} + J_{1,3} \end{bmatrix} \quad (16)$$

$$A_{1,1} = 2k\frac{R_V}{R}\left(1 - \frac{R_V}{R}\right)^3,\ A_{2,1} = k\left(1 - \frac{R_V}{R}\right)^3\left(0.5 + 1.5\frac{R_V}{R}\right),\ A_{3,1} = k\left(1 - \frac{R_V}{R}\right)^3\left(1 + \frac{R_V}{R}\right)$$

$$A_{4,1} = k\left(1 - \frac{R_V}{R}\right)^3\left(1.5 + 0.5\frac{R_V}{R}\right),\ A_{5,1} = 2k\left(1 - \frac{R_V}{R}\right),\ A_{1,2} = -24$$

$$A_{2,2} = -\{15 + k[1 - (R_V/R)]^2[0.7256 - 0.4473(R_V/R) - 0.2783(R_V/R)^2]\}$$

$$A_{3,2} = -\{6 + k[1 - (R_V/R)]^2[0.2188 - 0.375(R_V/R) + 0.1562(R_V/R)^2]\}$$

$$A_{4,2} = \left\{3 - k\left(1 - \frac{R_V}{R}\right)^2\left[-0.5888 + 0.3691\frac{R_V}{R} + 0.2197\left(\frac{R_V}{R}\right)^2\right]\right\},\ A_{5,2} = \left[12 + k\left(1 - \frac{R_V}{R}\right)^3\right]$$

$$A_{1,3} = 24,\ A_{2,3} = -\left\{3 + k\left(1 - \frac{R_V}{R}\right)^2\left[0.3748 - 0.1996\frac{R_V}{R} - 0.1753\left(\frac{R_V}{R}\right)^2\right]\right\}$$

$$A_{3,3} = -\{12 + k[1 - (R_V/R)]^2[0.3625 - 0.375(R_V/R) + 0.0125(R_V/R)^2]\}$$

$$A_{4,3} = -\{3 + k[1 - (R_V/R)]^2[0.3535 + 0.2005(R_V/R) + 0.153(R_V/R)^2]\}$$

$$A_{5,3} = \{24 + 0.8k[1 - (R_V/R)]^3\}$$

$$A_{2,4} = \left\{6.25 - k\left(1 - \frac{R_V}{R}\right)^2\left[0.1585 - 0.0784\frac{R_V}{R} - 0.0801\left(\frac{R_V}{R}\right)^2\right]\right\},\ (A_{1,4} = 0)$$

$$A_{3,4} = -\{10 + k[1 - (R_V/R)]^2[0.3542 - 0.3125(R_V/R) - 0.0417(R_V/R)^2]\}$$

$$A_{4,4} = -\{11.25 + k[1 - (R_V/R)]^2[-0.1837 + 0.0785(R_V/R) + 0.1052(R_V/R)^2]\}$$

$$A_{5,4} = \{40 + 0.6666k[1 - (R_V/R)]^3\}$$

$$A_{2,5} = \left\{7.265 - k\left(1 - \frac{R_V}{R}\right)^2\left[0.05998 - 0.0284\frac{R_V}{R} - 0.0316\left(\frac{R_V}{R}\right)^2\right]\right\},\ (A_{1,5} = 0)$$

$$A_{3,5} = -\{3.75 + k[1 - (R_V/R)]^2[0.2868 - 0.2344(R_V/R) - 0.0525(R_V/R)^2]\}$$

$$A_{4,5} = -\{19.02 + k[1 - (R_V/R)]^2[-0.0642 - 0.0066(R_V/R) + 0.0709(R_V/R)^2]\}$$

$$A_{5,5} = \{60 + 0.5714k[1 - (R_V/R)]^3\}$$

$$Z_2 = C_3^2(X^3 - X^4 + 0.3X^5) + C_4^2(X^4 - 1.2X^5 + 0.4X^6) + C_5^2\left(X^5 - \frac{4}{3}X^6 + \frac{10}{21}X^7\right) + C_6^2\left(X^6 - \frac{10}{7}X^7 + \frac{15}{28}X^8\right) + C_7^2\left(X^7 - \frac{3}{2}X^8 + \frac{7}{12}X^9\right)$$

$$\begin{bmatrix} B_{1,1} & B_{1,2} & B_{1,3} & B_{1,4} & B_{1,5} \\ B_{2,1} & B_{2,2} & B_{2,3} & B_{2,4} & B_{2,5} \\ B_{3,1} & B_{3,2} & B_{3,3} & B_{3,4} & B_{3,5} \\ B_{4,1} & B_{4,2} & B_{4,3} & B_{4,4} & B_{4,5} \\ B_{5,1} & B_{5,2} & B_{5,3} & B_{5,4} & B_{5,5} \end{bmatrix} \begin{bmatrix} C_3^2 \\ C_4^2 \\ C_5^2 \\ C_6^2 \\ C_7^2 \end{bmatrix} = \begin{bmatrix} J_{2,3} \\ 0.0625J_{2,1} + 0.25J_{2,2} + J_{2,3} \\ 0.25\ J_{2,1} + 0.5\ J_{2,2} + J_{2,3} \\ 0.5625J_{2,1} + 0.75J_{2,2} + J_{2,3} \\ J_{2,1} + J_{2,2} + J_{2,3} \end{bmatrix} \tag{17}$$

$$Z_3 = C_3^3(X^3 - X^4 + 0.3X^5) + C_4^3(X^4 - 1.2X^5 + 0.4X^6) + C_5^3\left(x^5 - \frac{4}{3}X^6 + \frac{10}{21}X^7\right) + C_6^3\left(X^6 - \frac{10}{7}X^7 + \frac{15}{28}X^8\right) + C_7^2\left(X^7 - \frac{3}{2}X^8 + \frac{7}{12}X^9\right)$$

$$\begin{bmatrix} B_{1,1} & B_{1,2} & B_{1,3} & B_{1,4} & B_{1,5} \\ B_{2,1} & B_{2,2} & B_{2,3} & B_{2,4} & B_{2,5} \\ B_{3,1} & B_{3,2} & B_{3,3} & B_{3,4} & B_{3,5} \\ B_{4,1} & B_{4,2} & B_{4,3} & B_{4,4} & B_{4,5} \\ B_{5,1} & B_{5,2} & B_{5,3} & B_{5,4} & B_{5,5} \end{bmatrix} \begin{bmatrix} C_3^3 \\ C_4^3 \\ C_5^3 \\ C_6^3 \\ C_7^3 \end{bmatrix} = \begin{bmatrix} J_{3,3} \\ 0.0625J_{3,1} + 0.25J_{3,2} + J_{3,3} \\ 0.25\ J_{3,1} + 0.5\ J_{3,2} + J_{3,3} \\ 0.5625J_{3,1} + 0.75J_{3,2} + J_{3,3} \\ J_{3,1} + J_{3,2} + J_{3,3} \end{bmatrix} \tag{18}$$

$$B_{1,1} = -24,\ B_{2,1} = -\left\{15 + k\left(1 - \frac{R_V}{R}\right)^2\left[0.7498 - 0.4957\frac{R_V}{R} - 0.2541\left(\frac{R_V}{R}\right)^2\right]\right\}$$

$$B_{3,1} = -\{6 + k[1 - (R_V/R)]^2[0.3626 - 0.6625\,(R_V/R) + 0.3\,(R_V/R)^2]\}$$

$$B_{4,1} = \left\{3 - k\left(1 - \frac{R_V}{R}\right)^2\left[-0.2354 - 0.3377\frac{R_V}{R} + 0.5731\left(\frac{R_V}{R}\right)^2\right]\right\},\ B_{5,1} = 12 + k\left(1 - \frac{R_V}{R}\right)^3\left(0.4 + 0.6\frac{R_V}{R}\right)$$

$$B_{1,2} = 24,\ B_{2,2} = -\left\{3 + k\left(1 - \frac{R_V}{R}\right)^2\left[0.3805 - 0.2109\frac{R_V}{R} - 0.1695\left(\frac{R_V}{R}\right)^2\right]\right\}$$

$$B_{3,2} = -\{12 + k[1 - (R_V/R)]^2[0.425 - 0.5(R_V/R) + 0.075(R_V/R)^2]\}$$

$$B_{4,2} = -\{3 + k[1 - (R_V/R)]^2[-0.1477 - 0.2111(R_V/R) + 0.3588(R_V/R)^2]\}$$

$$B_{5,2} = \{24 + k[1 - (R_V/R)]^3[0.4 + 0.4(R_V/R)]\}$$

$$B_{1,3} = 0,\ B_{2,3} = \left\{6.25 - k\left(1 - \frac{R_V}{R}\right)^2\left[0.16 - 0.0812\frac{R_V}{R} - 0.0787\left(\frac{R_V}{R}\right)^2\right]\right\}$$

$$B_{3,3} = -\{10 + k[1 - (R_V/R)]^2[0.3824 - 0.369(R_V/R) - 0.01339(R_V/R)^2]\}$$

$$B_{4,3} = -\left\{11.24 + k\left(1 - \frac{R_V}{R}\right)^2\left[-0.05656 - 0.1758\frac{R_V}{R} + 0.2323\left(\frac{R_V}{R}\right)^2\right]\right\},\ B_{5,3} = \left[40 + k\left(1 - \frac{R_V}{R}\right)^3\left(0.3808 + 0.2858\frac{R_V}{R}\right)\right]$$

$$B_{1,4} = 0,\ B_{2,4} = \left\{7.265 - k\left(1 - \frac{R_V}{R}\right)^2\left[0.0603 - 0.02907\frac{R_V}{R} - 0.0312\left(\frac{R_V}{R}\right)^2\right]\right\}$$

$$B_{3,4} = -\{3.75 + k[1 - (R_V/R)]^2[0.2999 - 0.2606(R_V/R) - 0.0393(R_V/R)^2]\}$$

$$B_{4,4} = -\{19.02 + k[1 - (R_V/R)]^2[0.01756 - 0.1702(R_V/R) + 0.1527(R_V/R)^2]\}$$

$$B_{5,4} = \{60 + k[1 - (R_V/R)]^3[0.3572 + 0.2142(R_V/R)]\}$$

$$B_{1,5} = 0,\ B_{2,5} = \left\{5.004 - k\left(1 - \frac{R_V}{R}\right)^2\left[0.02117 - 0.00986\frac{R_V}{R} - 0.01131\left(\frac{R_V}{R}\right)^2\right]\right\}$$

$$B_{3,5} = \{2.625 - k[1 - (R/R_V)]^2[0.2161 - 0.1764(R/R_V) - 0.0397(R_V/R)^2]\}$$

$$B_{4,5} = -\{48.11 + k[1 - (R_V/R)]^2[0.072 - 0.1721(R_V/R) + 0.1001(R_V/R)^2]\}$$

$$B_{5,5} = \{83.88 + k[1 - (R_V/R)]^3[0.3328 + 0.1666(R_V/R)]\}$$

In designing a rotor blade for bending, it is necessary to assume a bending rigidity EI of the blade in order to investigate the stress in the structure. The bending stress can be calculated if the applied forces, represented on the right-hand side of the matrix equations, and the parameter k are known for a certain helicopter or autogiro. The coefficients C_1^i, C_3^i, ... can then be determined from the matrix equations. The corresponding bending moments are:

$$M_1 = \frac{EI}{R}[6C_3^1X + 12(-C_3^1 + C_4^1)X^2 + 2(3C_3^1 - 12C_4^1 + 10C_5^1)X^3 + 2(6C_4^1 - 20C_5^1 + 15C_6^1X^4) + 20(C_5^1 - 3C_6^1)X^5 + 30C_6^1X^6]$$

$$M_2 = \frac{EI}{R}[6C_3^2X + 12(-C_3^2 + C_4^2)X^2 + 2(3C_3^2 - 12C_4^2 + 10C_5^2)X^3 + 2(6C_4^2 - 20C_5^2 + 15C_6^2)X^4 + 2(10C_5^2 - 30C_6^2 + 21C_7^2)X^5 + 2(15C_6^2 - 42C_7^2)X^5 + 42C_7^2X^7]$$

$$M_3 = \frac{EI}{R}[6C_3^3X + 12(-C_3^3 + C_4^3)X^2 + 2(3C_5^3 - 12C_4^3 + 10C_5^3)X^3 + 2(6C_4^3 - 20C_5^3 + 15C_6^3)X^4 + 2(10C_5^3 - 30C_6^3 + 21C_7^3)X^5 + 2(15C_7^3 - 42C_7^3)X^6 + 42C_7^3X^7]$$

$$M_{EL} = M_1 + M_2\cos\psi + M_3\sin\psi \qquad (19)$$

In case the assumed EI is not satisfactory—i.e., the structure is either too weak or too strong—a new value of EI may be assumed and a set of new coefficients calculated. The constants k and $J_{n,m}$ in the matrix Eqs. (16). to (18) may be changed simply by multiplying some of the terms by the factor $(EI_{new})/(EI)_{old}$. Hence, the calculation is considerably simplified.

Blade with Variable Mass Distribution

The expressions given in the previous section are valid only for a uniform mass, modulas of elasticity, and moment of inertia distribution along the span of the blade. When these parameters vary along the span of the blade, Eq. (10) may be rewritten in the form:

$$\eta(X)\frac{d^4Z}{dX^4} + 2\eta'(X)\frac{E_0'I_0'}{E_0I_0}\frac{d^3Z}{dX^3} - \left[k_0\xi(X)\left(1 - \frac{R_V}{R}\right)R_1(X) - \eta''(X)\frac{E_0''I_0''}{E_0I}\right]\frac{d^2Z}{dX^2} + 2k_0\xi(X)\left(1 - \frac{R_V}{R}\right)^3R_2(X)\frac{dZ}{dx} + \frac{2k_0}{\omega^2}\xi(X) \times \left(1 - \frac{R_V}{R}\right)^4\frac{d^2Z}{dt^2} = -\frac{R^3}{E_0I_0}\left(1 - \frac{R_V}{R}\right)^4\frac{dS}{dr} \qquad (20)$$

where

$$k_0 = \frac{m_0R^4\omega^2}{2E_0I_0},\quad \xi(X) = \frac{m(X)}{m_0},\quad \eta(X) = \frac{E(X)I(X)}{E_0I_0}$$

$$\eta'(X) = \frac{E'(X)I'(X)}{E_0'I_0'},\quad \eta''(X) = \frac{E''(X)I''(X)}{E_0''I_0''},$$

$$E'I' = \frac{d(EI)}{dX},\quad E''I'' = \frac{d^2(EI)}{dX^2}$$

The subscript 0 represents a specified reference section along the span of the blade.

The term dS/dr on the right-hand side of Eq. (20) differs from the expression given for it in Eq. (11) only in that m in the latter is changed to $\xi(X)m_0$.

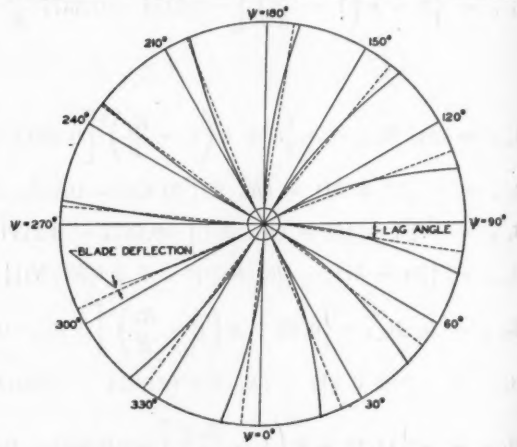

FIG. 5. Lag angles and deflections of rotor blade at various azimuth angles Ψ in plane of rotation calculated for typical tapered spare blade.

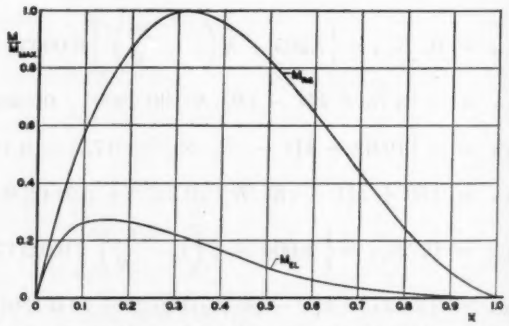

FIG. 6. Comparison of bending moments of rigid and elastic blade calculated for typical tapered spare blade.

In solving Eq. (20) the same method can be employed as that used in the solution of Eq. (10). This again leads to matrix equations from which the coefficients of X in the polynomials representing Z_1, Z_2, and Z_3 are determined. In the solution of the matrix equations the mass distribution function $\xi(X)$, bending rigidity function $\eta(X)$, and its derivatives $\eta'(X)$ and $\eta''(X)$ are specified at five stations along the blade span—namely, at $X = 0$, $1/4$, $1/2$, $3/4$, and 1. It was found that this approximate solution was accurate enough for practical applications.

Examples

Numerical examples were worked out in order to demonstrate the significance of the bending of the rotor blade in the plane of rotation and to show the differences in the bending moments calculated for a constant-section blade and an actual blade with variable mass and moment of inertia distribution. The results of the calculations are shown in Figs. 5 to 8. The numerical work was carried out according to the theory just presented, but on the basis of five rather than three terms in the Fourier expansions.

Fig. 5 shows the lag angles and deflections of a rotor blade at various values of ψ, the angle of rotation in the plane of rotation. In Fig. 6 the bending moments of the rigid blade are compared with those of the elastic blade. Fig. 7 presents a comparison of the bending moments along an assumed constant-section blade with those along a typical actual blade of variable section. Finally, in Fig. 8 the bending moments in the plane of rotation are compared with the bending moments in the flapping plane.

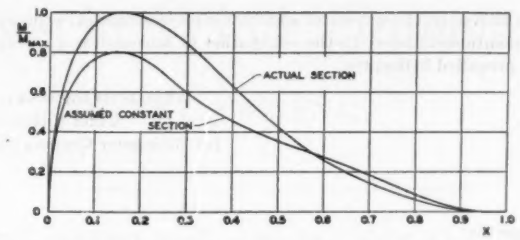

FIG. 7. Comparison of bending moments of actual section and assumed constant section.

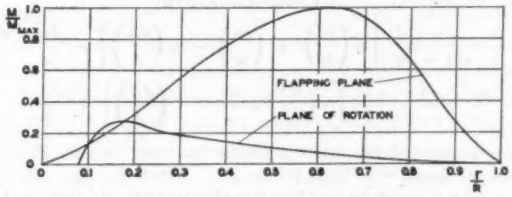

FIG. 8. Comparison of bending moments in the flapping plane and the plane of rotation for assumed constant section.

Bibliography

Frazer, R. A., Jones, W. P., Skan, S. W., *Approximations to the Function and to the Solution of Differential Equation*, R. & M. No. 1709, British ARC, 1937.

Huxton, Nutt, Bigg, and Beavan, *General Investigation into the Characteristic of the C-30 Autogiro*, R. & M. No. 1859, British ARC, 1939.

Letters to the Editor

Dear Sir:

I have read with considerable interest the paper "On the Steady Flow of a Gas Through a Tube with Heat Exchange or Chemical Reaction" by Paul Chambré and Chia-Chiao Lin, which appeared in the October, 1946, issue of the JOURNAL. I was, however, surprised to find several conclusions that were emphasized as if they were obtained by the authors, whereas, in fact, they were previously presented in more detailed and expressive form, by Szczeniowski in his paper entitled "Flow of Gas Through a Tube of Constant Cross-Section with Heat Exchange . . . .," which appeared in the January, 1945, issue of the *Canadian Journal of Research*.

The point is that, although Szczeniowski's paper is cited among the references by Messrs. Chambré and Lin, there is not the slightest mention in the text of their paper (even the footnote number is omitted in the text), while:

(1) The theory developed in Section 2 follows assumptions and lines similar to those of Szczeniowski.

(2) Investigations given in Section 3 are, in principle, identical with those of Szczeniowski.

(3) Several conclusions given by the authors in italics and concerning the velocity of flow in a tube of constant cross section, the tendency of flow to reach the sonic state, the temperature change (i.e., conditions for temperature decrease while heat is introduced and vice versa), etc., are simply borrowed from Szczeniowski's paper, with no mention made as to the origin.

Thus, the reader of the article is led to suppose that the authors have for the first time discovered a few interesting aerothermodynamic phenomena—which is not the case. Let me cite, for instance, the following sentence from the authors' conclusion: "This paper is. . . . . It is certainly only the beginning of a more extensive investigation but already it has brought out rather interesting results. For example, it must now be kept in mind that the addition of heat to a flow system does not necessarily lead to an increase in temperature. Such results are somewhat surprising. . . . ." Of course, they are no more surprising in October, 1946, than they were in January, 1945, when they were presented in Szczeniowski's paper.

I should like to take this opportunity of pointing out that introducing a change of mole number in computations, however interesting it may be theoretically, has no practical influence if applied to jet propulsion. It is known that this change of mole number is small even in theoretically correct burning mixtures; in burners of jet engines, moreover, a considerable air excess must be applied for technological reasons. The actual amount of air here exceeds the theoretical by not less than three times. This

was proved by the successful application of Szczeniowski's theory, as mentioned above, to the calculation of burners for a certain jet-propelled helicopter.

WITOLD BRZOZOWSKI
Chief Engineer
Jet Helicopter Corporation

Dear Sir:

Controlling the Eqs. (7)–(13) in the paper by Chambré and Lin we have found that a term dA/A is lost on the right side of Eqs. (10) and (11). They should be written

$$\frac{dT}{T} = \frac{1-\gamma M^2}{\gamma(1-M^2)}\left[\gamma\left(\frac{\delta a}{H}\right) + \left(\frac{\delta n}{n}\right) - \gamma\left(\frac{dA}{A}\right)\right] - \frac{dn}{n} + \frac{dA}{A}$$

$$\frac{da^2}{a^2} = \frac{1-\gamma M^2}{\gamma(1-M^2)}\left[\gamma\left(\frac{\delta Q}{H}\right) + \frac{\delta n}{n} - \gamma\left(\frac{dA}{A}\right)\right] + \frac{dA}{A}$$

We discovered this when treating the case "Steady Flow at Constant Speed with Heat Exchange." Then the Eqs. (7)–(13) gave (with $du = 0$) $dp = dT = 0$, which is obviously abnormal.

BENGT JACOBSSON
Svenska Flygmotor Aktiebolaget
Projektavdelningen, Sweden

Dear Sir:

The wide interest on the subject of gaseous combustion, as shown by the comments and criticisms on the paper by Chambré and Lin, is certainly encouraging. On the other hand, the misunderstanding associated with some of these comments is unfortunate. For instance, Mr. Brzozowski quoted that the authors described as surprising the phenomenon of a possible decrease of temperature of a flowing gas upon heat addition, while the authors actually meant to say that this phenomenon is *by no means* surprising. (The complete last sentence, partly quoted by Brzozowski from the original paper, reads: "Such results are somewhat surprising *if* one is not aware of the inertia forces that must enter the picture of rapid motion of fluids." Mr. Brzozowski omitted the conditional clause in his quotation.) In the text (col. 1, p. 539), as soon as this fact is stated, the physical interpretation is given and its consistency with the second law of thermodynamics is pointed out. A similar physical interpretation is repeated in the letter of Dr. Wood to the JOURNAL.

I should like therefore to explain a few things regarding the paper under discussion. The work was completed in late 1946 when the authors were beginning to study the problem of combustion. The chief concern was to stress the fact that *the aerodynamic forces must be considered in the problem of combustion and that the study of fuels of various types is probably not as important.* The authors then went on to the investigation of the effect of turbulence in the flame front, and this first part of the paper was left untouched. It was roughly edited and submitted when one of the authors was leaving the Jet Propulsion Laboratory, GALCIT. In the meantime, we read the paper of Professor Szczeniowski, and inserted a reference to it. Obviously, the reference number should be in the second sentence of the introduction, since the references are listed in the order in which they are cited. We wish to apologize to Professor Szczeniowski for this unfortunate omission. We wish also to thank Dr. Wood and Mr. Jacobsson for the correction of the other obvious slips, which occurred under similar circumstances.

We regret very much that we could not have given proper credit to Dr. Hicks. As far as we know, the report by Dr. Hicks was declassified and distributed at about the same time the paper appeared in print. (The first declassified copy was received here at Brown University on October 16, 1946.) It is clear that Dr. Hicks and Professor Szczeniowski reached similar results independently, although the declassification took place a year and a half after Professor Szczeniowski's paper had been published. There might conceivably be others who have reached similar results during these years of restricted publication.

We wish, however, to mention the following points to explain why Professor Szczeniowski's paper was not discussed in detail. In doing so, we hope also to make it clear that the main problems we have in mind are not the ones already considered.

(1) Our main interest is in the mechanism of combustion, which implies other considerations besides heat transfer. Only the part discussed in Section 3 is connected with Professor Szczeniowski's results. Even in this case, our discussions can be easily extended to include the case where γ is not a constant, while his discussions are essentially based on a constant value of γ.

(2) Indeed, after the general equations [Eqs. (7)–(13)] have been written down, many more conclusions can be obtained in addition to those given in the *special* case treated in Section 3 to which the main criticism was directed. Some of these are given in Section 4, which are related to condensation and detonation shocks. Even in the special case of constant mole number, the change of cross section has interesting consequences. For example, *in an expanding tube, the flow may depart more and more from the sonic state while it is being heated. In a contracting tube, the temperature of the gas may decrease during heating for a certain range of Mach Numbers less than* $1/\sqrt{\gamma}$. These conclusions follow immediately from our general equations, but do not seem to be in the scope of Professor Szczeniowski's paper.

(3) The second paragraph of Professor Szczeniowski's Abstract puzzles us very much. It states: "The conclusion is reached that the velocity of flow in the tube, if the tube is heated or cooled, shows a natural and permanent tendency to reach the velocity of sound, after which the heat exchange is no longer possible." As far as we can see, cooling does not lead the stream to the sonic state.

(4) It seems that Professor Szczeniowski hesitated to conclude the physical reality of decreasing temperature associated with heat addition. (Cf. the discussions after p. 8 of his paper.) So far as heat transfer is concerned, the frictional effect discussed by Dr. Wood is enlightening. So far as combustion is concerned, there is no doubt that such a phenomenon does occur.

Although our chief aim is to study the phenomenon of combustion without immediate concern toward application, I wish also to say one word about a remark of Mr. Brzozowski regarding the practical application of our results to jet propulsion. The use of monopropellants in rocket tubes is certainly an example of jet propulsion where the change of mole number should be considered.

Finally, I wish to reiterate that the purpose of the paper is to stress the point that in combustion problems it is important to *bear in mind* the dynamical forces. The individual conclusions are cited to exemplify this point. One should really not be too concerned with them. Also, the method of approach used is elementary and has been used by various authors.* We would like to admit the priority of Professor Szczeniowski and Drs. Hicks and Wood concerning the two results they obtained, but we believe that we have considered a much more general problem and added a few more conclusions. We still feel, however, that we are not very far in the problems of combustion, and we are humbly looking forward to some further developments in these directions instead of concentrating our attention on a few simple results already obtained.

C. C. LIN
Brown University

* E.g., Bailey, N. P., JOURNAL OF THE AERONAUTICAL SCIENCES, Vol. 11, p. 231, 1944.

Shock-Wave Oscillations in Wind Tunnels

HANS-WOLFGANG LIEPMANN* AND HARRY ASHKENAS†
California Institute of Technology

SUMMARY

A simple choking device for use in transonic flow experiments is described. It is shown that most observed shock-wave oscillations in wind tunnels are due to speed fluctuation and can be eliminated by using a choking device.

INTRODUCTION

SCHLIEREN OBSERVATIONS of shock waves in transonic flow, such as on airfoil sections, in ducts, etc., show that the waves are generally unsteady, oscillating over appreciable distances. This apparent unsteadiness of shock waves has often been accepted as a typical phenomenon of transonic flow. This view was supported by some flight observations of severe buffeting in transonic flow.

During investigations of the supersonic zone on airfoil sections at the GALCIT, it was realized that, in order to increase the accuracy of measurements, an attempt should be made to stabilize the flow. It was then found that *most observed shock-wave oscillations are introduced by the wind tunnel* and can be stopped by means of a "choking" device downstream from the model in the test section or diffuser. A simple device of this sort has been used with excellent results for some time in the 2- by 20-in. Transonic Tunnel at the GALCIT. The present paper describes this device and its application.

The stabilization of shock waves in wind tunnels and ducts is of considerable practical and theoretical importance. The usual rapid motion of a shock wave causes inherent errors in pressure distribution and force measurements because of the difficulty of obtaining these measurements with an instrument of small time lag. This shock-wave instability also introduces nonstationary effects that are difficult to evaluate. There are additional important consequences in connection with the comparison with free-flight data and especially shock-buffeting problems. From the analytical point of view, it is, of course, important to know whether the positions of the shock waves in flow with local supersonic regions are well defined or not.

The large-scale oscillations of the shock wave that were observed in the 2- by 20-in. Transonic Tunnel were, in general, due to fluctuations of the tunnel flow (i.e., to fluctuations in mean speed, not to turbulence). The shock oscillations appeared to be less pronounced than had been noted in previous observations elsewhere. This was attributed to the comparatively steady flow in the tunnel and led to an attempt to decrease the fluctuations and pulsations even more.

To obtain constant mass flow in the tunnel, a constriction of the test-section area was established downstream of the model, and the tunnel operated in such a fashion that this constriction "choked," i.e., sonic velocity was attained there. The Mach Number in the test section is then, as in supersonic wind tunnels, determined by the area ratio of test section to throat. This procedure proved successful and the shock waves became steady. This second throat also provides an excellent method of speed control. A change in the throat area can be calibrated directly in Mach Number regardless of Reynolds Number; or, at a given throat area, the Reynolds Number can be altered by changing the pressure in the tunnel while the Mach Number remains fixed by the area ratio.

The authors believe that the establishment of such a throat area is necessary for all measurements in the transonic range, except in cases in which the unsteadiness of flow and the subsequent loss of accuracy in the measurements are of minor importance. The important parameter in the transonic range is not the

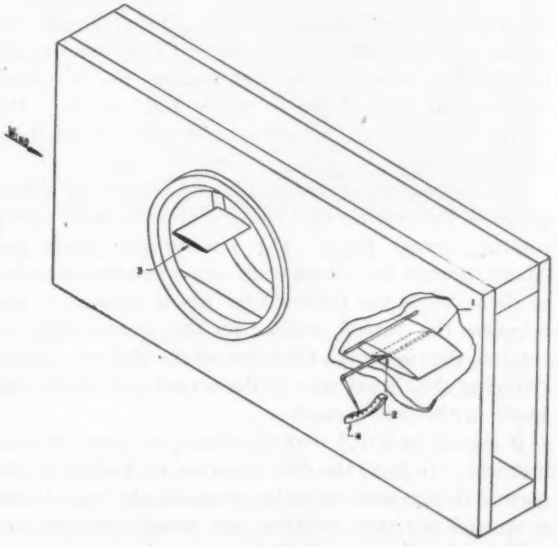

FIG. 1. Sketch of test section showing the choke, composed of flexible airfoil (1), with rotating center piece (2), downstream from the model (3). The position of the center piece is shown on the scale (4).

Received November 6, 1946.

* Associate Professor of Aeronautics.

† Research Assistant.

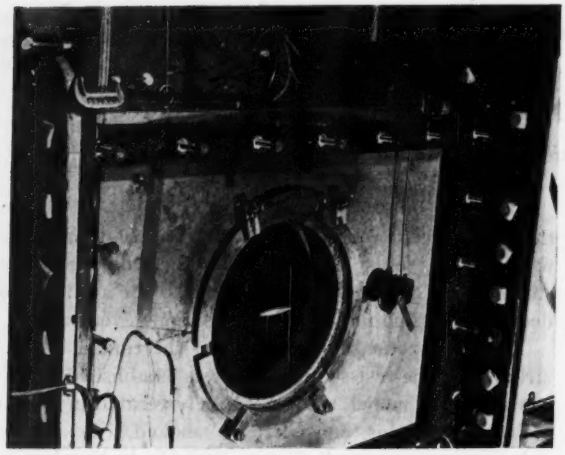

FIG. 2. Test section of the GALCIT 2- by 20-in. transonic wind tunnel, showing the motor drive for the choking unit speed control.

Mach Number, M, but the parameter $\beta = \sqrt{1 - M^2}$. The use of β instead of M shows immediately that the transonic speed range is not so small as it appears when the Mach Number only is considered. The necessary precision of Mach Number setting increases as M approaches unity, since

$$\left|\frac{d\beta}{\beta}\right| = \frac{M^2}{1 - M^2}\left|\frac{dM}{M}\right|$$

APPARATUS

Choke

The variable choking device is shown in Fig. 1. Fig. 2 is a photograph of the test section of the 2- by 20-in. Transonic Tunnel at GALCIT showing the motor drive for the choking unit. Using this device, the Mach Number in the test section can be varied continuously from 0.700 to 0.905, and values of the Mach Number may be reproduced with an accuracy of 0.5 per cent.

The choking device is a flexible airfoil formed of two pieces of thin spring steel, hinged at both ends, and a rotating center piece. The leading-edge hinge pin passes through the tunnel walls and is fastened securely to them, while the trailing-edge pin is allowed to slip between the tunnel walls. As the center piece is rotated, the maximum thickness of the choke is varied, changing the throat area of the tunnel and, hence, the speed in the test section.

It should be noted that the choke need not be symmetrical. In fact, the first experiments leading to the present design were made by spanning the tunnel with a streamlined strut section and merely rotating the strut. Observation with the tunnel schlieren apparatus does not reveal any asymmetrical flow conditions in the test section with such an asymmetrical choke.

Mach Meter

A simple and inexpensive form of Mach Number meter (Fig. 3) has been developed in conjunction with the speed control. The meter consists of a large board on which are mounted two mercury tubes, one of which is a barometer-type tube, measuring absolute pressure, while the other is a U-tube formed by a capillary tube and a large diameter reservoir. The static pressure is measured by the barometer tube, and the difference $(p_0 - p)$ between stagnation pressure (p_0) and static pressure (p) is measured by the U-tube. The scales of these two tubes are also the scales of a nomograph, the slanting scale of which is also mounted on the manometer board. Movable pointers run along the scales and the indicating line of the nomograph (in the form of a fine thread) is attached to the pointers. The Mach Number is read directly from the slanting scale, which has been calculated* through use of the well-known isentropic pressure relation:

$$p_0/p = \{1 + [(\gamma - 1)/2]M^2\}^{\gamma/(\gamma-1)}$$

* Calculation of the nomograph and the design of the meter are due to P. Johnson.

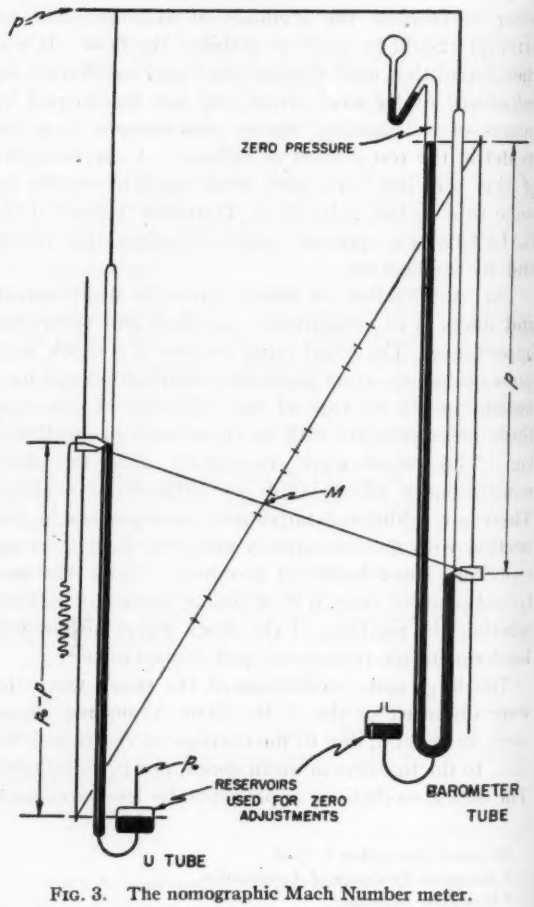

FIG. 3. The nomographic Mach Number meter.

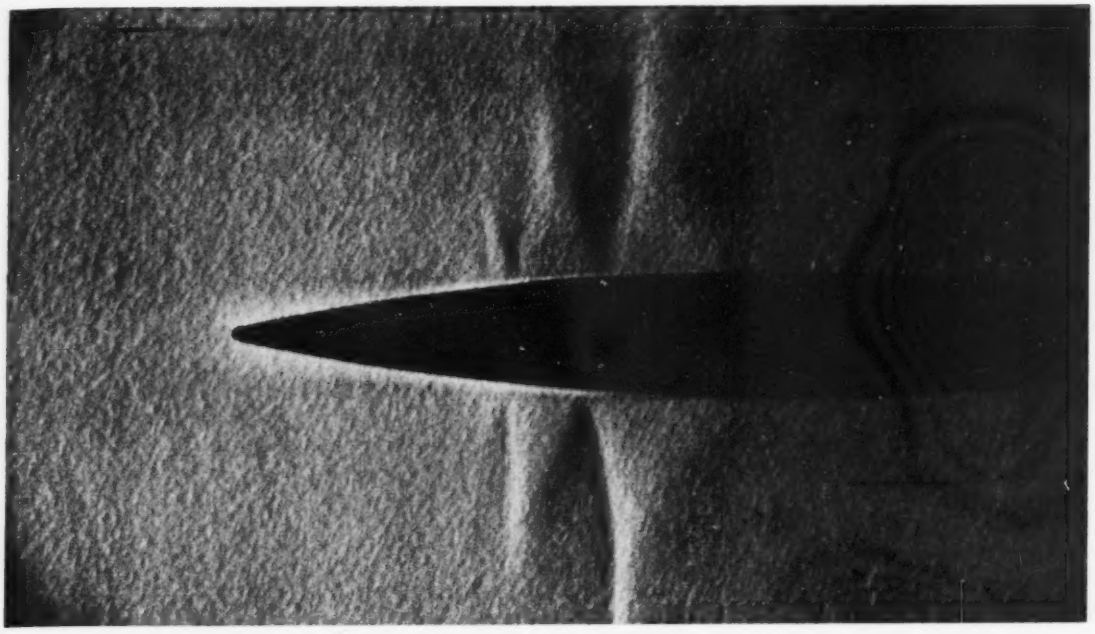

FIG. 4a. Schlieren photograph of flow past 3-in. by 12 per cent circular arc airfoil at $M_\infty = 0.844$. Tunnel choked. Exp., 1/100 secs. Knife edge normal to mean flow direction.

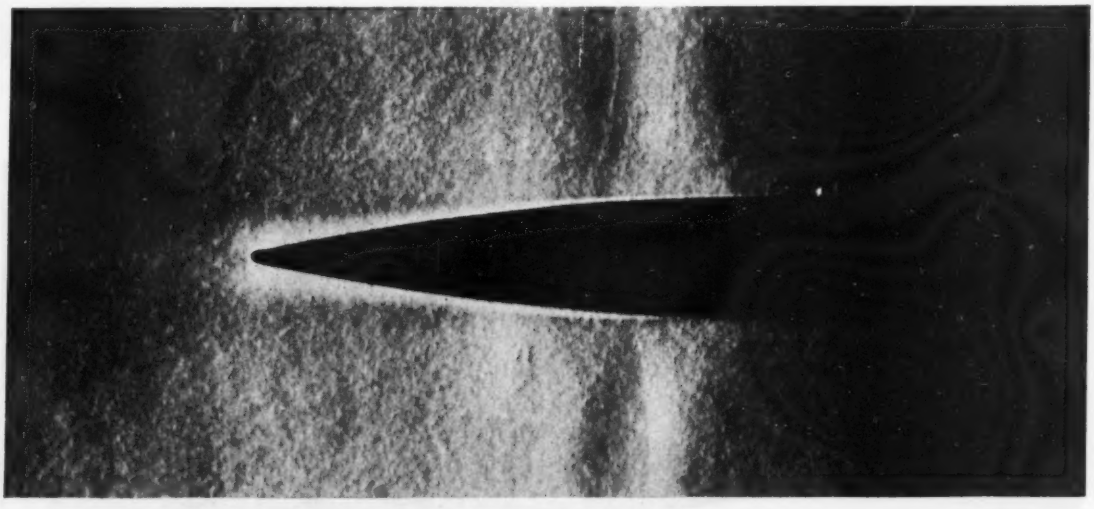

FIG. 4b. Schlieren photograph of flow past 3-in. by 12 per cent circular arc airfoil at $M_\infty = 0.844$. Tunnel not choked. Exp., 1/100 secs. Knife edge normal to mean flow direction.

The Mach Number scale is such that variations in the third decimal of the Mach Number are easily discernible.

RESULTS

The type of speed control described, in addition to providing maximum flexibility of operation, serves to decrease the oscillating nature of the shock wave. In the past, rapid fluctuations of the free-stream Mach Number due to diffuser separation and variation in other losses throughout the tunnel have caused the shock wave to oscillate over as much as 20 per cent of the airfoil chord at a given tunnel-speed setting. By creating a supersonic region (through use of the choke) at the exit of the test section, the disturbances from the diffuser are not allowed to travel upstream. Then, since the mass flow through the test section must remain constant by virtue of the sonic speed at the throat, it follows that the free-stream Mach Number in the test section must also remain constant and, thus, oscillations of the shock wave are kept to a minimum.

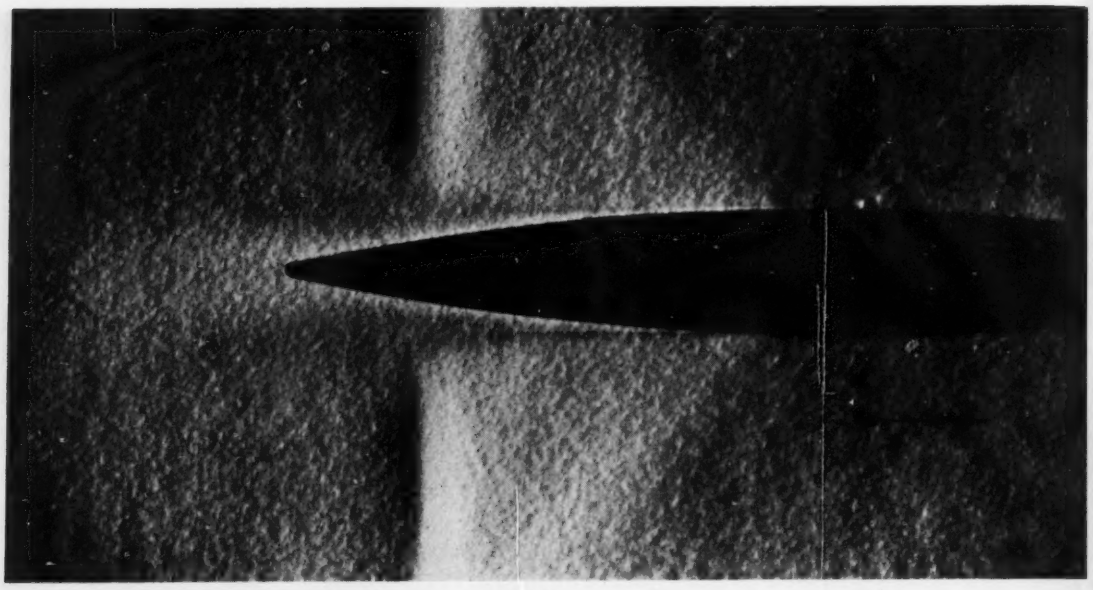

FIG. 5a. Schlieren photograph of flow past 3-in. by 12 per cent circular arc airfoil at $M_\infty = 0.902$. Tunnel choked. Exp., 1/100 secs. Knife edge normal to mean flow direction.

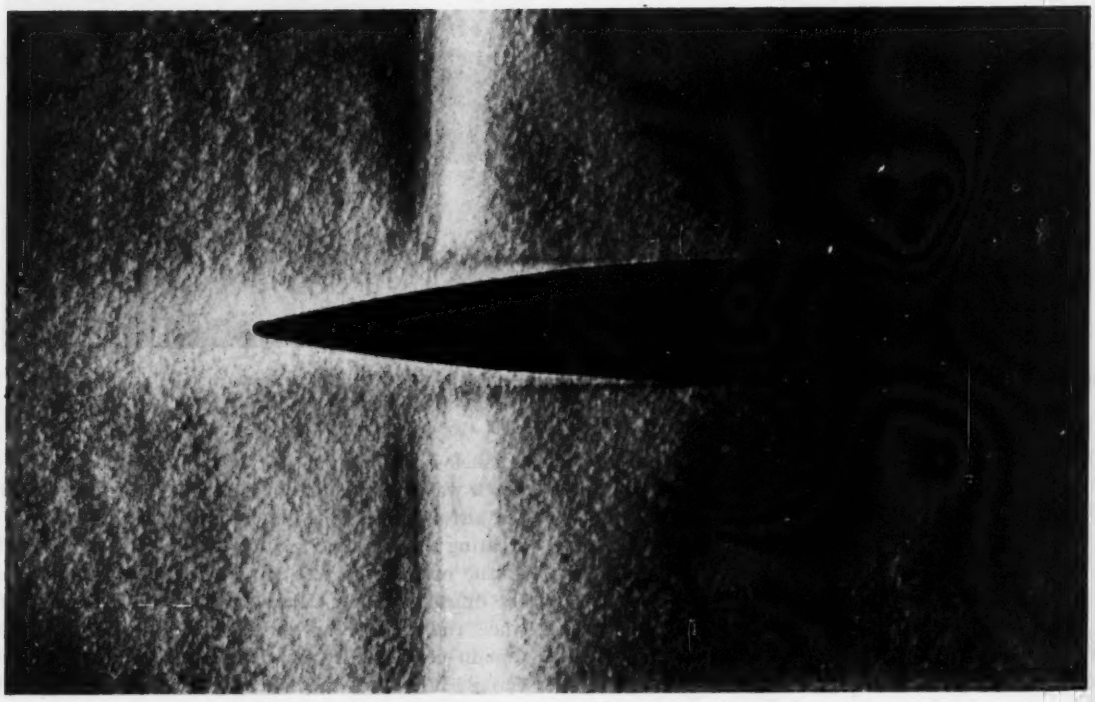

FIG 5b. Schlieren photograph of flow past 3-in. by 12 per cent circular arc airfoil at $M_\infty = 0.902$. Tunnel not choked. Exp., 1/100 secs. Knife edge normal to mean flow direction.

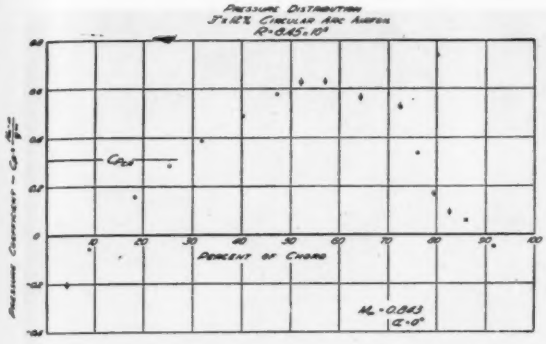

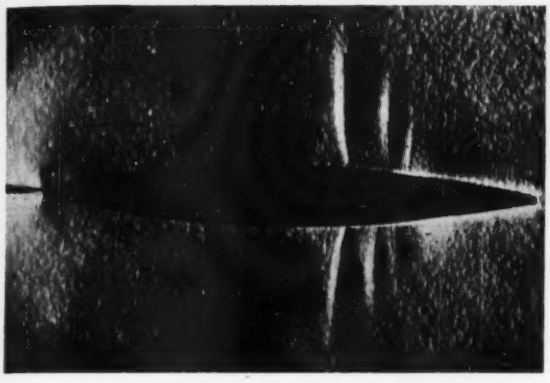

FIG. 6. Comparison between pressure distribution measurements (*top*) and schlieren photograph. Knife edge normal to mean flow direction. Exp., 1/100 secs.

The decrease in shock-wave fluctuation is graphically illustrated by Figs. 4 and 5, which were taken with continuous light at an exposure of $^1/_{100}$ sec. Figs. 4a and 5a show the shock wave on the airfoil with the tunnel running at the choked condition, while Figs. 4b and 5b show the same shock wave in the unchoked tunnel.

The effect of the choking speed control on pressure distribution surveys is as striking as that on shock-wave oscillations. Pressure-distribution measurements show none of the rapidly fluctuating qualities commonly associated with transonic pressure surveys. Pressure surveys may be compared directly with schlieren photographs. A typical comparison of a pressure measurement and a schlieren photograph is shown in Fig. 6.

The large shock "thickness" shown in Fig. 4a indicates that the shock wave is not completely motionless. This is evident from Figs. 7 and 8, where a comparison is made between schlieren photographs taken with a spark (Figs. 7a and 8a) at an exposure of 4×10^{-6} sec. and those taken with continuous light (Figs. 7b and 8b) at an exposure of $^1/_{100}$ sec. In order to determine the possible cause of the remaining oscillations of the shock wave, a curve of shock wave position vs. the transonic parameter $\beta = \sqrt{1 - M^2}$ (Fig. 9) has been plotted. The data from which this curve is drawn were taken from schlieren photographs made with continuous light; the position of the shock wave is easily read from such photographs.

This curve may be used to calculate approximately the change in throat area required to cause the shock "thickness" of Figs. 7b and 8b if the assumption is made that the thickness of the shock is due simply to

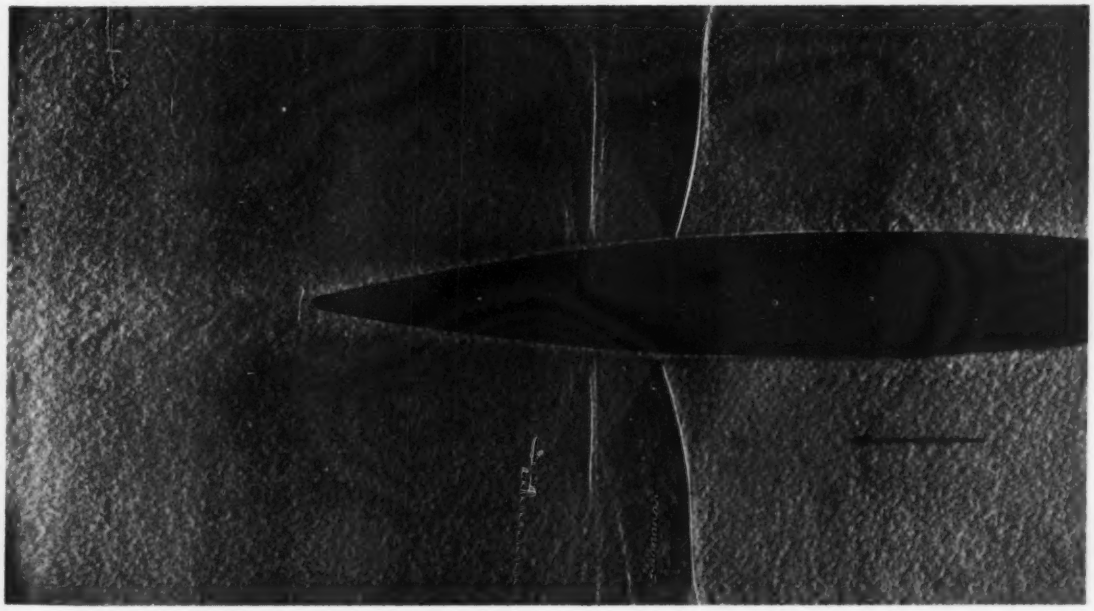

FIG. 7a. Schlieren photograph of flow past 3-in. by 12 per cent circular arc airfoil at $M_\infty = 0.844$. Tunnel choked. Exp., 4×10^{-6} secs. Knife edge normal to mean flow direction.

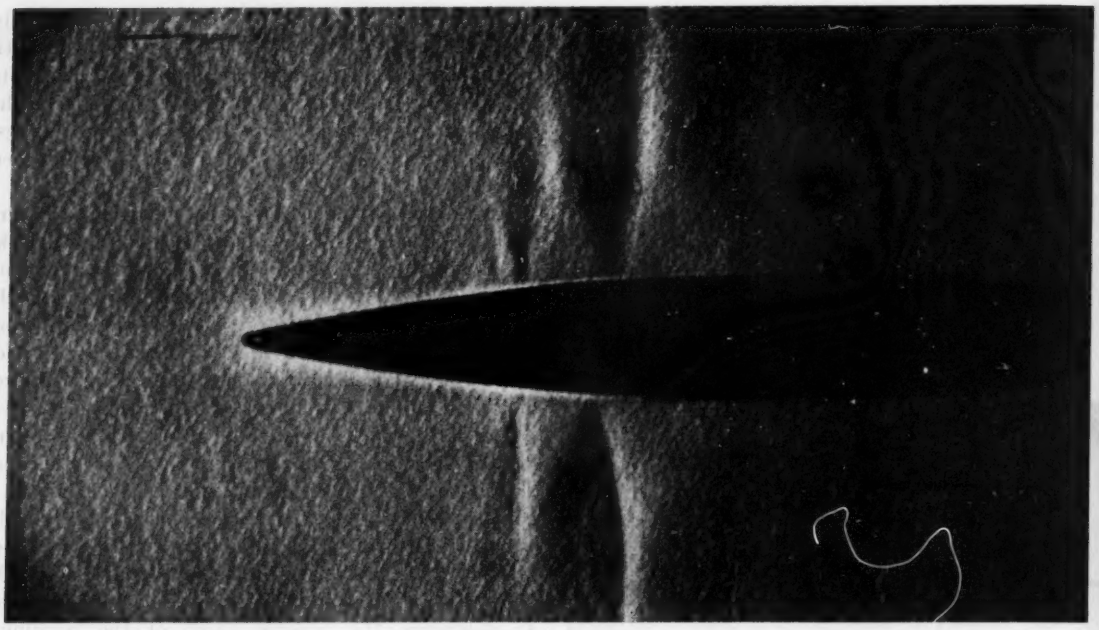

FIG. 7b. Schlieren photograph of flow past 3-in. by 12 per cent circular arc airfoil at $M_\infty = 0.844$. Tunnel choked. Exp., 1/100 secs. Knife edge normal to mean flow direction.

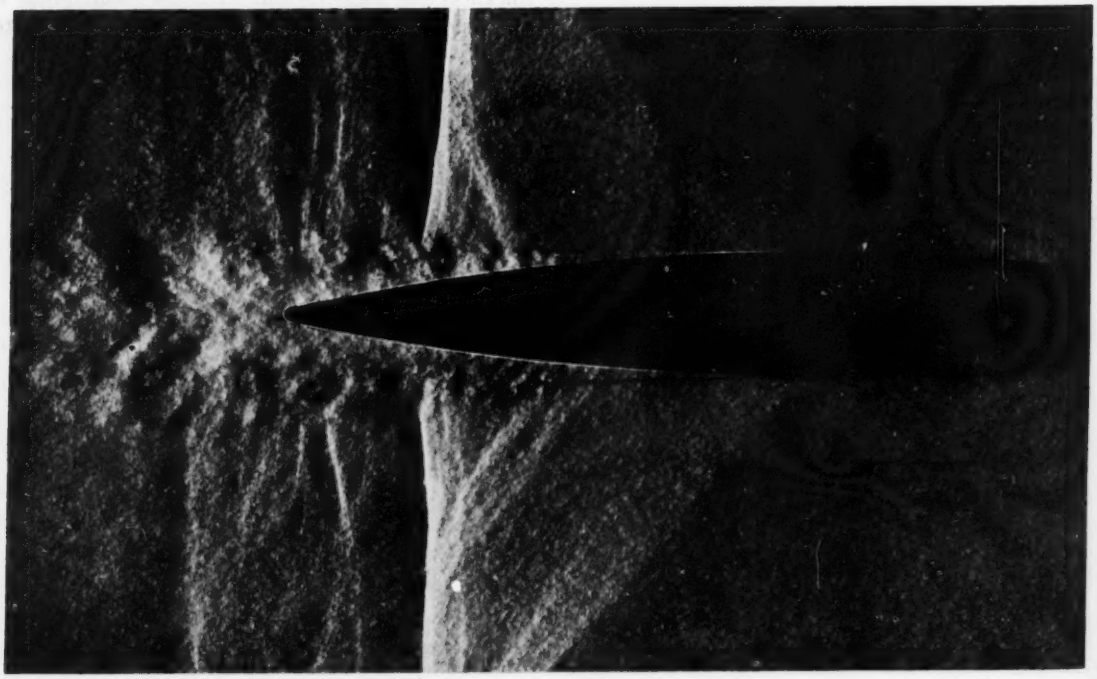

FIG. 8a. Schlieren photograph of flow past 3-in. by 12 per cent circular arc airfoil at $M_\infty = 0.902$. Tunnel choked. Exp., 4×10^{-6} secs. Knife edge normal to mean flow direction.

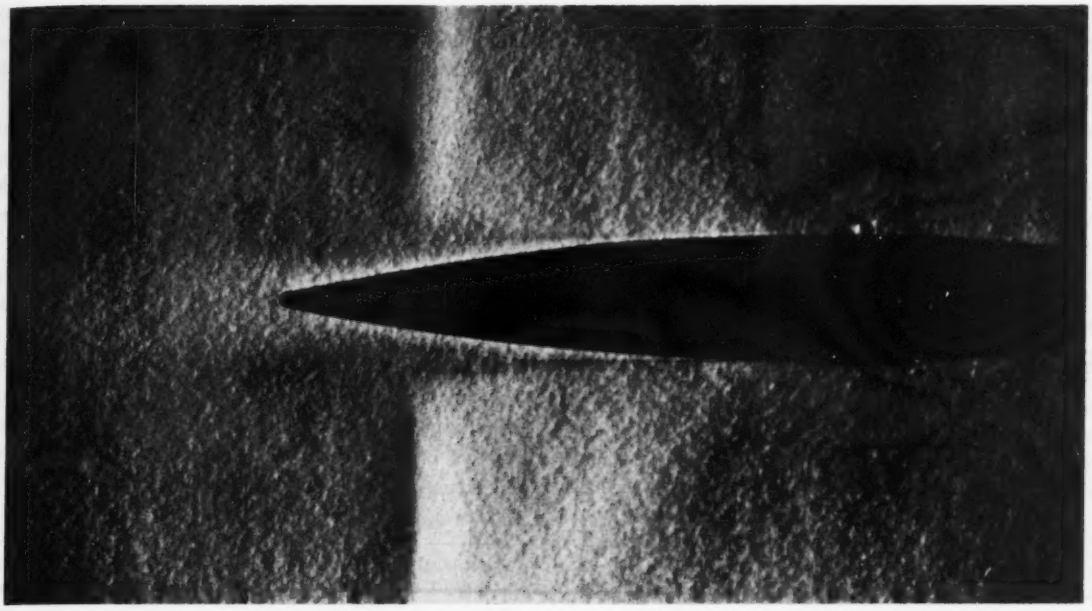

FIG. 8b. Schlieren photograph of flow past 3-in. by 12 per cent circular arc airfoil at $M_\infty = 0.902$. Tunnel choked. Exp., 1/100 secs. Knife edge normal to mean flow direction.

the fact that the shock is moving during the exposure of the film. Using simple one-dimensional gas dynamics, the variation of Mach Number with throat area may be determined; thus:

$$\frac{A}{A^*} = \left(\frac{2}{\gamma+1}\right)^{(\gamma+1)/2(\gamma-1)} \times \left[\left(1+\frac{\gamma-1}{2}M^2\right)^{(\gamma+1)/2(\gamma-1)} / M\right]$$

or

$$\frac{dM}{dA^*} = \frac{\left(\frac{\gamma+1}{2}\right)^{(\gamma+1)/2(\gamma-1)}}{A} \times \left[\frac{\left(1+\frac{\gamma-1}{2}M^2\right)^{(3\gamma-1)/2(\gamma-1)}}{1-M^2}\right]$$

dx/dM may be measured from Fig. 9; dA^* may then be computed for any apparent shock thickness.

Computation shows that a change of 0.001 in. in all dimensions at the throat could account for a Mach Number variation sufficient to cause the apparent "thickness" of the shock wave. Changes of this magnitude can be due to fluctuations in the thickness of the boundary layer. Thus, with the present arrangement it is difficult to determine how much of the remaining shock oscillation is "real" and how much is due to the wind tunnel. There is little doubt that a certain amount of the shock oscillation must be due to boundary-layer fluctuations on the model itself and, thus, is "real"—that is, is independent of the tunnel characteristics. Subsequent investigations must show the magnitude of these oscillations. At this time, real shock-wave fluctuations have been definitely observed only when the base of the shock wave almost coincides with the transition point of the boundary layer on the model.

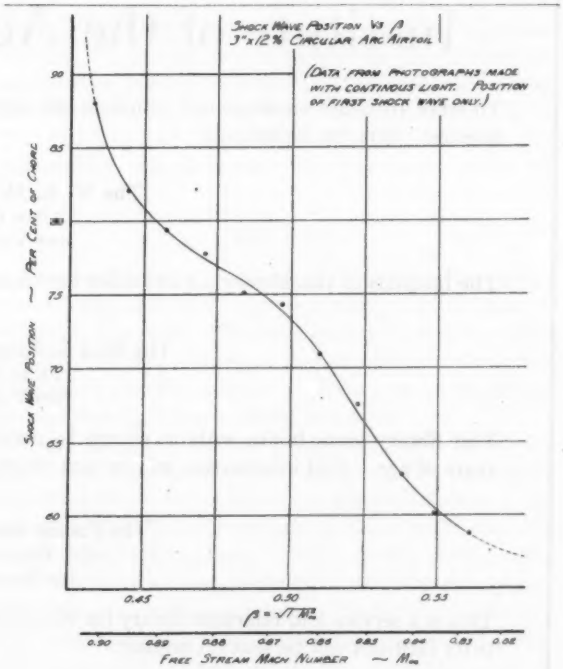

FIG. 9.

Conclusions

The speed control of wind tunnels operating in the transonic range must be considerably more precise than that of subsonic wind tunnels. The use of a choking device to stabilize and control the Mach Number appears to be the best choice for a transonic wind tunnel. It should be noted, however, that the use of such a device in a tunnel requires the expenditure of considerably more power than is ordinarily necessary. The energy ratio of a tunnel operated with a choking device is thus far lower than that of an ordinary subsonic tunnel. Such an increase in power consumption, however, is well warranted by the advantages to be gained. If a transonic wind tunnel is to be equipped with such a device, it should be remembered that the speed fluctuations due to oscillation of the wall boundary layer can be reduced by using large test-section cross sections.

The conditions prevailing in a choked transonic wind tunnel are, in general, nearly the same as those present in a normal supersonic tunnel. The fact that the quality of the flow downstream from the throat of a transonic tunnel is of no importance merely represents a greater latitude in the design of such a tunnel and makes the use of a variable throat area much simpler for operation in the transonic region than in the supersonic region.

The results presented here show that *observed buffeting phenomena in transonic flight are not connected with the hitherto observed shock oscillations in wind tunnels*. The buffeting is likely to be caused by a combination of structural oscillations and airspeed fluctuations rather than by any inherent characteristics of transonic flow. Further research is evidently needed to clarify this point.

Library Facilities of the Institute of the Aeronautical Sciences

To serve Institute members and others in the aeronautical industry, the Institute of the Aeronautical Sciences offers the facilities of:

The W. A. M. Burden Library
2 East 64th Street
New York 21, N.Y.

The facilities of this library are available for reference study at the Institute.

The Paul Kollsman Lending Library
2 East 64th Street
New York 21, N.Y.

This library loans books without charge to members and others in the United States over eighteen years of age. Full information will be sent on request.

The Pacific Aeronautical Library
6715 Hollywood Boulevard
Los Angeles 28, Calif.

This is a service and reference library for West Coast members and organizations. Full information as to its facilities will be sent on request.

The Rate of Descent of Parachutes from Various Altitudes

KENNETH E. PENROD,* GEORGE L. MAISON,* AND JAMES E. McDONALD†

Boston University School of Medicine and Iowa State College

SUMMARY

One-hundred and eleven observations were made on the descent times of 200-lb. torso dummies attached to 28-ft. silk, 28-ft. nylon, and 24-ft. nylon parachutes. These observations were made from various launching altitudes up to 40,000 ft. A C_dS value was computed for each descent from the formula $C_dS = 2W/\rho V^2$, where W = weight of the dummy plus parachute and ρV^2 was calculated from the observed atmospheric conditions. The mean C_dS values thus computed were: for 28-ft. silk parachutes, 531; for 28-ft. nylon, 483; and for 24-ft. nylon, 336.

By using the mean C_dS value computed for each type of parachute, a formula has been developed to predict the time of descent from any altitude to any altitude if the type parachute, weight of the man, and certain atmospheric conditions are known.

An improved method of comparing performance of experimental parachutes is presented which negates the necessity for attempting to duplicate a given density altitude on successive flights.

A method is presented for calculating velocity at any instant in parachute descent. Landing velocities at different ground levels and with different types of parachutes and different weight men are discussed.

INTRODUCTION

A KNOWLEDGE OF THE TIME REQUIRED to reach the ground when a parachute is opened at a specified altitude is sometimes highly useful. Moreover, information concerning the rate of descent is necessary for the calculation of landing impact when the ground is reached. Heretofore, all tables of rates of parachute descent have been based on calculations extrapolated from a few observations of parachute descents from near the ground. It has been presumed, but never proved, that the rate of descent at any given altitude would vary inversely with the square root of the density ratio of the air at that altitude. In connection with tests conducted for the measurement of impact forces of parachute openings at altitude, the occasion was presented to observe experimentally the effect of altitude on parachute descent.

METHOD

The technique of release of the 200-lb. hard rubber torso dummies was described in a previous report.[1] Briefly, the parachutes were opened by 25-ft. static lines attached to the airplane. Parachutes were released at approximately 7,000, 15,000, 26,000, 33,000, and 40,000 ft. density altitude, and at each release accurate data as to indicated altitude, air speed, and temperature were kept. Flight instruments had been previously calibrated by the Flight Test Branch of the Air Matériel Command, Wright Field. In addition to the usual aircraft altimeter, the altitude of release was recorded by a radio altimeter and a recording barograph.

The timing was done visually by ground observers for the lower altitudes, and for the higher altitudes radio contact between the plane and the ground was maintained and stop watches were started at a signal from the plane. The parachutes were released in succession with sufficient intervals between to allow individual timing. The watch was stopped with the first contact of the dummy with the ground. The ground was a dried desert lake bed, the altitude of which was +2,800 ft. The location was near Kingman, Ariz.; the period of observation was November 30, 1944, to February 10, 1945.

RESULTS

Since the primary purpose of these parachute drops was to measure and compare opening shock forces of different sizes and kinds of parachutes, a given drop usually included a mixture of parachutes. Thus, the number of observations on a given type of parachute for any one flight varied from two to six.

Some variation existed among altitudes of release with different flights. For instance, the calculated density altitude at release of the silk parachutes at the so-called "26,000-ft." level ranged between 25,850 and 27,050 ft. density altitude. Since there is good reason to presume, as will be shown later, that the rate of descent of a parachute is related to the density of the air, it is misleading to group all the observed descent times from one approximate altitude. Also atmospheric conditions between the altitude of release and the ground will vary from day to day. The observations herein reported were made at the same geographic location but over a period of some 10 weeks. Therefore, it should prove more fruitful to treat each flight individually, taking into consideration the actual observed atmospheric conditions for that day. To this end the Kollsman number, or altimeter setting, at take-

Received January 10, 1947.

* Departments of Physiology and Pharmacology, Boston University School of Medicine. Formerly at the Aero Medical Laboratory, Air Matériel Command, Wright Field.

† Department of Physics, Iowa State College.

off and landing and the atmospheric temperature at each 2,000-ft. stratum were recorded for each flight.

Terminal velocity of a freely falling body is reached when its aerodynamic drag is equal to its weight. This relationship is expressed thus:

$$D = W = C_d S(\rho V_t^2/2) \qquad (1)$$

where

D = drag (lbs.)
W = weight (lbs.)
C_d = drag coefficient
S = drag area (sq.ft.)
ρ = air density (slugs per ft.^{3})
V_t = terminal velocity (ft. per sec.)

If the density of the atmosphere did not vary with altitude, then any falling body, as soon as it had been accelerated to the terminal velocity specified by Eq. (1), would fall with that constant velocity throughout its entire descent, and the problem of predicting total time of descent would be comparatively easy. But in the actual atmosphere, air density is not constant in space, or in time, so the terminal velocity of a body falling through the earth's atmosphere becomes a variable depending not only on its shape and weight but also on the value of the air density at each successive point in its descent. Since a body falling through the atmosphere is continuously moving into regions of greater density, Eq. (1) tells us that this is equivalent to saying that it is always falling from regions of higher terminal velocity into regions of lower terminal velocity; so, strictly speaking, we must conclude that in all but the first few seconds, during which the chute is opening, this steady deceleration implies that the actual velocity of descent must always be slightly greater than the theoretical value determined by Eq. (1). That is, the drag force, D, must always be slightly greater than the weight, W, with the net effect that the body undergoes a steady deceleration, as is actually observed to occur. The rate of increase of density with decreasing altitude is, however, gradual enough to make this slight disequilibrium and its consequent velocity lag negligible in our calculations. Thus, in summary, Eq. (1) presents the following picture of the variation in rate of descent of any large body (if we agree to equate D and W, and thus to neglect any velocity lags): For a body of given weight, W, drag area, S, and drag coefficient, C_d, the velocity at any point in its descent is inversely proportional to the square root of the density. From this basic relationship, formulas expressing the dependence of total time of descent on atmospheric conditions and on parachute type will now be developed.

The weight of our dummies, with parachutes attached, was constant at 225 lbs., plus or minus a few pounds. The ρV^2 values would be expected to vary with the changes in atmospheric conditions from flight to flight. These ρV^2 values were computed from the data of each flight as follows:

Let

$$\rho V^2 = k = 2W/C_d S$$

Then

$$V = \sqrt{k/\rho}$$

also

$$1/V = \sqrt{\rho/k}$$

If, now, we imagine the atmosphere to be divided into a series of strata, each 2,000 ft. in vertical thickness, then the time required to pass through the ith stratum will be

$$t_i = 2{,}000/V_i$$

The sum of these 2,000-ft. stratum times represent the total time

$$\Sigma t_i = \sum \frac{2{,}000}{V_i} = 2{,}000 \sum \frac{1}{V_i}$$

But

$$1/V = \sqrt{\rho/k}$$

so

$$\Sigma t_i = 2{,}000 \sum \sqrt{\frac{\rho_i}{k}} = \frac{2{,}000}{\sqrt{k}} \Sigma \sqrt{\rho_i} \qquad (2)$$

Now from the General Gas Law we have

$$P = \rho RT$$

in which

P = pressure in inches of mercury
ρ = the air density expressed in slugs per ft.^{3}
R = the gas constant for dry air (in suitable units)
T = air temperature in degrees Kelvin (°K.)

Then $\rho = P/RT$ and

$$\sqrt{\rho} = \sqrt{P/RT} = (1/\sqrt{R})\sqrt{P/T} = \left.\begin{array}{r} \\ \sqrt{\dfrac{3.38639 \times 10^4 \times 1.951875 \times (P/T)}{2.8886 \times 10^6}} = \\ 0.15126\sqrt{P/T} \end{array}\right\} \qquad (3)$$

This expression can then be substituted in Eq. (2), yielding

$$\Sigma t_i = \frac{2{,}000 \times 0.15126}{\sqrt{k}} \sum \sqrt{\frac{P_i}{T_i}} = \frac{302.52}{\sqrt{k}} \sum \sqrt{\frac{P_i}{T_i}} \qquad (4)$$

where P_i/T_i represents average pressure and temperature conditions for the ith 2,000-ft. stratum.

If the observed time of descent for each parachute is now substituted in Eq. (4), we may rearrange and solve for k:

$$k = \left(\frac{302.52 \sqrt{P_i/T_i}}{\text{observed time}}\right)^2 \qquad (5)$$

TABLE 1A

Computed ρV^2 and C_dS Values for Each Observed 24-Ft. Nylon Parachute Descent

Flight No.	Density Altitude	Observed Time, Sec.	ρV^2	C_dS
12	15,550	477	1.27	353.5
		464	1.35	334.6
		454	1.41	320.3
		474	1.29	349.1
		477	1.27	353.5
		456	1.39	323.0
16	15,800	455	1.43	314.0
		472	1.33	337.8
		426	1.64	275.2
		468	1.35	332.4
23	15,650	465	1.33	339.1
		440	1.48	303.6
		504	1.13	398.2
19	26,300	828	1.24	363.8
		785	1.38	326.3
36	26,400	783	1.42	316.2
		789	1.40	321.2
		787	1.41	319.6
		815	1.31	342.7
34	32,740	924	1.47	305.9
		925	1.47	306.8
		1,047	1.15	393.0
40	39,000	1,150	1.22	370.1
		1,149	1.22	369.5
Mean			1.348	336.23
Standard Deviation			±0.116	±29.1

TABLE 1B

Computed ρV^2 and C_dS Values for Each Observed 28-Ft. Nylon Parachute Descent

Flight No.	Density Altitude	Observed Time, Sec.	ρV^2	C_dS
9	7,750	204	1.07	419.0
		204	1.07	419.0
		214	0.98	461.1
		213	0.99	456.4
14	7,800	212	1.00	450.9
		203	1.09	413.6
		224	0.89	503.3
		219	0.94	481.3
4	16,000	605	0.83	540.2
		540	1.05	430.2
		538	1.05	426.9
6	15,875	557	0.93	484.4
		559	0.92	488.1
		543	0.98	460.6
8	15,750	552	0.99	454.5
		578	0.90	498.3
		563	0.95	472.7
13	15,850	565	0.93	482.3
		612	0.80	565.3
21	15,950	568	0.93	485.4
		574	0.91	495.6
		571	0.92	490.2
5	27,050	927	1.02	440.3
		998	0.88	510.2
7	26,600	949	0.94	476.2
		963	0.92	490.2
11	25,850	999	0.86	523.9
		995	0.86	520.2
		958	0.93	481.8
15	26,360	973	0.89	503.4
		981	0.88	511.9
		968	0.90	498.3
19	26,300	976	0.89	505.6
		954	0.93	482.8
36	26,400	907	1.06	424.5
		943	0.98	458.7
10	39,400	1,241	1.10	408.3
		1,460	0.80	565.3
		1,428	0.84	540.9
18	40,000	1,410	0.86	525.7
		1,294	1.02	442.9
		1,342	0.94	476.2
		1,386	0.89	507.9
40	39,000	1,350	0.88	510.2
		1,352	0.88	511.4
		1,356	0.88	514.3
Mean			0.938	482.83
Standard Deviation			±0.077	±38.75

Referring again to Eq. (1), it is seen that C_dS values may be then calculated by the equation

$$C_dS = 2W/\rho V^2 \qquad (6)$$

where the value of ρV^2 has been obtained from Eq. (5) and where W is the known weight of dummy plus parachute.

C_dS values have been calculated for 24 observed descents of 24-ft. nylon parachutes, for 46 28-ft. nylon, and 41 28-ft. silk parachutes. These data are presented in Tables 1A, 1B, and 1C.

COMPUTATION OF APPROXIMATE DESCENT TIME

Using the above relationship, it is possible to predict with reasonable accuracy the time it will take a man to reach the ground from any altitude if we know his weight, the type of parachute used, and the ground-level elevation.

Transposing Eq. (5),

$$\text{descent time} = \frac{302.52\Sigma\sqrt{P_i/T_i}}{\sqrt{\rho V^2}} \qquad (7)$$

If the mean C_dS values for each of the three standard types of parachutes are used, the formulas become:

For 24-ft. nylon parachutes:

$$\text{descent time} = \frac{302.52\Sigma\sqrt{P_i/T_i}}{\sqrt{2w/336}} \qquad (8)$$

For 28-ft. nylon parachutes:

$$\text{descent time} = \frac{302.52\Sigma\sqrt{P_i/T_i}}{\sqrt{2w/483}} \qquad (9)$$

For 28-ft. silk parachutes:

$$\text{descent time} = \frac{302.52\Sigma\sqrt{P_i/T_i}}{\sqrt{2w/531}} \qquad (10)$$

The value for $\Sigma\sqrt{P_i/T_i}$ is a function of the space through which the parachute travels. If the ground

TABLE 1C

Computed ρV^2 and C_dS Values for Each Observed 28-Ft. Silk Parachute Descent

Flight No.	Density Altitude	Observed Time, Sec.	ρV^2	C_dS
1	7,500	224	0.87	517.8
		210	0.99	455.0
		233	0.80	560.4
9	7,750	246	0.74	608.9
		232	0.83	541.5
14	7,800	242	0.77	587.5
		213	0.99	455.5
		240	0.78	577.7
4	16,000	583	0.90	501.7
		539	1.05	428.6
6	15,875	589	0.83	542.2
		572	0.88	511.4
		613	0.77	586.7
8	15,750	562	0.95	471.2
		600	0.84	537.0
		602	0.83	540.9
		615	0.80	564.6
13	15,850	600	0.83	543.5
		558	0.96	470.2
		607	0.81	556.2
		552	0.98	460.1
21	15,950	609	0.81	557.6
		586	0.87	516.6
5	27,050	998	0.88	510.2
		1,115	0.71	636.5
		1,032	0.82	545.5
		1,017	0.85	530.0
7	27,600	970	0.91	497.2
		990	0.87	517.8
15	26,360	1,022	0.81	555.6
		1,032	0.80	564.6
19	26,300	984	0.88	513.7
		964	0.91	493.4
10	39,400	1,585	0.67	666.7
		1,372	0.90	499.5
11	40,050	1,389	0.90	499.5
		1,388	0.90	499.5
		1,389	0.90	499.5
		1,448	0.83	542.8
18	40,000	1,417	0.85	531.3
		1,461	0.80	564.6
Mean			0.855	530.74
Standard Deviation			±0.077	±48.63

elevation is at sea level, the appropriate $\Sigma\sqrt{P_i/T_i}$ may be read directly from the graph shown in Fig. 1. For ground-level elevations higher than sea level, the appropriate correction value can be obtained by moving up the altitude scale (ordinate) to the altitude at the ground level then moving out along this altitude value until the plotted curve is intersected. The abscissa of this point of intersection is the necessary correction value that must then be subtracted from the value of $\Sigma\sqrt{P/T}$ shown for the launching altitude. Thus, if the ground level is 1,000 ft., the value 0.15 would be subtracted from the value for the launching altitude. If we wish to calculate the descent time from 20,000 to 1,000 ft., we would read the value for 20,000 ft. from the graph, 2.77 and subtract the 0.15 for the 1,000-ft. landing elevation, getting 2.62 as the appropriate value of $\Sigma\sqrt{P/T}$.

The value for $\Sigma\sqrt{P/T}$ shown in Fig. 1 was computed from U.S. Standard Atmosphere tables. Hence, the error of prediction should be in proportion to the variation of the actual atmospheric conditions of the day from the standard atmosphere. However, this error is probably less than the errors introduced by the variation among parachutes. It is seen from the data of Table 1 that identical parachutes dropped in succession from a plane at a constant altitude will vary considerably in the time they take to reach the ground. This variation can be partially accounted for by rising and descending air currents and the amount of pendulum swing; hence, spilling of air. For this reason it is possible to predict only approximately the actual time of descent of a lone parachute. Therefore, the figures calculated by the above method should be taken to represent the mean, or average, descent times of groups of identical parachutes and loads.

COMPARISON OF PARACHUTE DESCENT TIMES

For the purposes of comparing various types of parachutes it is believed that a computation of C_dS values would yield better results than does a simple comparison of observed descent times. Such computations would relieve the necessity for attempting to duplicate pressure altitudes on different flights, as well as

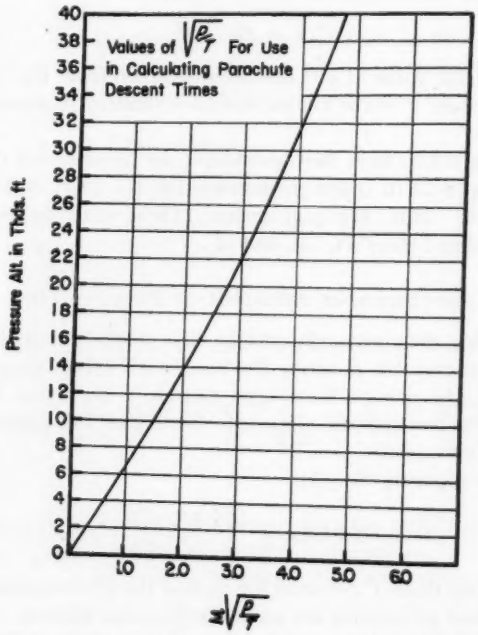

FIG. 1. Graph of $\sqrt{P/T}$ values, computed from U.S. Standard Atmosphere Tables, for use in calculating parachute descent times from the formula

$$\text{descent time} = (302.52\ \Sigma\sqrt{P/T})/\sqrt{2W/C_dS}$$

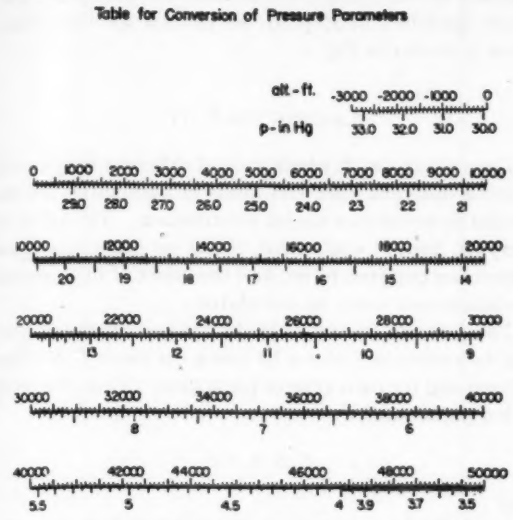

FIG. 2. The actual, or true, pressure at a given altitude is computed by setting one leg of a pair of dividers on zero and the other leg on the appropriate Kollsman number and by applying this correction to each altitude in question. Table adopted from Bellamy.[2]

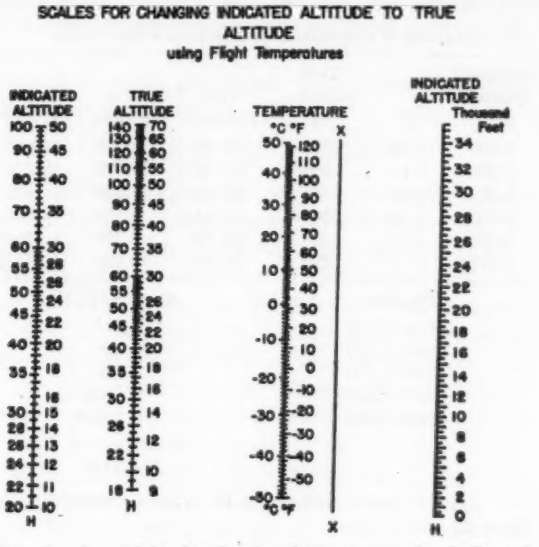

FIG. 3. A straightedge is placed to correct the indicated altitude of the right-hand column with its observed temperature. This locates a point on the line X. The straightedge is then rotated about this point so as to connect it with the indicated altitude in the left-hand column. True altitude is then read at the point where this line intersects the "True Altitude" scale.

rule out the effect of changing atmospheric conditions between tests.

For such a calculation the Kollsman number, or altimeter setting of the day, the temperature of the air at each 2,000-ft. level, the exact indicated altitude and temperature at time of drop, and a knowledge of the ground-level elevation are needed for each flight. The altitude of release need not be the same on successive flights. With these data at hand the method of calculation is as follows:

(a) True pressure can be obtained by entering Fig. 2 with a pair of dividers, one leg of which is set on zero altitude (29.92-in. pressure) and the other leg set on the figure for the altimeter setting of the day.[2] Thus, if such settings were greater than 29.92, the top line would be used, and, if it were less than 29.92, the second line would be used. The setting of the dividers so obtained represents a pressure correction that is used for each 2,000-ft. level as follows: Place one leg of the set dividers on the 2,000-ft. level in question and swing the other leg to right or left depending on whether the Kollsman number for the setting was to right or left of the zero point of 29.92 in. Hg. Read the pressure indicated by the second leg. This represents the actual pressure at the given indicated altitude. By doing this for each 2,000-ft. level, true pressures are obtained for each of these levels at which temperature is known. (Temperature readings were taken at every 2,000-ft. level of indicated altitude on each flight.)

(b) Next, the true altitude can be obtained from the nomogram shown in Fig. 3. To use this nomogram, a straightedge is placed on the right-hand portion of the nomogram in such a way as to connect the indicated altitude with its appropriate temperature. This locates a point on the line X. Next, the straightedge is rotated about that point on the line X and made to connect that point with the observed indicated altitude on the scale to the left. Then the true altitude may be read off the "True Altitude" scale at the point where the straightedge crosses that scale.

(c) The value for $\sqrt{P/T}$ can now be calculated for each of the successive levels for which true pressures have been determined in step (a), whose temperatures were recorded during flight, and whose true altitudes have been determined nomographically in step (b). The data up to this point had best be tabulated as shown in Table 2.

(d) The next step involves plotting the true altitudes vs. $\sqrt{P/T}$ values. From this graph the mean $\sqrt{P/T}$ value for each 2,000-ft. stratum may then be read directly. A second table should now be made showing the mean value of $\sqrt{P/T}$ for each complete 2,000-ft. stratum from ground altitude up to altitude of release.

The $\sqrt{P/T}$ values of the above table may now be summed and used in Eq. (5). Finally, Eq. (6) will give the C_dS value for the known weight, W, of dummy and parachute.

The above procedure may be illustrated with a hypothetical case in which a 200-lb. dummy with a 24-ft. nylon parachute (total weight 215 lbs.) is dropped from a 9,875-ft. indicated altitude, the time of descent being recorded as 382 sec. Altimeter setting is 30.20 and ground level is +300 ft. The observed temperature and indicated altitudes are shown in Table 2, along with the

TABLE 2
Example of Calculation of C_dS from Flight Data

Indicated Altitude, Ft.	°C.	Temperature, °A.	True Pressure	True Altitude	$\sqrt{P/T}$
+300	+23	296	29.86	308	0.3175
2,000	+15	288	29.09	2,020	0.312
4,000	+13	286	26.09	4,050	0.302
6,000	+12	285	24.21	6,150	0.292
8,000	+11	284	22.43	8,250	0.2805
9,875	+ 9	282	20.89	10,220	0.2722

Stratum	Mean $\sqrt{P/T}$
300 to 2,300	0.315
2,300–4,300	0.306
4,300–6,300	0.296
6,300–8,300	0.2855
8,300–9,875	0.2163*
	Σ 1.4188

* 1,575/2,000 of 0.2758 (mean for 8,300 to 10,300 stratum).

From Eq. (5)

$$\rho V_2 = (302.52 \times 1.4188/382)^2 = 1.2625$$

From Eq. (6)

$$C_dS = 430/1.2625 = 340.6$$

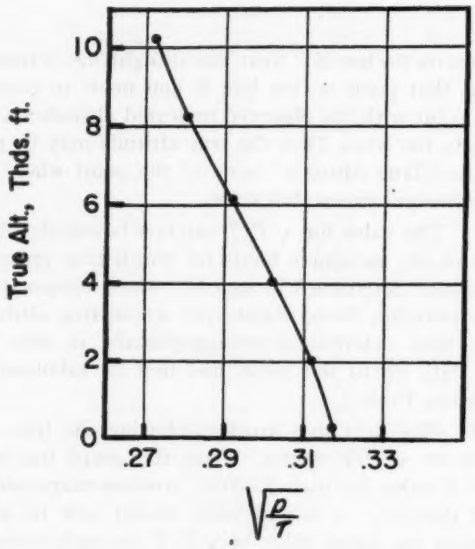

FIG. 4. Graph of true altitude vs. $\sqrt{P/T}$ for a sample calculation of parachute descent time. From this graph the mean $\sqrt{P/T}$ value for each 2,000-ft. stratum may be read directly. These values, together with their sum, are shown in Table 2.

entire calculation. The top stratum will not, in general, be a full 2,000-ft. stratum; therefore, since the coefficient 302.52 in Eq. (5) is based on 2,000-ft. strata, it is clear that the average $\sqrt{P/T}$ value for the top stratum must not be added directly along with the $\sqrt{P/T}$ values for the full 2,000-ft. strata but must be weighted by a fractional factor given by top-stratum-thickness-in-feet per 2,000 ft. An example of this weighting process is included in the sample calculations of Table 2. The graph described in step (d) as plotted for this calculation is shown in Fig. 4.

LANDING VELOCITY

The velocity with which men of different weight and wearing different sizes and kinds of parachutes hit the ground is sometimes useful information. The effect of carrying heavy equipment, such as paratroops are sometimes required to do, and the effect of high ground elevations can easily be calculated.

The velocity at any altitude can be calculated from the data contained above by using the mean C_dS values determined for each type of parachute. Thus, for 28-ft. nylon parachutes,

$$C_dS = 483$$

But

$$\rho V^2 = 2W/C_dS$$

So

$$V = \sqrt{2W/C_dS\rho} = \sqrt{2W/483\rho} \qquad (11)$$

The quantity ρV^2, as expressed above, is seen to be a constant during any given descent (fixed W and parachute type). Therefore, $\rho_1 V_1^2 = \rho_2 V_2^2$, so

$$V_2 = \sqrt{\rho_1/\rho_2}(V_1) \qquad (12)$$

where

V_1 = velocity at first altitude
V_2 = velocity at second altitude
ρ_1/ρ_2 = ratio between the densities of the two altitudes

The validity of the relationship expressed above can be put to test using the observed descent times listed in Table 1. In Fig. 5 the observations on descent times of 28-ft. nylon parachutes have been averaged for each of four approximate altitudes and plotted as launching altitude versus total time of descent to 2,800 ft. (ground level in these tests). Then a theoretical curve has been constructed using Eq. (12), where V_2 = velocity at 2,800 ft., ρ_2 = density at 2,800 ft., and the resulting curve is plotted to the same axes. The V_2 used in this calculation was derived from Eq. (11), using standard ρ for 2,800 ft.

It is evident that the observed mean descent times from the four different altitudes fall very close to this theoretical curve. Since the same relative correlation was found when the 24-ft. nylon and 28-ft. silk parachute descent time data were plotted against such a theoretical curve, it would appear to be safe to accept the validity of Eq. (12).

If we wish to determine the sea-level velocity of men weighing 225 lbs. wearing a 28-ft. nylon parachute, we may refer to Eq. (11) above and use any convenient

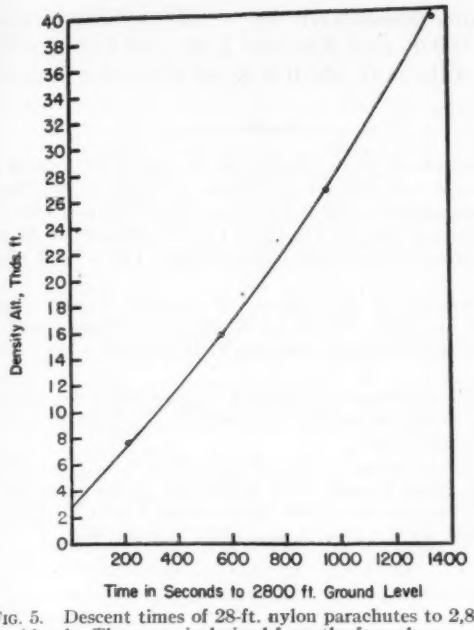

FIG. 5. Descent times of 28-ft. nylon parachutes to 2,800-ft. ground level. The curve is derived from the formula

$$V_\alpha = V_{2,800}/\sqrt{\rho\alpha/\rho_{2,800}}$$

where V_α = velocity at launching altitude, $V_{2,800}$ = velocity at 2,800 ft., ρ_α = air density at launching altitude and $\rho_{2,800}$ = air density at 2,800 ft. The four points represent means of four groups of observed descent times.

altitude. If we choose 10,000 ft., ρ_1 becomes 0.001756 and V_1 becomes 23.11. Then, using Eq. (12),

$$23.11 \times 0.859 = 19.85 \text{ ft. per sec. at sea level}$$

where 0.859 is the square root of the density ratio for 10,000 ft. The comparable sea-level velocities for 24-ft. nylon and 28-ft. silk parachutes are 23.78 and 18.96, respectively.

The precise effect of weight change on the rate of descent of parachutes cannot be shown by our data, since we used only one weight dummy. In general, we know that the heavier the weight the faster the rate of descent and, hence, the greater the landing impact; but one fundamental question remains unanswered: Does the weight of the incorporated air mass combine with the effect of dummy weight to determine the actual descent rates? If it does not, then the effect of the weight of the man on descent rate is easily calculated as follows:

For 24-ft. nylon parachutes with man-shaped dummies, the C_dS value is 336. Then,

$$\rho V^2 = 2W/C_dS = 2W/336$$

Next, applying the above in Eq. (11), using the appropriate value of ρ in slugs per cu.ft., the velocity may be calculated. Table 3 shows the results of such a calculation for sea-level velocities. If the weight of the air mass does enter into the problem, it would have a damping effect on the change in velocity, since the incorporated air mass should remain relatively constant with changes in weight of men. Hence, the percentage change in weight of the whole system would be less and the total spread in velocity shown in Table 3 would be too great. Thus, for the larger weights in Table 3, the velocities may involve small errors, but it is to be noted that any errors are on the safe side, since, at worst, the landing velocities in Table 3 are overestimated.

TABLE 3

Calculated Effect of Varying Weights of Men on the Sea-Level Velocity of a Standard 24-Ft. Nylon Parachute

Weight, Lbs.	Velocity, Sea Level, Ft. per Sec.
150	19.38
175	20.93
200	22.37
225	23.78
250	25.02
275	26.27
300	27.40

In this treatise no account is taken of the effect of the so-called "ground reflection" of air on the landing velocity of the parachute. This phenomenon, said by Stasevich[3] to give a retardation of 10 to 20 per cent, is a variable factor and has not, to our knowledge, been subjected to scientific measurement. This effect is presumed to be due to two factors: (1) rising air currents near the ground due to ground heat and (2) the striking of the ground of the air mass being pushed ahead of the canopy.

Practical experience in both the United States and British airborne services and air forces has shown that an increase in ground altitude of 5,000 ft. has been sufficient to increase greatly the number of landing injuries beyond those encountered in descents to near sea level.[4] It is generally assumed that this rise of injury rate is due to a rise in landing velocity occasioned by the reduced density of the air at the ground level in elevated areas. To show more clearly the effect of altitude on

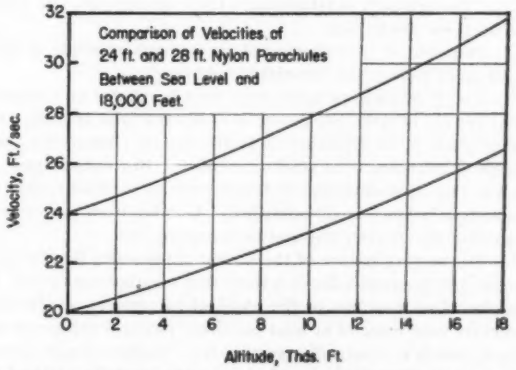

FIG. 6. The curves are derived from the formula $V_\alpha = V_0 \div \sqrt{\rho\alpha/\rho_0}$, where V_α = velocity at any altitude, V_0 = velocity at sea level, and ρ_α/ρ_0 = the density ratio.

landing velocities, Fig. 6 represents the theoretical increase in landing velocities of 24 and 20 ft. per sec., respectively.[5]

It may seem surprising, since the landing velocity at 5,000 ft. in a 24-ft. nylon parachute is less than 2 ft. per sec. faster, that the injury rate should be appreciably higher. However, it must be recalled that the kinetic energy of a falling body increases as the square of the velocity. This relationship is given by the formula

$$E_k = {}^1/_2 M V^2$$

Thus, calculation shows that the kinetic energy to be dissipated upon striking the ground at 5,000 ft. is some 17 per cent greater than at sea level for the same weight of man and same type of parachute. On the other hand, it may be calculated from the same formula that the kinetic energy associated with the 28-ft. parachutes is considerably less than for the 24-ft. parachutes at the same ground level. In the case of the 28-ft. nylon, for a 200-lb. man, it is some 43 per cent less, and in the case of the 28-ft. silk, it is 57 per cent less at sea level.

References

[1] Hallenbeck, G. A., Penrod, K. E., and MacCardle, R. C., *Magnitude and Duration of Opening Parachute Shock*, The Air Surgeon's Bulletin, Vol. 2, No. 2, pp. 35–37, February, 1945.

[2] Bellamy, John C., *The Use of Pressure Altitude and Altimeter Corrections in Meteorology*, Jr. Meteorology, Vol. 2, No. 1, March, 1945.

[3] Stasevich, R. A., *Dynamics of Parachute Jumps*, Samolet, No. 6, pp. 24–25; No. 8, pp. 37–38, 1937. Translation No. 7, Air Service Command, Patterson Field, Fairfield, Ohio, October, 1943.

[4] Maison, George L., Penrod, K. E., and Hall, F. G., *Parachute Shock Forces*, The Air Surgeon's Bulletin, Vol. 2, No. 10, pp. 350–353, October, 1945.

[5] Maison, George L., Penrod, K. E., Hall, F. G., *Descent Times of 200-Pound Dummies with 28-foot Silk, 28-foot Nylon and 24-foot Nylon Parachutes*, AAF Memorandum Report No. TSEAL3-696-66H, 30 May 1945, Wright Field, Dayton, Ohio.

Letter to the Editor

Dear Sir:

Mr. Krzywoblocki's Letter to the Editor (JOURNAL OF THE AERONAUTICAL SCIENCES, pp. 23–24, January, 1947) is so significant and representative of the opinion of a certain group of students of the problem of jet and rocket propulsion that it seems desirable to discuss further the definition of propulsive efficiency.

The formula for propulsive efficiency was established correctly many decades ago. It reads, using Mr. Krzywoblocki's notation:

$$\eta_p = \frac{2[(W_a + W_f)v_j - W_a V]\,V}{[(W_a + W_f)v_j^2 - W_a V^2]} \qquad (1)$$

Let us remember a few basic laws and principles of elementary physics:

(1) Velocity and force are vectors; the same is true for momentum, while kinetic energy is a scalar. Therefore, the direction of velocity vector is of importance in computing momentum, while it is immaterial in computing kinetic energy.

(2) The principle of relativity, a few centuries old, still holds true in classic mechanics.

(3) Principle of conservation of energy and principle of conservation of momentum invariably hold true.

(4) Every problem of mechanics must be placed in a certain given system of reference before it is theoretically treated. Of course, there is no difference as to the system chosen—i.e., one system of reference is as good as another. But once chosen, it must be respected until the whole computation of either energy or momentum balance is accomplished. Leaping from one system to another during the computation is inadmissible.

(5) In the very nature of the notion of efficiency lies the fact that its 100 per cent value is a limit that is either asymptotic in function of at least one of the physical parameters involved or occurs for zero value of at least one other physical parameter involved, which is essentially positive (i.e., absolute temperature, mass, etc.). This limit is, of course, not actually attainable, but it must be logically admissible. This means that practically attainable values of efficiency may be imagined as close to 100 per cent as the technical facilities now available permit, and there is no limit in improving these facilities so as to approach more closely the 100 per cent value in the future. Any formula for efficiency giving a theoretical maximum value of efficiency less than 100 per cent is erroneous. To illustrate the above, let us take the theoretical efficiency of the Otto cycle, which has an asymptotic limit of 100 per cent for the volumetric compression ratio infinitely large. Another example is the efficiency of Carnot cycle

$$\eta = \frac{(T_1 - T_2)}{T_1}$$

which has either an asymptotic limit of 100 per cent for the absolute temperature T_1 infinitely large or a limit of 100 per cent for the absolute temperature T_2 equaling zero; of course, the absolute temperature cannot be negative.

Mr. Krzywoblocki's assumption (2) is erroneous. Taking the propelled unit as a system of reference, air enters the engine at the rate of W_a lbs. per sec. and with the speed V; the input momentum is, therefore, $(W_a/g)\,V$ and the input kinetic energy is $(W_a/2g)\,V^2$; this is an actual fact. Ascribing this latter energy to the thermal efficiency would only displace its asymptotic limit from the 100 per cent value, which is wrong. The energy to be produced by the engine is, therefore, only

$$[(W_a + W_f)/2g]\,v_j^2 - (W_a/2g)\,V^2$$

Now, Mr. Krzywoblocki changes to another system of reference. Energy L_1 given by his Eq. (2) was computed relative to the propelled unit. Now he adds the kinetic energy L_2, given by his Eq. (3), relative to the earth. This energy is, of course, nil in the former system of reference. A further step along the path chosen by Mr. Krzywoblocki may be made. The earth as a system of reference is no better than any other system. Let us take the sun as a system of reference. The velocity V in Mr. Krzywoblocki's Eq. (3) for L_2 will become about 90,000 ft. per sec. The "most favorable conditions" in which the maximum energy can be imparted to the jet unit become still more favorable. Any other fixed star or even the Milky Way may also be chosen as a

system of reference. The only condition is to keep the direction of flight perpendicularly to the corresponding gravitational field. But this is not all. The internal energy of the fuel (not to be confused with the intramolecular—i.e., chemical energy) is, in fact, molecular kinetic energy. Why not add this energy also? True, molecular velocities have many different directions, but this makes no difference, since kinetic energy is not a vector. Mention should be made of the intra-atomic energy also.

Mr. Krzywoblocki's statement that "undoubtedly, the best speed of an airplane occurs when the optimum value of the useful power may be achieved" is misleading. It follows from his further reasoning that he speaks about the *unit* power, as obtained per 1 lb. of air involved. One B.t.u. in hydrogen weighs three times less than in gasoline. Does this mean that hydrogen is three times better than gasoline as fuel for combustion engines? Of course, the increase in air output of a jet engine will increase its bulk. But we are discussing only the problem of efficiency of the engine, other aspects of the propelled unit being, therefore, logically immaterial here. But even if they were involved, the best total useful power—and, consequently, the best speed of an airplane—would certainly not occur at the maximum of the unit power but somewhere between this maximum and the maximum efficiency.

The same kind of misunderstanding appears in Mr. Krzywoblocki's criticism expressed as follows: "One may ask what this 'propulsive' efficiency represents if it is not equal to zero and both the propulsive force and propulsive power are equal to zero." This applies to the "airscrew" case, $W_f/W_a \sim 0$, thus $\eta_p = 2V/(v_j + V)$, according to Eq. (1), where $v_j = V$. The point is that the statement that propulsive force and power are zero here is untrue. The air output is in this case infinitely large and the product $(\infty \times 0)$ is finite. This is, of course, an abstraction. But similar abstractions occur in theoretical physics so often that every physicist and even every college student must be familiar with them. The abstractive limit $(\infty \times 0)$ cannot be, of course, actually achieved. But we can approach it as close as the actual technical facilities now available permit. A very large output together with an extremely small increase in velocity may be actually applied, thus giving an efficiency close to the theoretical limit. The usual airscrew is certainly close to this limit. A 100 per cent efficiency is here an asymptotic limit in function of air output W_a. Assuming the propulsive force is given as (Th), we get:

$$\left.\begin{aligned} v_j &= V + [g(Th)/W_a V] \\ \eta_p &= 2V/\{2V + [g(Th)/W_a]\} \end{aligned}\right\} \tag{2}$$

Let us, finally, consider the case of a pure rocket, where $W_a = 0$ in Eq. (1), i.e.:

$$\left.\begin{aligned} \text{propulsive force } (Th) &= \frac{W_f v_j}{g} \\ \text{propulsive power } P = V(Th) &= \frac{WVv_j}{g} \\ \text{efficiency } \eta_p &= \frac{2V}{v_j} = \frac{2V}{w+V} \end{aligned}\right\} \tag{3}$$

where $w = v_j - V$ is the velocity of burnt gases relative to the earth. Consider the earth as a system of reference. During the energy release (i.e., by combustion) the velocity of the fuel relative to the earth changed from $(-V)$ to w. Therefore, the energy released, if its total is represented as kinetic energy (thermal efficiency 100 per cent), will correspond to the numerical value of the vecto- $[w - (-V)]$, i.e.:

$$P_{\text{tot.}} = \frac{W_f}{2g}[w - (-V)]^2 = \frac{W_f v_j^2}{2g}$$

The fuel traveling with the rocket had, before combustion and relative to the earth, kinetic energy $(W_f/2g)V^2$. The burnt gases leave the engine with the kinetic energy $(W_f/2g)w^2$, relative to the earth. The energy lost, which is gone uselessly to the surroundings, is therefore

$$P_{\text{loss}} = (W_f/2g)(w^2 - V^2) \tag{4}$$

and this energy has been borrowed from the total energy released. The fact that V and w have opposite directions is immaterial, since kinetic energy is a scalar. Therefore, the useful energy must be

$$P_{\text{tot.}} - P_{\text{loss}} = (W_f/g)Vv_j$$

which is in accordance with the propulsive power P found directly as a product of velocity V and force (Th) acting with this velocity (always relatively to the earth).

The energy lost P_{loss} as expressed by Eq. (4), is an essentially positive physical quantity. It would be illogical to suppose that this loss, dispersed in the surroundings, may be negative—i.e., that kinetic energy may be derived from surroundings that are at rest. In other words, it is impossible to transfer any part of the initial kinetic energy of fuel $W_f V^2/2g$ to the rocket, since both move with the same speed V—i.e., one is at rest relative to another. The theoretical upper limit for efficiency is, therefore, given by $P_{\text{loss}} \geq 0$, i.e.:

$$\left.\begin{aligned} w &\geq V \\ V &\leq {}^1/_2\, v_j \end{aligned}\right\} \tag{5}$$

Impulse drawn from the reaction of surroundings does not exist here. The picture is different when it does—e.g., in a gun, where the impulse balanced by the reaction of the earth is imparted and the theoretical limit for velocity becomes $V \leq v_j$. The case of pure jet ("airscrew") is somewhat analogous. Here, the impulse of surroundings (which belong to the earth system and are at rest relative to it) exists and may be explained as being in balance with the reaction of the surrounding air; this reaction is due to the inertia of air mass. In the general case, where $W_a \neq 0$ and $W_f \neq 0$, the impulse exists and involves in the energy balance a certain work.

The new "theories" as criticized above may cause so much harm in the era where the problem of dynamic propulsion is so intensively studied and so much time and money has been and still is being spent for experiment that it seems desirable to refute them at once.

B. Szczeniowski
Associate Professor
École Polytechnique
University of Montreal

Services of the Libraries of the Institute of the Aeronautical Sciences

The services of the Libraries are available to all members of the Institute, to Corporate Members, to advertisers in the AERONAUTICAL ENGINEERING REVIEW and AERONAUTICAL ENGINEERING CATALOG, and, under usual library limitations, to the public. Four specialized services are available.

The Paul Kollsman Lending Library

This lending library service makes available, *without charge*, the latest and more important aeronautical books.

Members may request the loan of any aeronautical or technical book they wish to borrow. Through an exchange agreement with the Engineering Societies Library, any book on general engineering may be borrowed from its great collection of over 160,000 volumes.

A photostating service is available at usual library rates.

Applications for membership in the library and further information will be sent on request.

The W. A. M. Burden Reference Library

This reference library contains over 12,000 aeronautical books, magazines, pamphlets, and reports gathered from world-wide sources and is one of the most complete aeronautical libraries in the world. Material from this library is not available for loan but may be used for reference purposes.

The Pacific Aeronautical Library

6715 Hollywood Boulevard
Los Angeles 28, California

Established in cooperation with the aircraft companies the library serves. The leading aircraft companies in or near Los Angeles participate in its support and operation.

This service library for aeronautical research is available to the public for reading privileges. Source material includes aerodynamic and structural research reports, as well as books on drafting, production methods, history, and allied sciences. It furnishes books, periodicals, and pamphlet material to the participating aircraft companies to supplement their engineering libraries.

Technical Information Service

This service has experienced personnel under the supervision of trained aeronautical engineers to compile any information desired. The services range from listing specialized reference books to the preparation of exhaustive bibliographies, digesting of reports, and general surveys of any aeronautical subject. Some of the available services are:

Bibliographies on any aeronautical subject.
Reports on any aeronautical subject.
Digests of aeronautical books, papers, periodicals, and references.
Translations.
Engineering investigations of special aeronautical subjects.
Biographies of individuals engaged in aeronautics.
Photostats of any aeronautical or general engineering material.
Microfilms made on special order.
Photographs made from the Institute's photographic collection.
Drawings and tracings made.

In addition to the services mentioned any commission which comes within the scope of the Service will be accepted. Special arrangements may be made for work requiring several weeks or months.

Translators are available for accurate transcriptions of all foreign language data. Translations are carefully edited by trained engineers.

Reproductions of any material in the collections of the Institute may be ordered at standard photostat rates.

INSTITUTE OF THE AERONAUTICAL SCIENCES, INC.
2 EAST 64TH STREET, NEW YORK 21, N.Y.